PB81-222259

Mixing Phenomena in Industrial Fume Afterburner Systems

Battelle Columbus Labs., OH

Prepared for

Industrial Environmental Research Lab.
Research Triangle Park, NC

Jul 81

U.S. Department of Commerce
National Technical Information Service
NTIS

PB81-222259

IERL-RTP-1224

MIXING PHENOMENA IN INDUSTRIAL FUME AFTERBURNER SYSTEMS

by

A. A. Putnam and H. A. Arbib

BATTELLE COLUMBUS LABORATORIES
505 King Avenue
Columbus, Ohio 43201

Contract No. 68-02-2629

EPA Project Officer: John H. Wasser

Industrial Environmental Research Laboratory
Office of Environmental Engineering and Technology
Research Triangle Park, NC 27711

Prepared for

U.S. ENVIRONMENTAL PROTECTION AGENCY
Office of Research and Development
Washington, DC 20460

REPRODUCED BY
NATIONAL TECHNICAL
INFORMATION SERVICE
U.S. DEPARTMENT OF COMMERCE
SPRINGFIELD, VA 22161

NOTICE

THIS DOCUMENT HAS BEEN REPRODUCED FROM THE BEST COPY FURNISHED US BY THE SPONSORING AGENCY. ALTHOUGH IT IS RECOGNIZED THAT CERTAIN PORTIONS ARE ILLEGIBLE, IT IS BEING RELEASED IN THE INTEREST OF MAKING AVAILABLE AS MUCH INFORMATION AS POSSIBLE.

IERL-RTP-1224	TECHNICAL REPORT DATA *(Please read Instructions on the reverse before completing)*	
1. REPORT NO. EPA-600/7-81-110	2. ORD Report	3. RECIPIENT'S ACCESSION NO. PB81 222259
4. TITLE AND SUBTITLE **Mixing Phenomena in Industrial Fume Afterburner Systems**		5. REPORT DATE July 1981 6. PERFORMING ORGANIZATION CODE
7. AUTHOR(S) **A.A. Putnam and H.A. Arbib**		8. PERFORMING ORGANIZATION REPORT NO.
9. PERFORMING ORGANIZATION NAME AND ADDRESS **Battelle-Columbus Laboratories 505 King Avenue Columbus, Ohio 43201**		10. PROGRAM ELEMENT NO. EHE624A 11. CONTRACT/GRANT NO. 68-02-2629
12. SPONSORING AGENCY NAME AND ADDRESS **EPA, Office of Research and Development Industrial Environmental Research Laboratory Research Triangle Park, NC 27711**		13. TYPE OF REPORT AND PERIOD COVERED Topical; 8/79-6/81 14. SPONSORING AGENCY CODE EPA/600/13

15. SUPPLEMENTARY NOTES **IERL-RTP project officer is John H. Wasser, Mail Drop 65, 919/541-2476. EPA-600/7-79-096 is a related report.**

16. ABSTRACT **The report reviews the physical-mixing phenomena involved in the reactions that occur in afterburners or fume incinerators. It considers mixing in afterburners from three points of view. It first covers typical designs of afterburner components that are involved in the mixing phenomena: with the paucity of performance information available, there is no clear-cut indication of the superiority of any particular design. Secondly, it considers the possible application of mathematical modeling principles developed for studies of conventional furnaces to afterburner design: although the problem for the afterburner is basically simpler, practical application of mathematical modeling still seems some time off. Thirdly, it presents empirical relations available in the literature for describing the performance of jet flow systems similar to various afterburner components: these relations permit an estimate of time/temperature histories of various flow paths through different afterburner designs. Overall, the design of adequate afterburners from the mixing point of view seems well within the current state of the art.**

17. KEY WORDS AND DOCUMENT ANALYSIS

a. DESCRIPTORS		b. IDENTIFIERS/OPEN ENDED TERMS	c. COSATI Field/Group	
Pollution	Burners	Pollution Control	13B	13A
Afterburners	Mathematical Models	Stationary Sources	21J	12A
Fumes	Jet Flow	Fume Incinerator Design		20D
Mixing			13H, 07A	
Incinerators				
Combustion			21B	

18. DISTRIBUTION STATEMENT	19. SECURITY CLASS *(This Report)*	21. NO. OF PAGES
Release to Public	**Unclassified**	107
	20. SECURITY CLASS *(This page)* **Unclassified**	22. PRICE

EPA Form 2220-1 (9-73)

ABSTRACT

This is a companion report to "Chemical Aspects of Afterburner Systems", EPA-600/7-79-096, April, 1979, which reviews the chemistry and reaction kinetics of oxidation and pyrolysis reactions that occur in afterburners or fume incinerators. This report reviews the physical mixing phenomena involved in the reactions that occur in afterburners or fume incinerators.

Mixing in afterburners is considered from three points of view. First, the typical designs of afterburner components that are involved in the mixing phenomena are covered. With the paucity of information available on performance, there is no clear-cut indication of the superiority of any particular design. Second, consideration is given to the possible application of mathematical modeling principles developed for studies of conventional furnaces to afterburner design. Although the problem for the afterburner is basically simpler, practical application of mathematical modeling still seems some time off. Third, empirical relations available in the literature for describing the performance of jet flow systems similar to various afterburner components are presented. Use of these relations permits an estimate of time-temperature histories of various flow paths through different afterburner designs. Overall, the design of adequate afterburners from the mixing point of view seems well within the current state of the art.

This report was submitted in partial fulfillment of Contract No. 68-02-2629 by Battelle's Columbus Laboratories under the sponsorship of the U.S. Environmental Protection Agency. It covers an effort conducted over the period August 1, 1979 to October 31, 1980, and work was completed as of October 31, 1980.

CONTENTS

Abstract ii

1. Introduction. 1
2. Review of Direct Flame Afterburner Systems. . . . 4
   - Burners 6
     - Line Burners 6
     - Multijet Burners 8
     - Ring Burners 8
     - Grid Burner 8
     - Distributed Source Burners 8
     - Discrete Source Burners. 13
     - Premix Burners 13
     - Delayed-Mixing Burners 13
     - Nozzle-Mix Burners 18
   - Combustion Chamber 21
     - Simple Combustion Chambers 21
     - Combustion Chamber with Symmetric Baffling 21
     - Combustion Chamber with Asymmetric Baffles 25
     - Side-Fired Burners 25
     - Compact Combustion Chamber 25
     - Regenerative Fume Incinerator 25
   - Approach Section
     - Slotted Duct System. 32
     - Approach with Abrupt Turn. 32
     - High Velocity Approach Section 34
3. Mathematical Modeling of Turbulent Combustion . . 35
   - Some Physical Features of Turbulence. 37
     - Vortex Stretching. 37
     - Correlations, Scales, and Spectra. . . . 39
     - Turbulence and Combustion. 44
   - Fundamentals of Turbulent Combustion Modeling. 46
     - The Flow. 46
     - Thermal and Chemical Properties 49
     - The Computation 51
     - Some Remarks about Radiation Transfer . 52
   - Recommendations for Modeling Turbulent Combustion in Industrial Afterburners . . 52
     - Flow Geometry. 52
     - Turbulence Model 52
     - Kinetic Model. 53

CONTENTS
(continued)

	Page
4. Jetlike Components of Afterburners	55
Circular Turbulent Free Jets.	57
Plane Turbulent Free Jets	63
Free Compound Jets.	64
Enclosed Compound Jets.	69
Circular Jet With Swirl	76
Jets in Cross Flow.	79
Jet Impingement	82
Flow Field	82
Heat Transfer.	86
Nomenclature for Section 4 only	89
5. Summary and Conclusions.	91
References	95

FIGURES

Number		Page
1	Fume afterburner with mixing-plate burner and recuperator	5
2	Maxon line gas burner with profile plates	7
3	Hirt multijet gas burner	9
4	Ring burners	10
5	North American flame grid burner	11
6	Distributed-source burner	12
7	Discrete-source burners	14
8	Flame retention type premix burner and one discrete source use	15
9	Multiple port premix burner	16
10	Delayed mixing burners	17
11	Nozzle-mixing burners	19
12	Common industrial flame types	20
13	Simple afterburner combustion chamber shapes	22
14	Flow patterns in combustion chamber of uniform diameter	23
15	Symmetric baffle systems	24
16	Combustion chambers with bridge wall baffles	26
17	Combustion chamber with side firing	27
18	Suggested arrangements for cross-stream mixing of flame and fume in rectangular box	28
19	Compact combustion chamber	29
20	Recirculation regions with 180° and 90° turns	30
21	Proctor-Schwartz system with regenerative heat recovery	31
22	Afterburner approach section with slotted duct	33
23	Vortex phenomena	38
24	Production of small scale isotropy by vortex stretching	40
25	Correlated and uncorrelated fluctuations	41
26	Typical transverse correlation coefficient	43
27	Typical isotropic turbulent energy spectrum	45
28	Regions of jet	48
29	Distribution of centerline velocity for flow from orifice according to Albertson, et al.	59
30	Reichard's velocity profile in the downstream part of a circular jet	61
31	Golubev-Klimkin profiles of downstream part of circular jet	62
32	Boundary of an axially symmetric jet	65
33	Boundary of a plane jet	66
34	Predicted and experimental half-radius for different velocity ratios	67
35	Predicted and experimental center line velocity for different velocity ratios	68

FIGURES
(continued)

Number		Page
36	Map of the recirculation for a ducted axisymmetric jet.	70
37	Position of recirculation eddy in confined jet. . .	71
38	Maximum recirculation flow rate versus $m^{1/2}$	73
39	Excess velocity as a function of axial distance . .	74
40	The axial growth of the velocity half-radius. . . .	75
41	Radial distribution of axial velocity	77
42	Radial distribution of swirl velocity	78
43	Geometry of the kidney shape of the circular jet in cross-flow	81
44	Flow field of normally impinging jet.	83
45	Inclined impinging jet.	87

TABLES

Number		
1	Jet-Type Variations Classified in Sets . . .	56
2	Coefficients for Incompressible Turbulent Jets	57

SECTION 1

INTRODUCTION

The aim in an industrial afterburner is to consume a pollutant down to a safe lower level while balancing the economics of auxiliary fuel requirements, afterburner size and complexity, operating and maintenance costs, and meeting any other specific requirement, such as turndown capabilities. While the kinetics of the specific reactions that are desired will control minimum time-temperature-concentration requirements, the mixing patterns in the afterburners will be critical in providing these conditions. Furthermore, the complexities of providing mixing patterns of a desired size will control the size of the afterburner, the amount of auxiliary fuel actually required, and the pressure drop through the afterburner. It is therefore clear that a detailed consideration of the various mixing phenomena that occur in industrial afterburners could result in significant advances in their design.

One might designate three characteristic times in an afterburner system, namely:

1. Chemical time, τ_c. For a first-order reaction, τ_c is proportional to $1/k$ where k is the rate constant. For other orders, the rate constant is multiplied by an appropriate average concentration.

2. Mixing time, τ_d. The mixing time is proportional to L^2/D_v where L is a characteristic linear dimension and D_v is the effective diffusion coefficient.

3. Residence time, τ_r. The residence time is proportional to L/V where V is an average gas velocity.

One notes that the ratio of the mixing time to residence time is proportional to the Reynolds' number, which is expected to be high in the usual afterburner. This means that mixing across the combustor must be examined critically. While the procedure for computing the flow and mixing in nonreacting systems can be quite satisfactory, where reaction systems are considered, the problem of "unmixedness" enters. Unmixedness was first discussed in some depth by Hawthorne, et al.,[1], using a Gaussian distribution as a basis for their computational procedure. In their discussion, it is pointed out that a turbulent diffusion flame is made of pockets of unreacted fuel, air, unreacted mixture, reacting mixture, and products of combustion. A similar situation occurs for a turbulent premixed flame. As a result, a sampling at one point may show both reaction products, and fuel, oxygen, and nitrogen. In dealing through mathematical modeling with the physical (as contrasted to the chemical) aspects of combustion in a combustion system, the phenomenon of unmixedness must be added to the other flow considerations. And in most of the literature this is done, usually in the same spirit as in the Hawthorne, et al.,[1] paper. However, it is well known that the jets and vortex flow systems that make up the usual combustion system do not show a Gaussian-type distribution on the scale of interest. Quite common in the literature[2,3,4,5] are pictures and sketches of the rolling-up vortices at the region of highest velocity gradient, which normally is in the highest reaction rate region.

The ratio of the chemical time to the residence time is V/kL, the reciprocal first Damkohler group. If the rate constant is very high, or V/kL is low, the reaction can be inhibited by lack of proper mixing but not the chemistry. This is the usual case in combustion systems. However, in fume incinerators, it is possible that the rate constant for the fumes [not the fuel for the gas burner(s)] is low and the performance will be limited by both the reaction time and the mixing time. As a result, an optimum fume incinerator must be designed for a particular class of fumes.

To complicate these chemical aspects further, in 1970, Pauletta[6] pointed out that "the presence of a flame is important for contaminant removal. Evidence indicates that when using electric heat energy much

higher temperatures are required--1500 to 1800 F--to obtain the same efficiency achieved with a direct-flame system at 1000 to 1400 F. If satisfactory incineration is to be achieved at the lowest possible temperature, the type of flame and the design of the combustor are also important factors to be considered". In 1980, Gruzdev, et al.,[7] studied self-ignition temperature of kerosene sprays downstream of a gas turbine combustor can. The temperatures varied from about 500 K to 1300 K, with an inverse correlation of the self-ignition temperature with a measure of the non-equilibrium ionization of the igniting gas from the turbine. This would indicate that the more intimately and quickly the primary products of combustion in a fume incinerator mixed with the polluted secondary air, the lower the temperature or the shorter the time could be for complete combustion of the fumes.

Estimates of the chemical reaction time for various fumes is covered in Reference 8, a parallel study to the present one. In the present study, the factors entering into the estimate of the mixing time are reviewed. The review covers three aspects of the mixing problem, namely, a consideration of the various direct flame afterburner systems that are in present use, a consideration of the possible mathematical modeling of fume incineration systems, and a review of the performance parameters associated with the various components of an afterburner.

SECTION 2

REVIEW OF DIRECT FLAME AFTERBURNER SYSTEMS

An effective direct flame afterburner provides (a) contact between the contaminants in the air and the burner flame, (b) time for the combustion process to be completed, (c) sufficiently high temperature for the complete oxidation of the combustibles, and (d) flow patterns that ensure adequate mixing while preventing excessive quenching. (It is common for legislation or regulations to prescribe a pair of fixed values, such as 0.3 sec for "b" and 1300 F for "c", without regard to type of pollutant. The analysis in Reference 8 shows this is not an adequate approach.) To do this, the contaminated gases are delivered to the afterburner where they are mixed with the burner flame or flames in the upstream part of the unit, normally a refractory-lined chamber. They then pass through the remainder of the chamber, where the combustion process is completed prior to discharge to the atmosphere. Figure 1 is a sketch of a typical fume afterburner using a mixing plate or grid burner. An array of line burners, multijet burner, a nozzle-mix burner, or a premix burner could be used in the same general location. Variations on the recuperator from no recuperator to more extensive ones can also be made. A catalytic afterburner would have the catalyst section inserted at the downstream end of the combustion chamber, and the combustion chamber would not run as hot, thus saving on the required amount of supplemental fuel.

In the following discussion, emphasis is placed on three areas important to the turbulence mixing process, namely, the burner, the approach section to the burner, and the combustion chamber. (Much of this discussion is based on material in Reference 9. Many of the associated figures are also based on figures in Reference 9.) The aim at this point is not to consider the details of mixing, but the generic types of components that enter into these portions of an afterburner system.

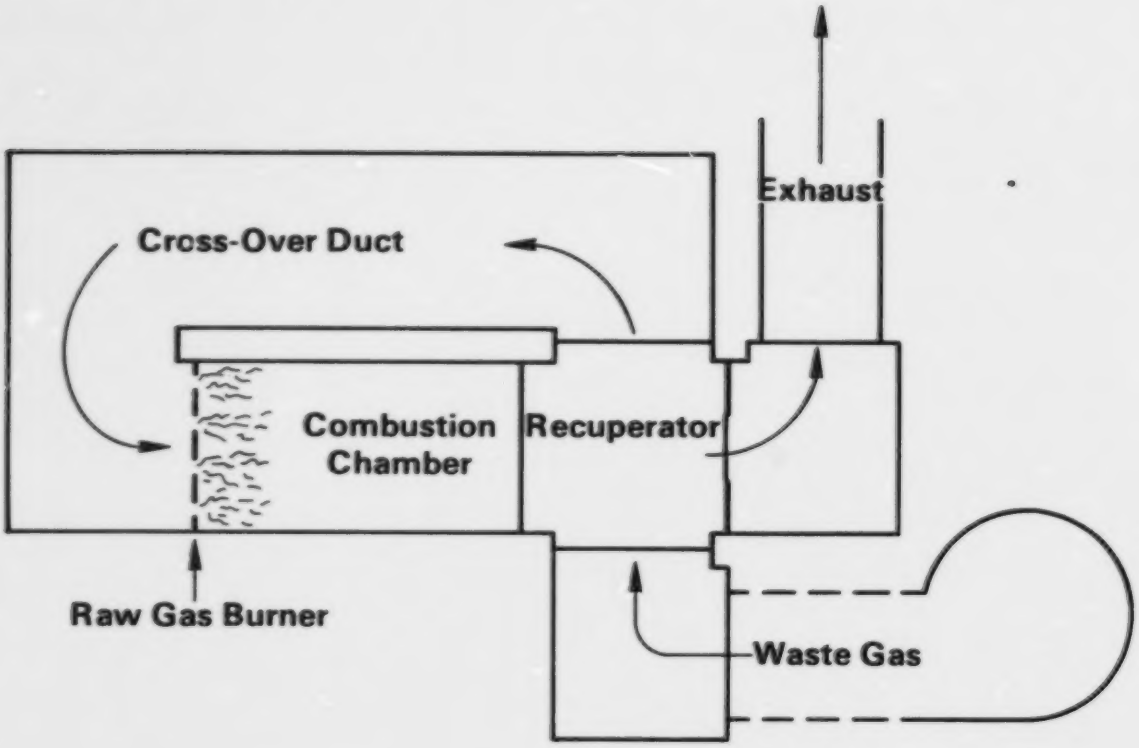

FIGURE 1. FUME AFTERBURNER WITH MIXING-PLATE BURNER AND RECUPERATOR

BURNERS

In the usual type of fume incinerating afterburner, the aim is to use a burner that will permit the minimizing of the auxiliary fuel requirements while permitting the complete mixing of the main body of fume pollutant air with the burner products without quenching the reaction. A multitude of classical burner designs permit the achieving of this goal, with no clear-cut advantage in cost and performance. As a result, various builders of afterburner incinerators have used or adapted their particular burner designs in the development of this new product.

In this treatment, six general types of gas burner arrays are distinguished, 1) line burners, 2) multijet burners, 3) ring burners, 4) grid or plate burners, 5) distributed source burners, and 6) discrete source burners. Three different types of gas-burner mixing systems are also distinguished, premix, delay mix, and nozzle mix. These nine items are discussed below, in turn.

Line Burners

Line burners, along with multijet burners and grid burners, are distinguished by being an array of components, and being confined to a rather narrow cross-section in the afterburner system. Because these are composed of a multiplicity of elements, their performance may be analyzed on the basis of a single component, with the properly chosen boundary conditions.

Figure 2 shows three 6-in. elements of a Maxon line burner. For larger areas, these elements plus cross elements are used to build up an open grid pattern. Then profile plates are added to block part of the remaining open area, and thus to balance off the air flow between burner elements and intraspaces. It is seen that intimate mixing of the primary air with the fuel takes place. The secondary air is then aspirated into the flame from a slot along the burner element. There also have to be large recirculation patterns behind the profile plates. It is clear that the time-temperature history will vary with flow path.

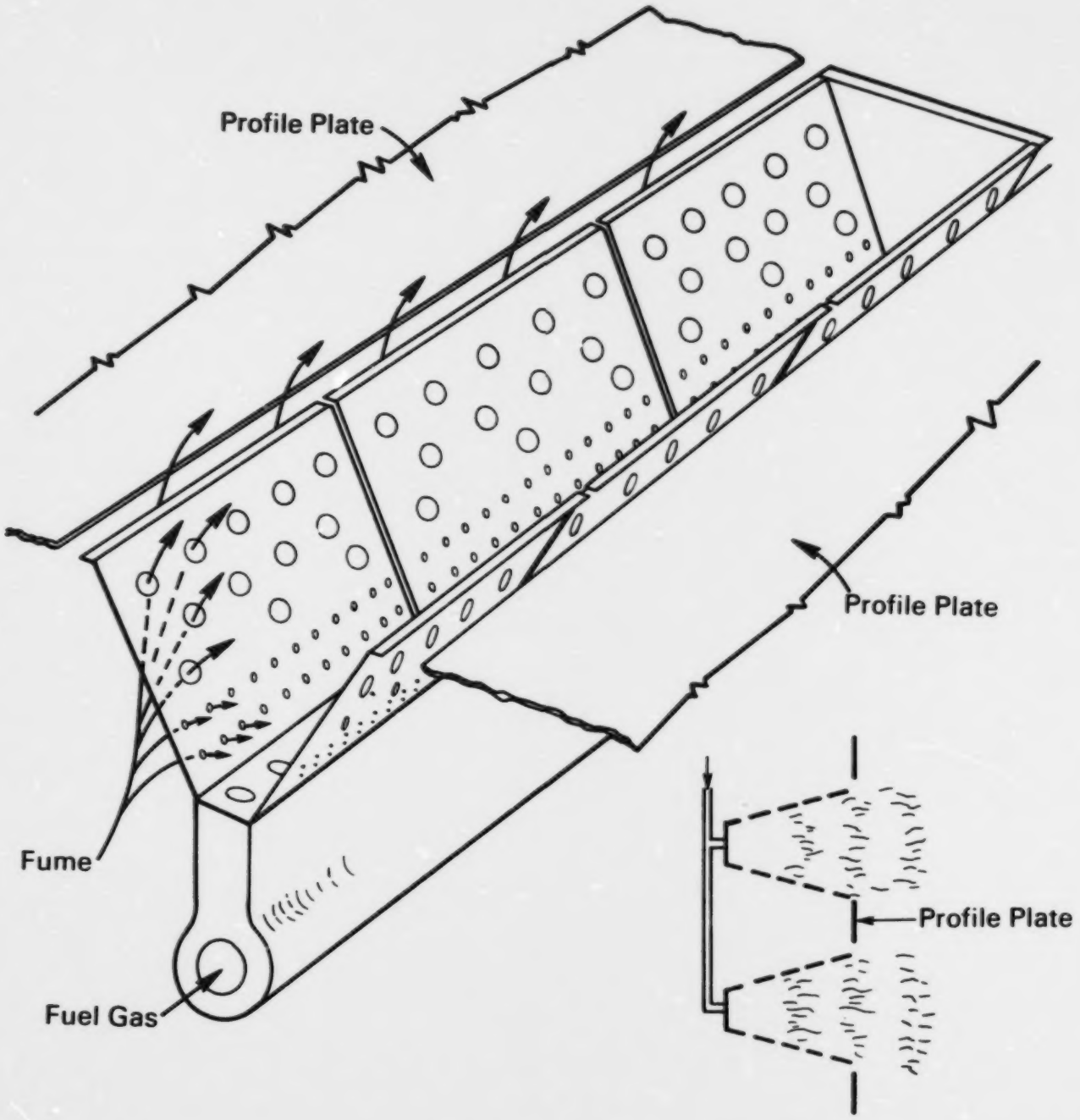

FIGURE 2. MAXON LINE GAS BURNER WITH PROFILE PLATES

Multijet Burners

Figure 3 shows a typical multijet burner. Small individual raw gas burners aspirate the required amount of fume-polluted primary air to burn as individual flames. An array of these burners (16 in figure) is then placed in the combustion duct, with the remaining fume-polluted secondary air bypassing the burner array and mixing downstream with the products of combustion. A problem with this system is ensuring adequate mixing downstream.

Ring Burners

Figure 4 shows two raw gas ring burners; the Midland-Ross unit is used in a stack afterburner. In this unit, the raw gas is impinged on a rod to improve mixing and stabilize the flames, as indicated in the accompanying sketch (for a somewhat different design). In the John Zink unit, a ledge is used to impact the gas, stabilize the flames, and increase the rate of mixing. There is no sharp demarcation of primary air and secondary air such as there is in the multijet burner. However, the concept of multiple individual flames is the same.

Grid Burner

Figure 5 shows a typical grid burner. A series of fuel ducts support the open grid with oblong holes (about 1 in. x 3 in.). Drilled ports permit the raw gas to exit at a low Reynolds' number into the blockage region between the holes. A certain amount of air is aspirated into the recirculation region to burn with the fuel. Further fuel combustion may take place immediately downstream, followed by spreading of the flame through the remainder of the fume-contaminated air.

The grid is intended to cover the entire cross section of the combustion duct.

Distributed Source Burners

The distributed source burner is quite similar to the multijet burner (Fig. 3). However, the burners act independently and the flames are separated by the fume polluted gases moving between the burners. Figure 6a shows one example of the type of array. Figure 6b shows a second arrangement of burners. The burners may be either nozzle mix, delayed mix, or premix in type (see below).

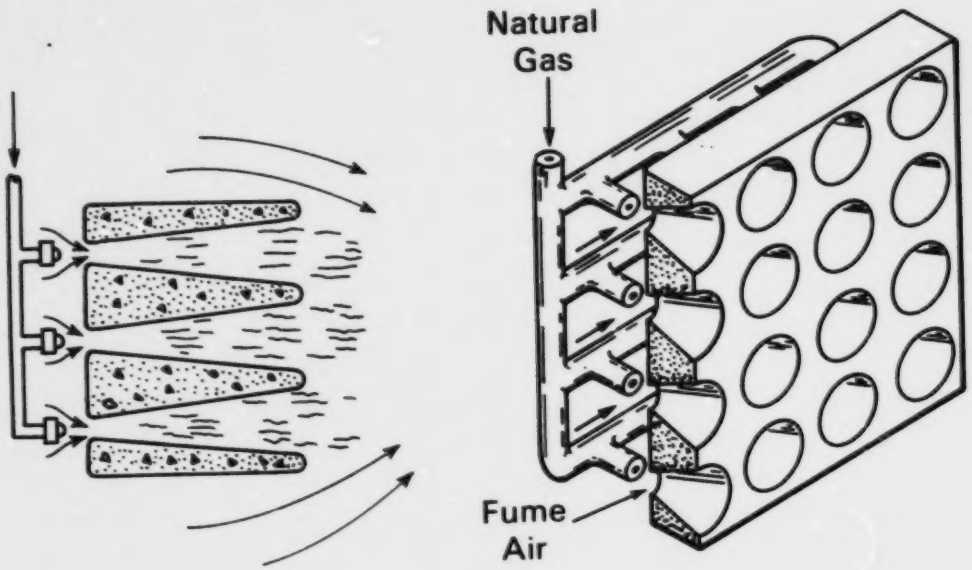

FIGURE 3. HIRT MULTIJET GAS BURNER

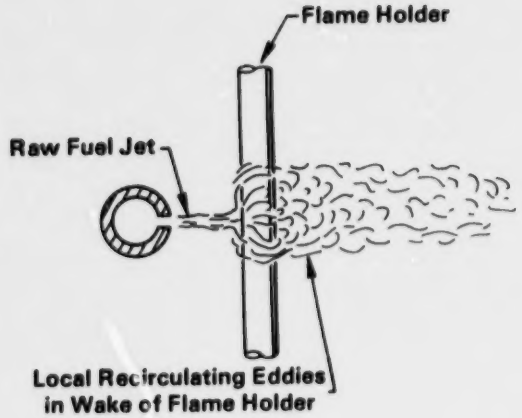

(a) Detail

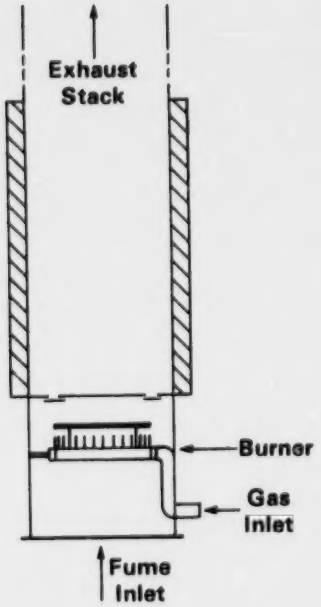

(b) Midland Ross

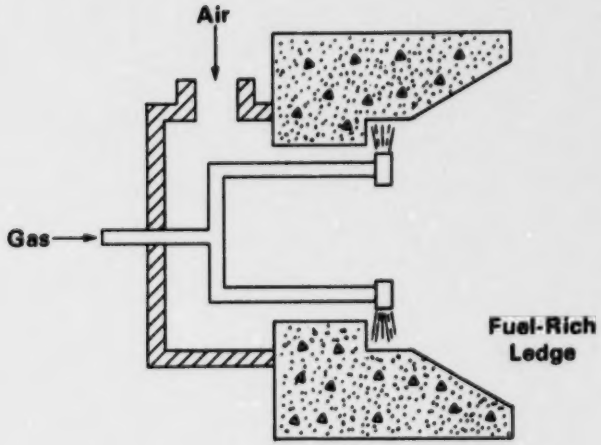

(c) John Zink

FIGURE 4. RING BURNERS

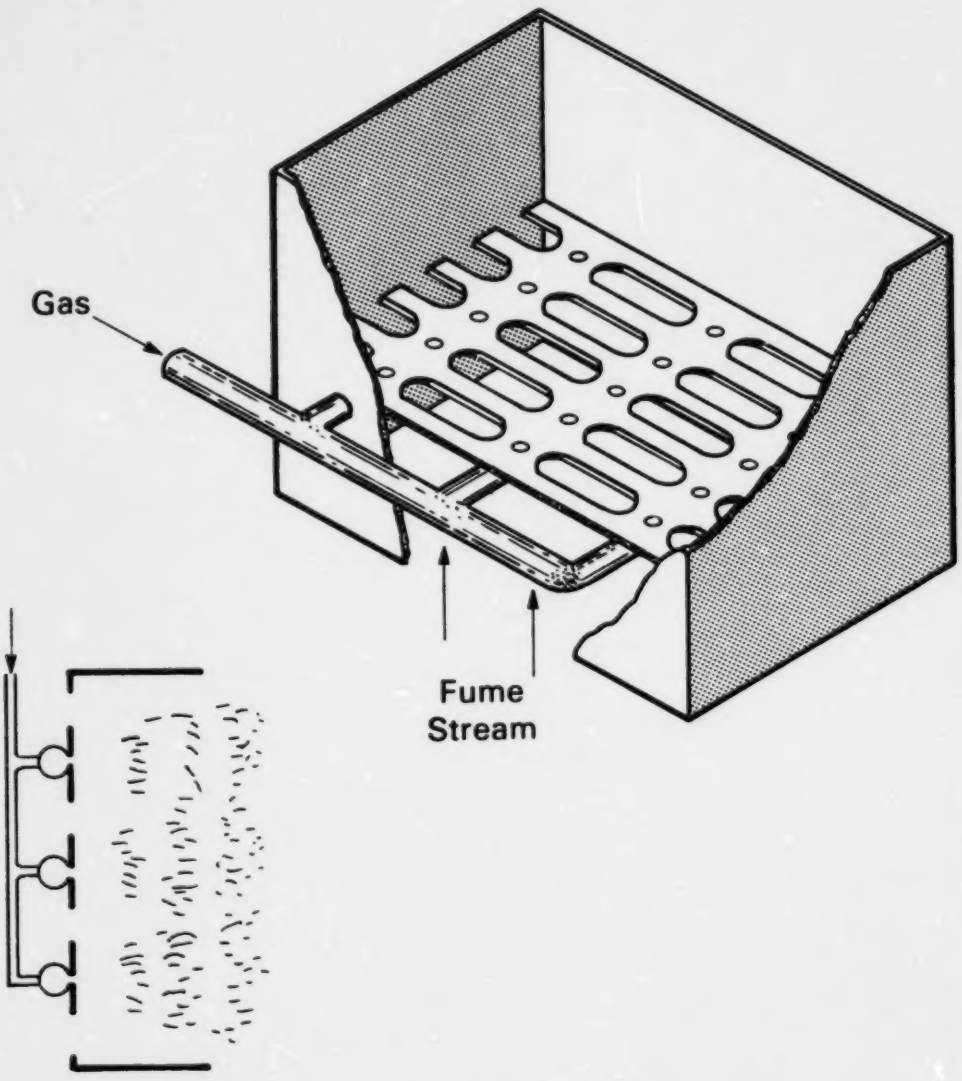

FIGURE 5. NORTH AMERICAN FLAME GRID BURNER

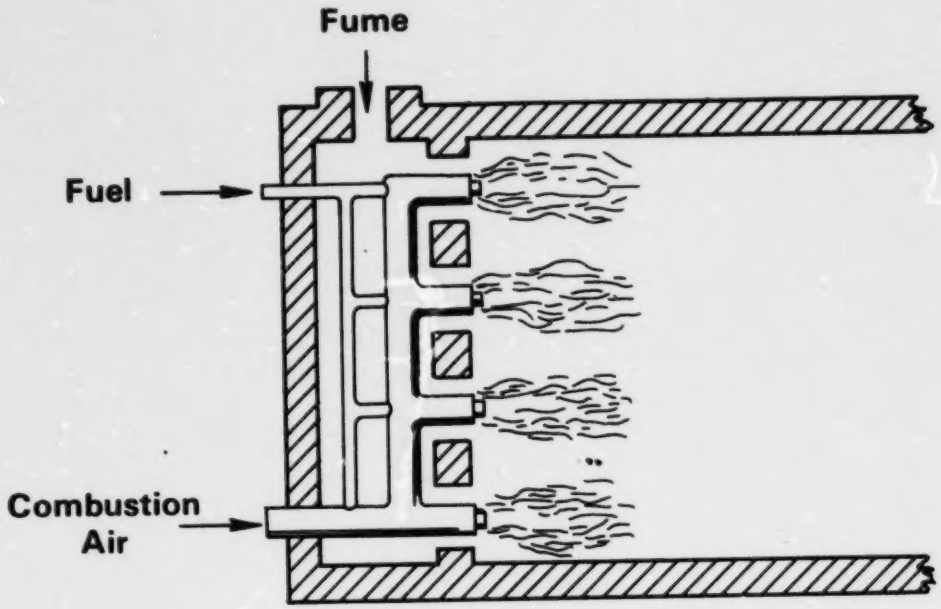

(a) Parallel Flow

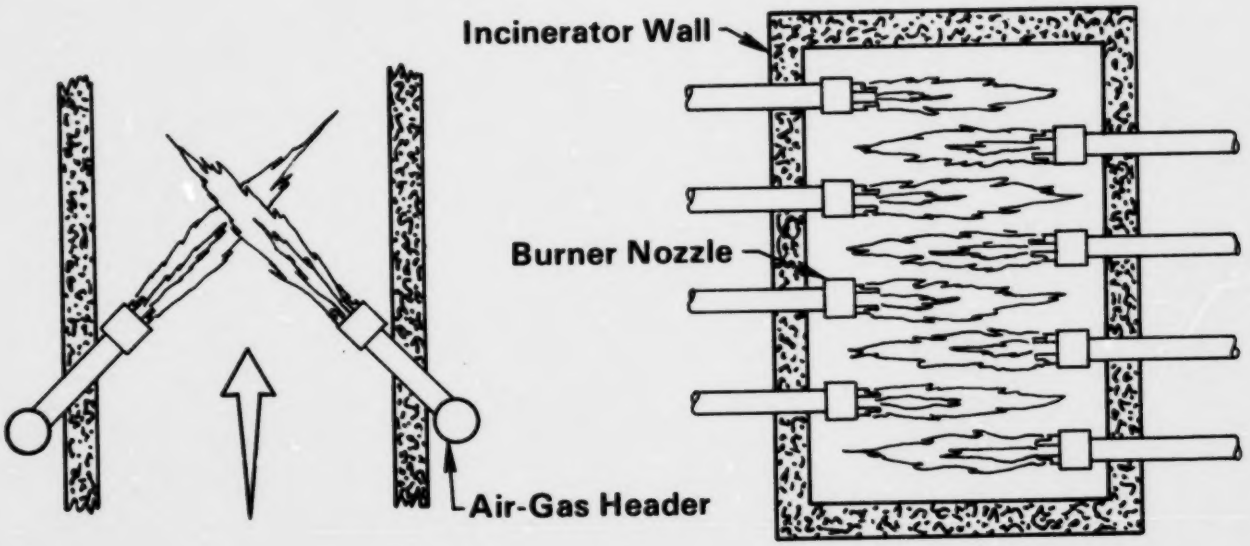

(b) Cross Flow

FIGURE 6. DISTRIBUTED-SOURCE BURNER

Discrete Source Burners

Two discrete source burners are shown in Figure 7. While the burner may be more economical to build and control, the mixing problem is obviously increased as compared to a multiple source system with interspace for the secondary polluted air to come through. In addition to the end wall position shown here, the sources may be directed in from a side wall, toward the axis or with some tangential component (producing swirl).

Premix Burners

A premix burner is defined as a burner in which the gas and air have been previously mixed, or a burner in which the gas and air are mixed before they reach the nozzle.

In a premix burner, the premixed fuel and air are usually supplied to the region from an inspirator or Venturi mixer, an aspirator or suction-type mixer, or a fan mixer. The burner may be a small port or ported manifold type, a large port (or pressure type), a tunnel burner, or a flame-retention type burner, in which some of the combustible mixture is slowed down and diverted into an annular combustion region. The flame in the protected annular region acts as a pilot to maintain or hold the main flame. In closed systems (such as tunnel burners), steps, recesses, grids, and other obstaclles are often used to hold the flame. These form protected recirculation zones, which hold the flame and from which the flame spreads. Figure 8a might be used singly in a large size, such as with a flame distirbuter in Figure 8b, or as a multiple set in a pattern similar to Figure 6. Figure 9 shows another version of the premix burner, in which one mixing chamber supplies a multiple set of ports. This burner is similar in concept to the ones used in many residential gas-fired heating units.

Delayed-Mixing Burners

Delayed mixing burners as those in which the fuel and air leave the burner nozzle unmixed and thereafter mix relatively slowly, largely through diffusion. This results in a long luminous flame called a diffusion flame, luminous flame, a long flame. Figure 10 shows one example of such burners. Because of their slow mixing, they are not used as discrete sources in fume afterburners. In smaller sizes as a distributed source, as in Figure 6a, they may be used.

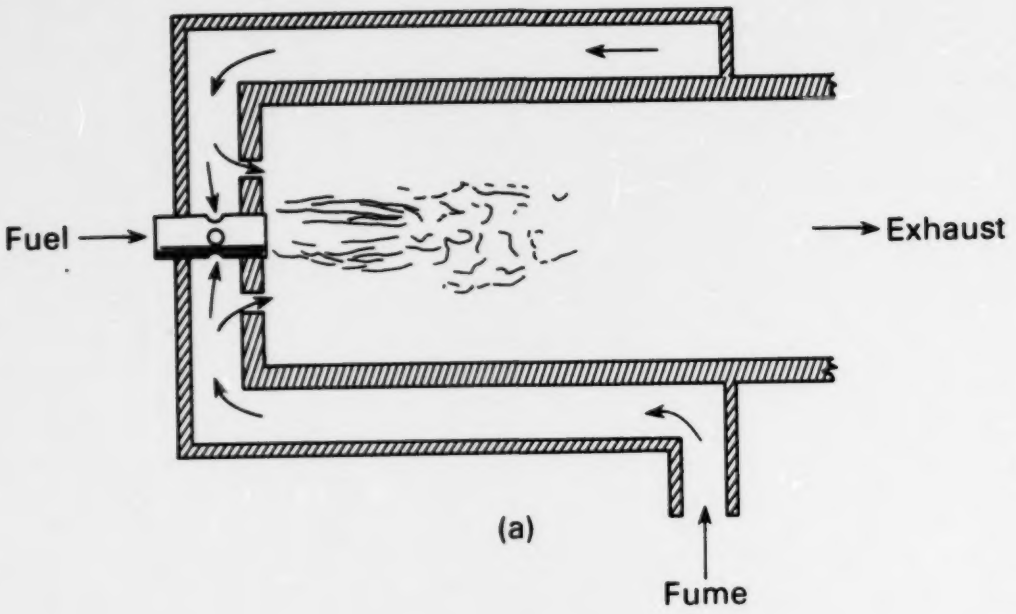

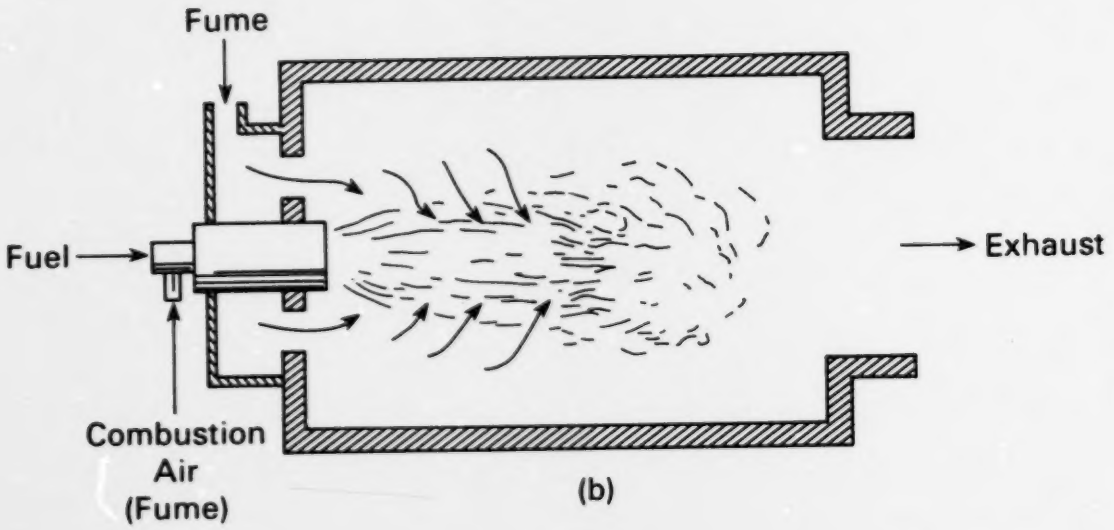

FIGURE 7. DISCRETE-SOURCE BURNERS

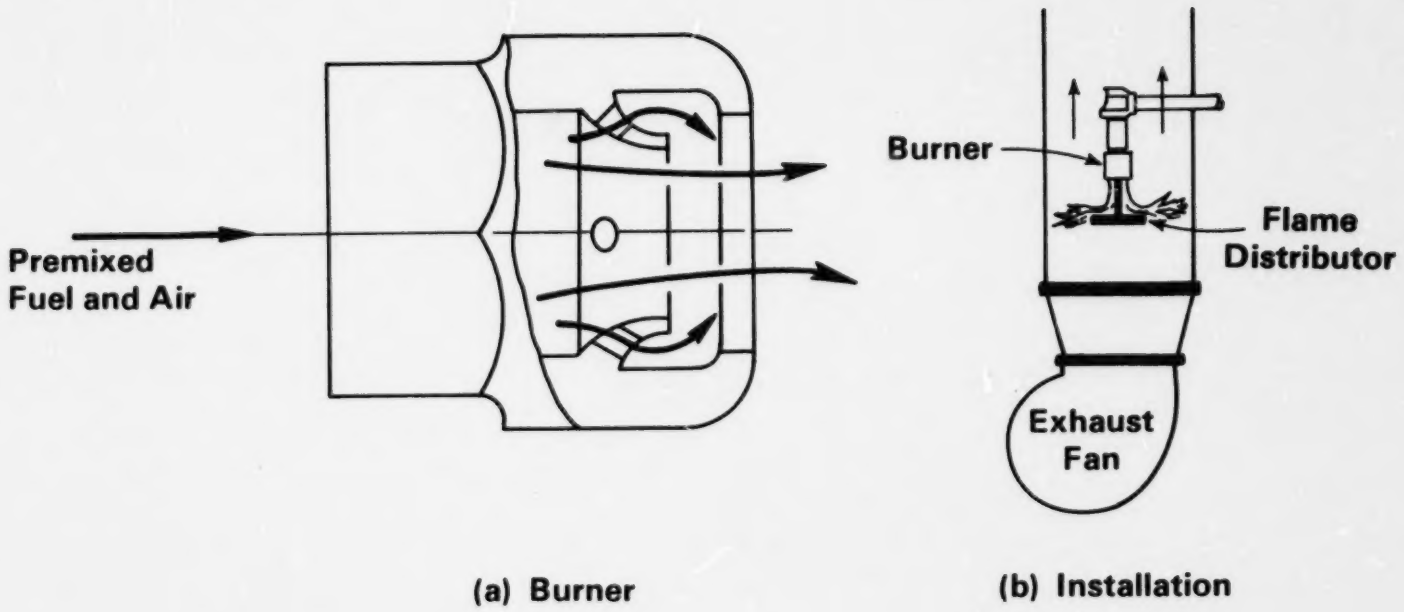

FIGURE 8. FLAME RETENTION TYPE PREMIX BURNER AND ONE DISCRETE SOURCE USE.

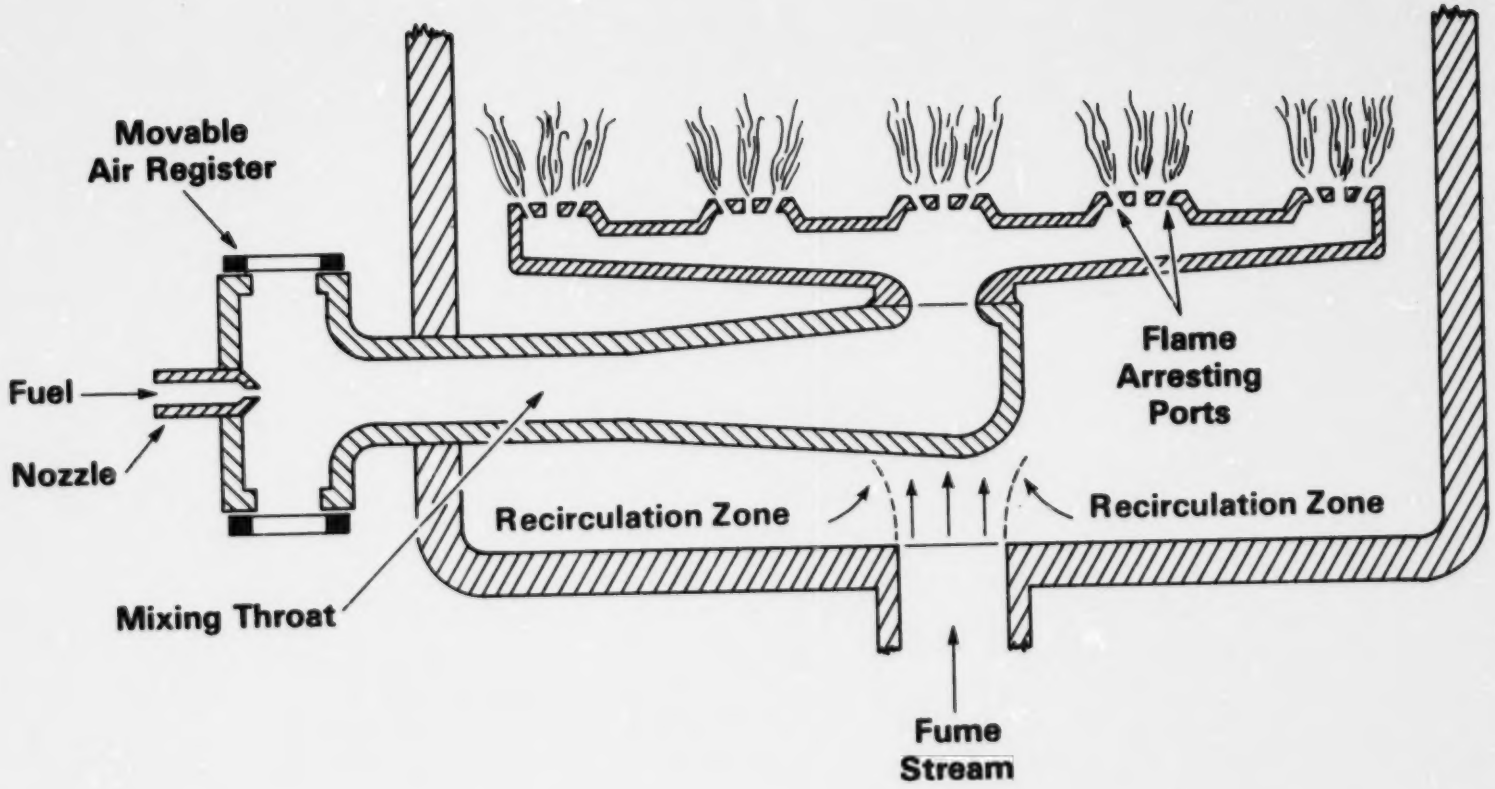

FIGURE 9. MULTIPLE PORT PREMIX BURNER

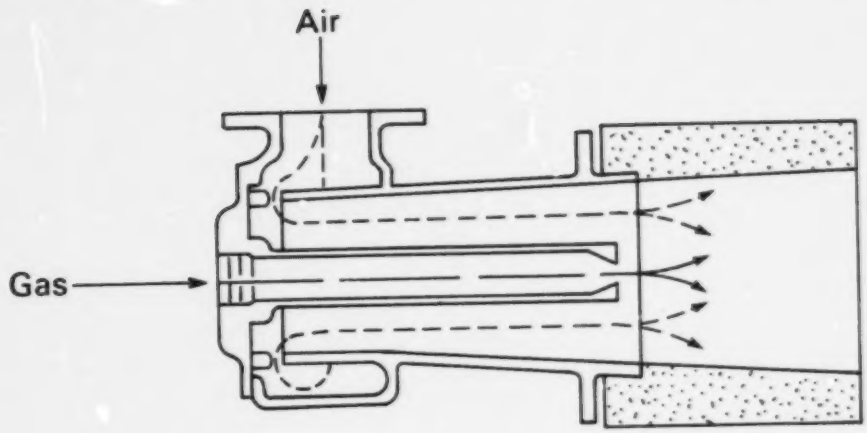

FIGURE 10. DELAYED MIXING BURNERS

Nozzle-Mix Burners

A nozzle-mix burner is one in which fuel and air are not mixed until just as they leave the burner port, after which mixing is usually very rapid. The flame cannot flashback in this type of burner. Nozzle-mix burners combine the advantage of the relatively short flame of the premix burner and the lack of flashback problems of the diffusion flame. The short flames are obtained by three different methods. Figure 11a shows the use of multiple high-velocity air jets parallel with the fuel jet. The air jets aspirate the fuel in around them and form short flames because of the small jet diameter and potential core length. Figure 11b shows the use of nonparallel jets. These may impinge, may interlace (with multiple fuel jets as well as air jets), or may be canted to produce a swirl flame and even a heavy recirculation zone on the burner axis. Figure 11c shows a burner similar in spirit to the Maxon line burner (Figure 2). Again, the air is mixed rapidly with the fuel, following which the highly turbulent product jet aspirates the remaining fume-polluted air into itself.

Nozzle-mix burners with large variation in the degree of swirl are available. Reed[10] presents the classification of flame types in Figure 12. He also notes that "swirl improves flame stability by forming toroidal recirculation zones that recirculate heat and active chemical species to the base of the flame and thereby broadens the range of velocities in which flame stabilization is possible. These toroidal zones form when the swirl number is greater than 0.6. Swirl number, S, is defined as the ratio of axial flux of angular momentum to the product of radius and axial flux of linear momentum, where the radius is that of the exit port. Swirl has two additional benefits--it shortens combustion time by causing high rates of entrainment of ambient fluids, and it provides quick mixing in the vicinity of the burner nose and along the boundaries of recirculation zones."

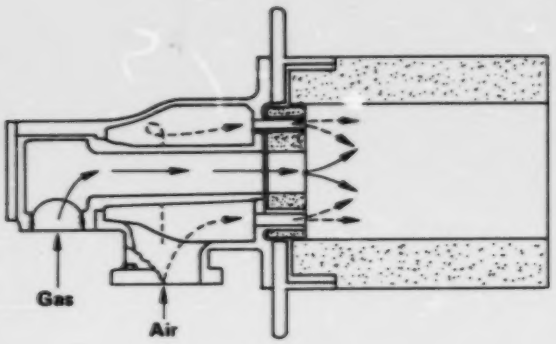

(a) North American 2236 Gas Burner

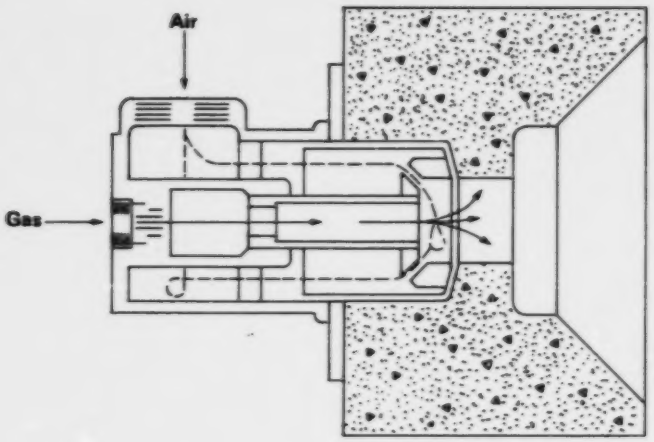

(b) Bloom HTR Gas Burner

(c) UOP Raw Gas Burner

FIGURE 11. NOZZLE-MIXING BURNERS

Type		Flame description	Swirl	Recirculation	Jet description[C]	Mixing rate
1†		Conventional forward flame	none, or weak in center only	little or none	axial	moderate
2†		"Headpin" flame	some	between pri and sec jets	pri jet penetrates internal reverse flow pri jet vel>sec jet vel	moderate
3†		Ball of flame	considerable, S>0.6	hot reverse flow into center	sec jet vel>pri jet vel	intense
4		Conical flame	high, S>1	cold reverse flow into center	sec jet vel>>pri jet vel	intense
5		Coanda burner flame	very high	minimal	radial or swirled flow contained by a refractory shape	fast
6	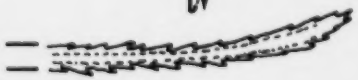	Long, luminous, lazy flame	none	none	fuel jet vel and air jet vel equally low (laminar)—bouyancy controlled	delayed, slow, diffusion
7	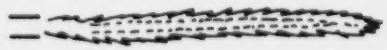	Long luminous "fire hose" flame	none	none	fuel[□] jet vel>>air jet vel—thrust controlled	delayed
8	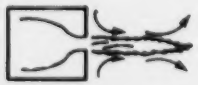	High velocity	low	small scale internally, large scale externally	flow contained by refractory shape—burning inside and outside tile	fast

[C] pri = primary—refers to central jet.
sec = secondary—refers to outer jet.
†Type numbers 1, 2, and 3 were established by the International Flame Research Center of Ijmuiden, Netherlands. Type 3 corresponds to Type B and 5 to C in Reference 51.
[□] Or fuel and atomizing medium.

FIGURE 12. COMMON INDUSTRIAL FLAME TYPES

COMBUSTION CHAMBER

The purpose of the combustion chamber in a fume afterburner is to provide the necessary time and temperature to consume the pollutants uniformly. With perfect mixing of the secondary polluted air with the products of combustion of the fuel and the primary polluted air, a simple plug flow system would minimize the combustion chamber size. Because of various economic and constructional considerations, type of pollutants and variability of supply rates, necessity of turn-down capacity, and other problems, this perfect situation does not exist. Thus there are departures from the ideal solution. In this section, examples of the various types of combustion chambers encountered in practice are considered.

Simple Combustion Chambers

The simplest combustion system is the rectangular or the cylindrical duct. Figure 13 shows such systems using a distributed source burner in one case, and a discrete source burner in the second case. With the distributed source, the ideal plug flow situation is well approximated on a gross scale. With the discrete source, consideration has to be given to the effect of the discrete jet. Figure 14 presents three examples of jet-induced flow patterns using a discrete source. In Figure 14a, the blockage around the entrance results in a recirculation zone with a length of the same order of magnitude as the width. When intense swirl is added, a central recirculation zone is added to the flow pattern. The third example shows that even if there is no blockage, but just a slow velocity uniform stream surrounding a high velocity jet (as from a burner), a recirculation zone can be set up. These recirculation zones may be helpful in moving hot products of combustion upstream where they can act to ignite the fresh mixture. On the other hand, they can take up space that adds nothing to the needed reaction time.

Combustion Chamber With Symmetric Baffling

Figure 15 shows two examples of combustion chambers with symmetric baffles. These chambers may be circular, or square with baffles on all sides, or rectangular with baffles on two opposite sides. It is not obvious that they necessarily lead to the desired degree of mixing; an annulus of unreacted fume-air mixture could pass through the entire combustion chamber of improper design.

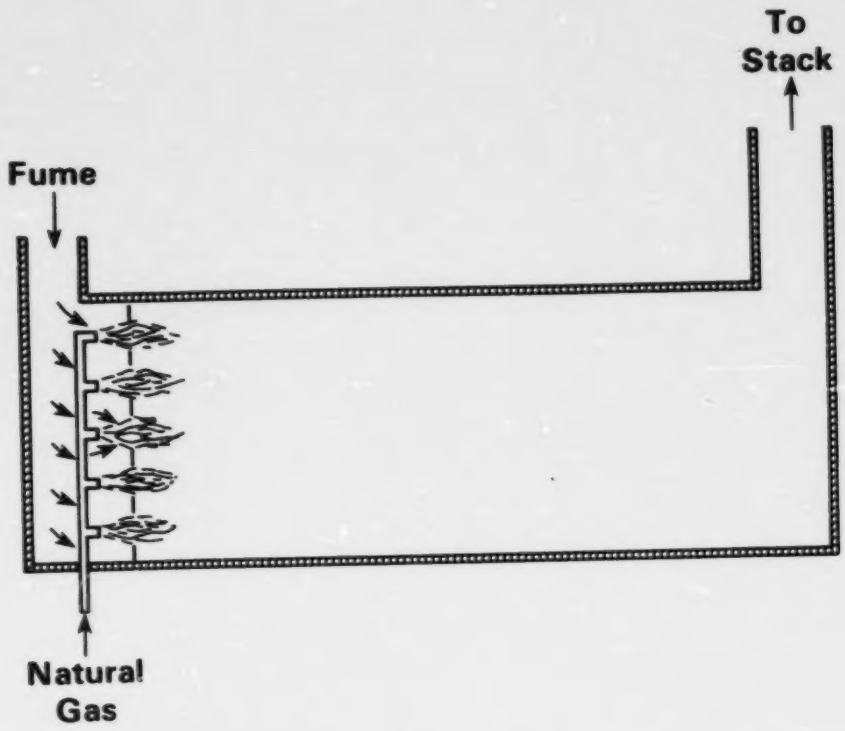

(a) Afterburner With Distributed Burner

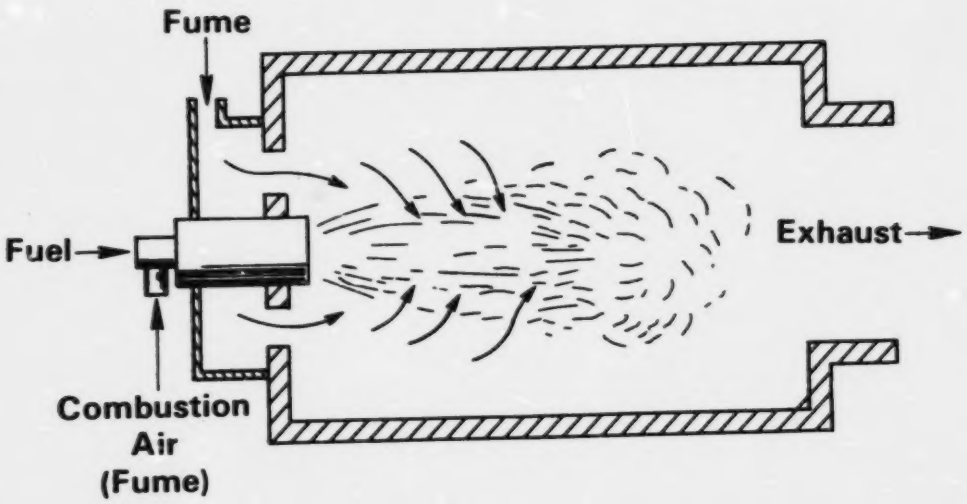

(b) Afterburner Using a Discrete Burner

FIGURE 13. SIMPLE AFTERBURNER COMBUSTION CHAMBER SHAPES

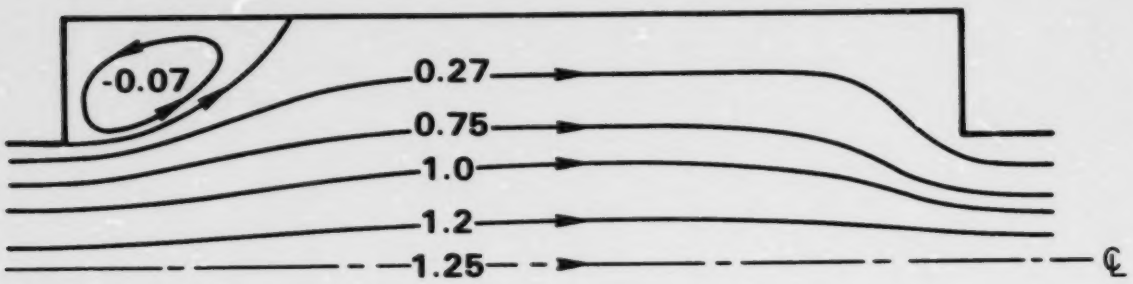

(a) Low Swirl

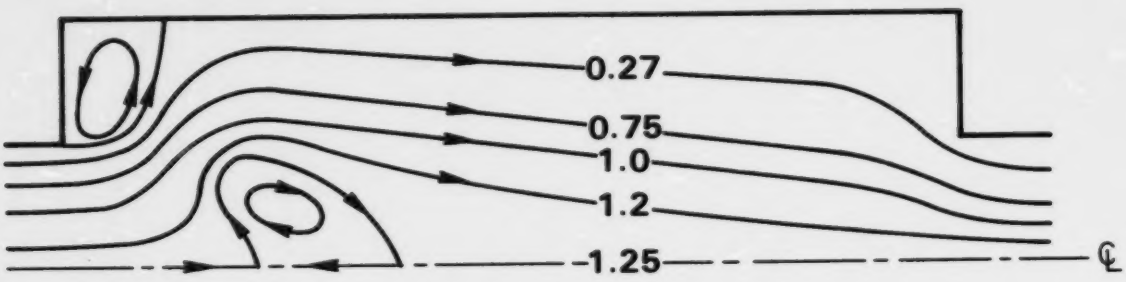

(b) High Swirl

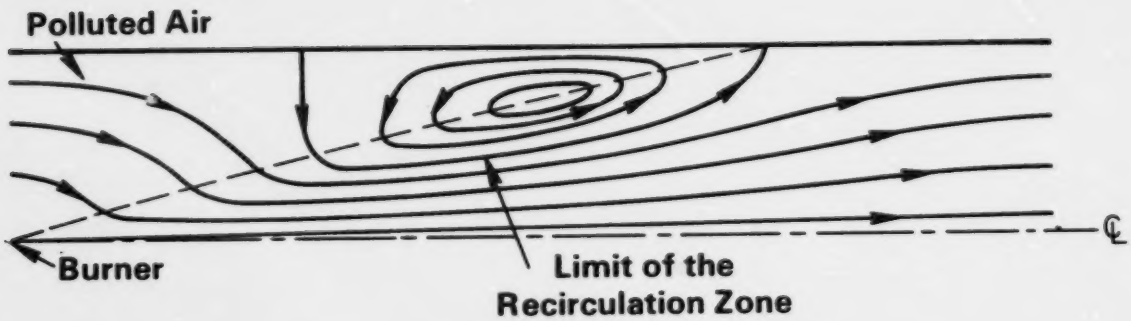

(c) Uniform Low Velocity at Entrance

FIGURE 14. FLOW PATTERNS IN COMBUSTION CHAMBER OF UNIFORM DIAMETER

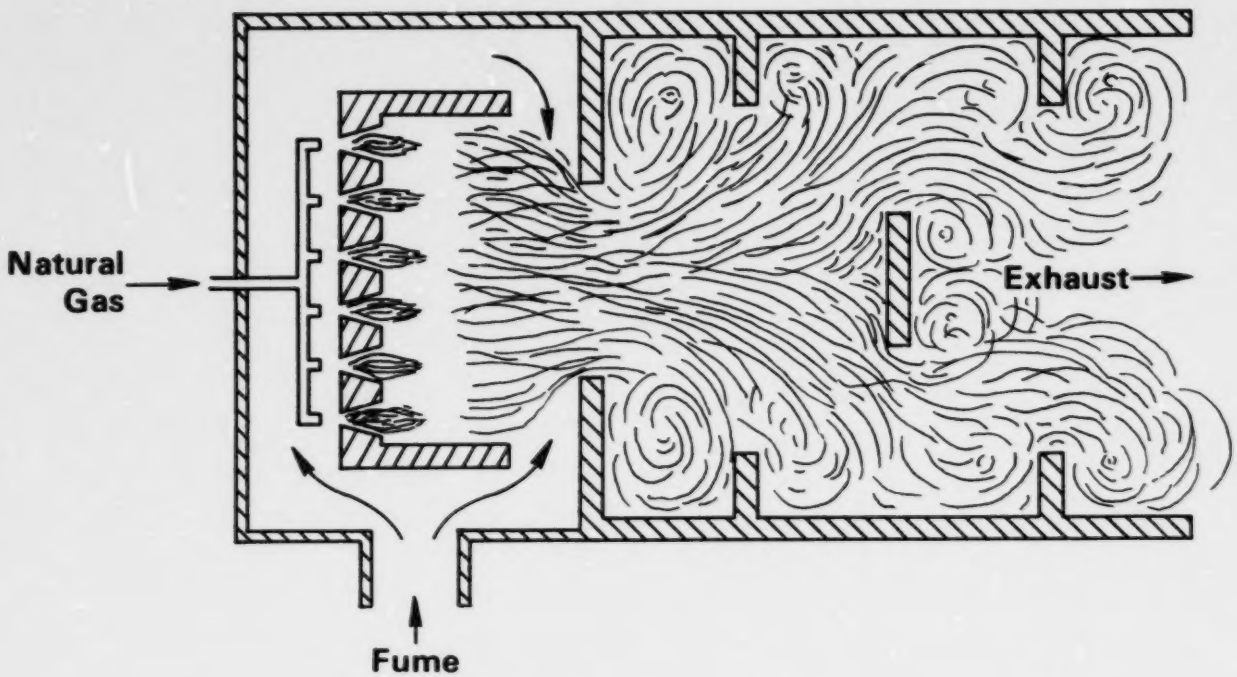

(a) Multiple Jet Gas Burner

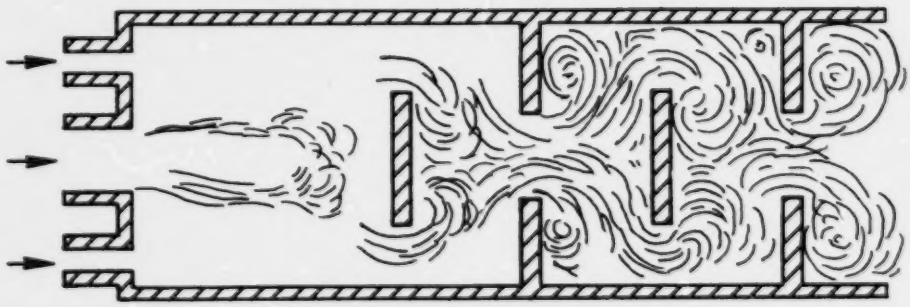

(b) Discrete Gas Burner

FIGURE 15. SYMMETRIC BAFFLE SYSTEMS

Combustion Chamber With Asymmetric Baffles

Rectangular combustion chambers can have one or more bridge walls to mix the products of combustion and the fume-laden air. The gross flow patterns are simple to deduce when zero swirl burners are used. When a high swirl burner is used, the presence of the swirl induces further mixing, as shown in Figure 16b.

Side-Fired Burners

Figure 17 shows the possible arrangements for side firing a combustor chamber. In Figure 17a, the gas (or products of combustion) is fired tangentially into the chamber, resulting in flame impingement on the wall and rapid mixing. There may be single or multiple recirculation annuli, depending on the end conditions of the chamber. Figure 17c shows how the tangential entrance of the combustion products induces swirl into the fume air. In the case of Figure 17b, the gases impinge on the opposite wall, and spread in both directions. No net swirl is present. Variations of this can have multiple entrances, as in Figure 17d.

Figure 18 shows a variation on the swirl theme suggested by Rolke, et al.[9]. Each diagonal pair of fume entrances result in a vortex.

Compact Combustion Chamber

Figure 19 shows a combustion chamber in which the flow is turned 180° to result in a compact recuperator-combustor system. With the distributed combustion, the arrangement does not cause any segregation problems. However, as shown in Figure 20, this 180° turn can result in a reduction in effective residence time. The same results follow for a configuration with a 90° turn. If a multiple burner or a discrete source burner were used, the abrupt turn can cause an additional problem in obtaining uniform combustion of the fumes.

Regenerative Fume Incinerator

Figure 21 shows a fume incinerator with a regenerative system for heat recovery rather than a recuperator system. With the direct cross flow of the fume containing gas it is clear that the problem is to ensure good mixing with the combustion products of the burner in the short path available.

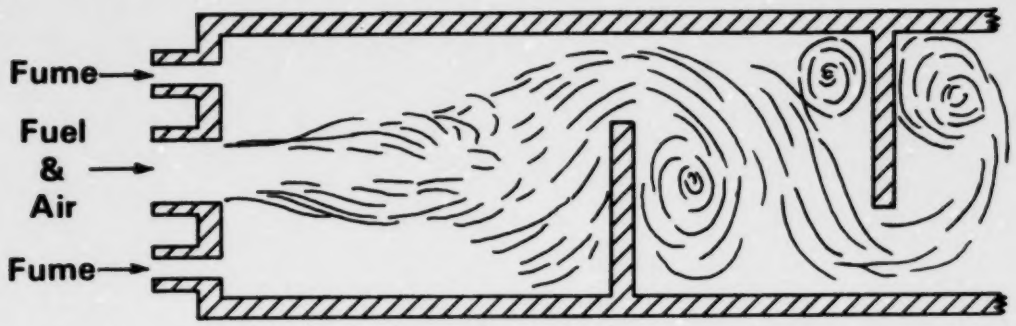

(a) Non-Swirl Burner

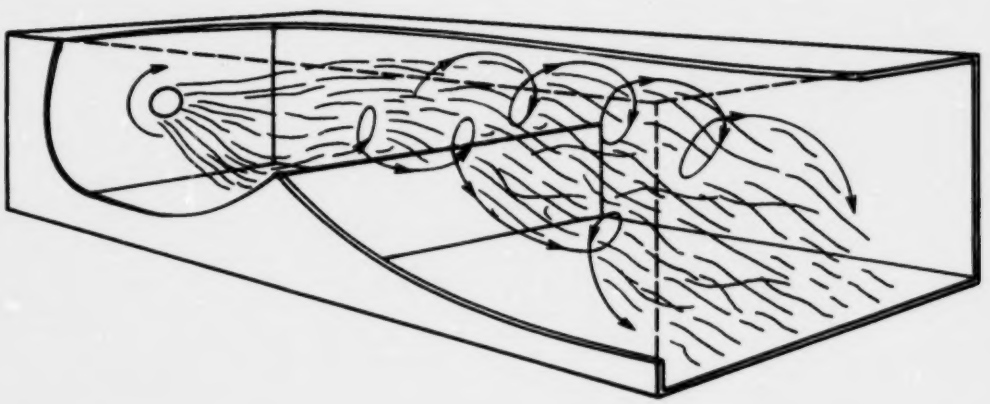

(b) Swirl Burner

FIGURE 16. COMBUSTION CHAMBERS WITH BRIDGE WALL BAFFLES

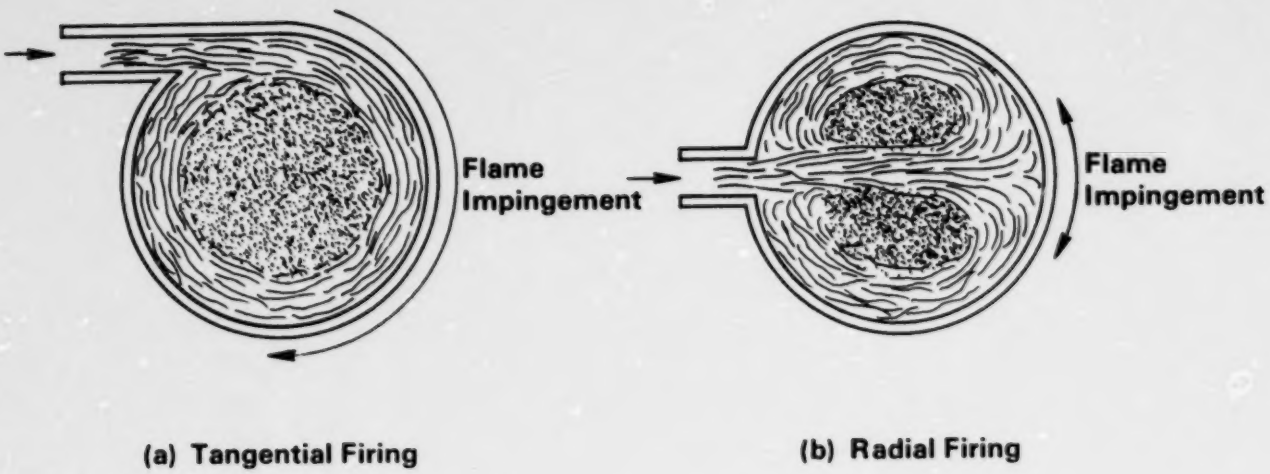

(a) Tangential Firing

(b) Radial Firing

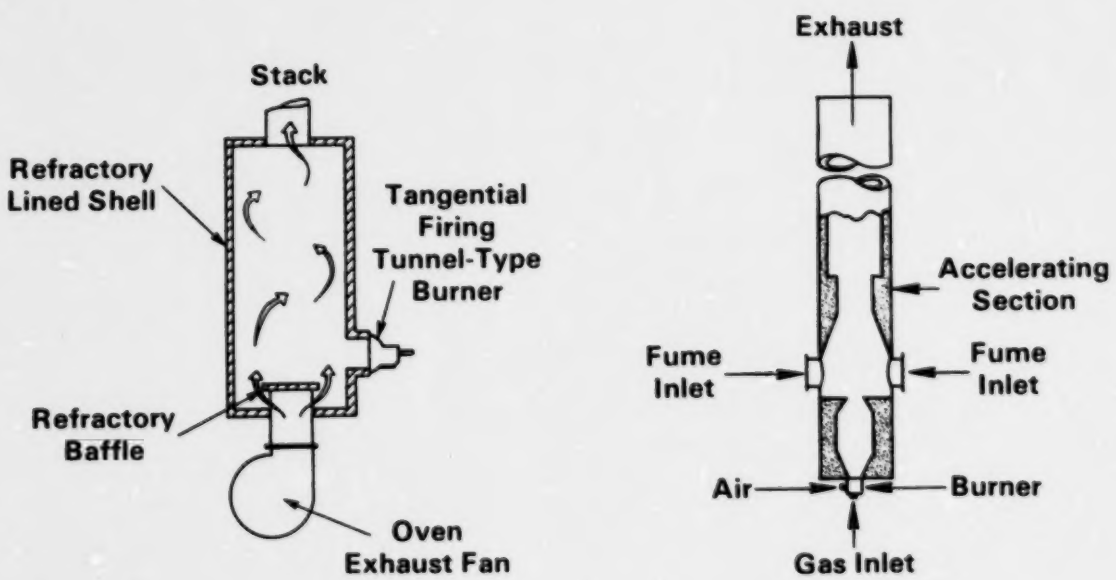

(c) Waste Gas Incinerator

(d) Jet Incinerator

FIGURE 17. COMBUSTION CHAMBER WITH SIDE FIRING

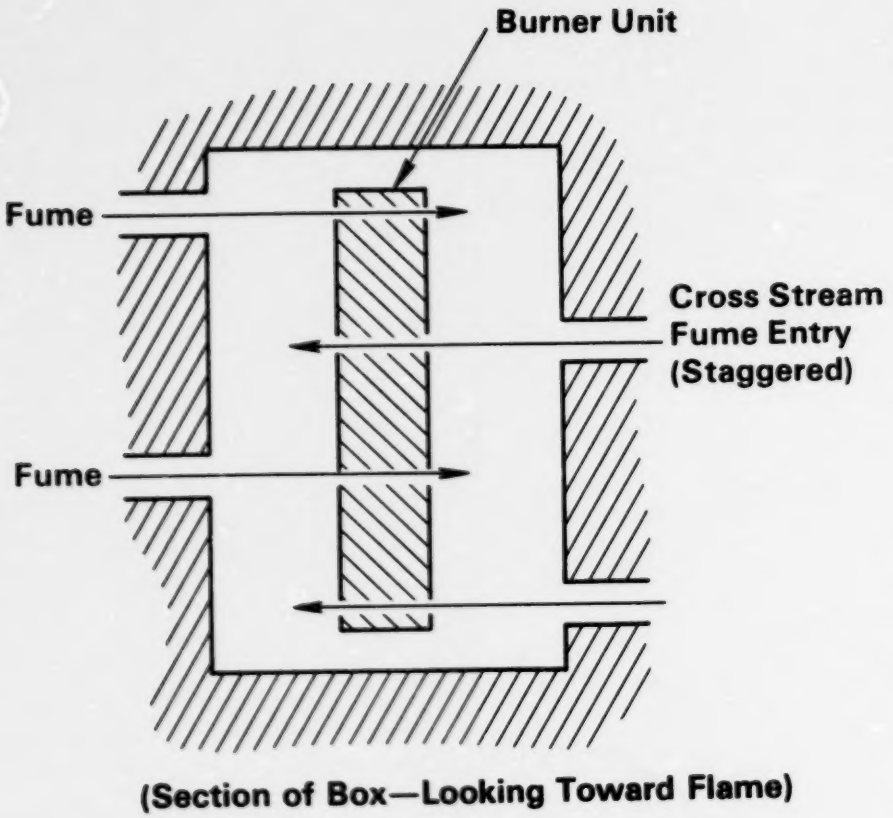

FIGURE 18. SUGGESTED ARRANGEMENTS FOR CROSS-STREAM MIXING OF FLAME AND FUME IN RECTANGULAR BOX

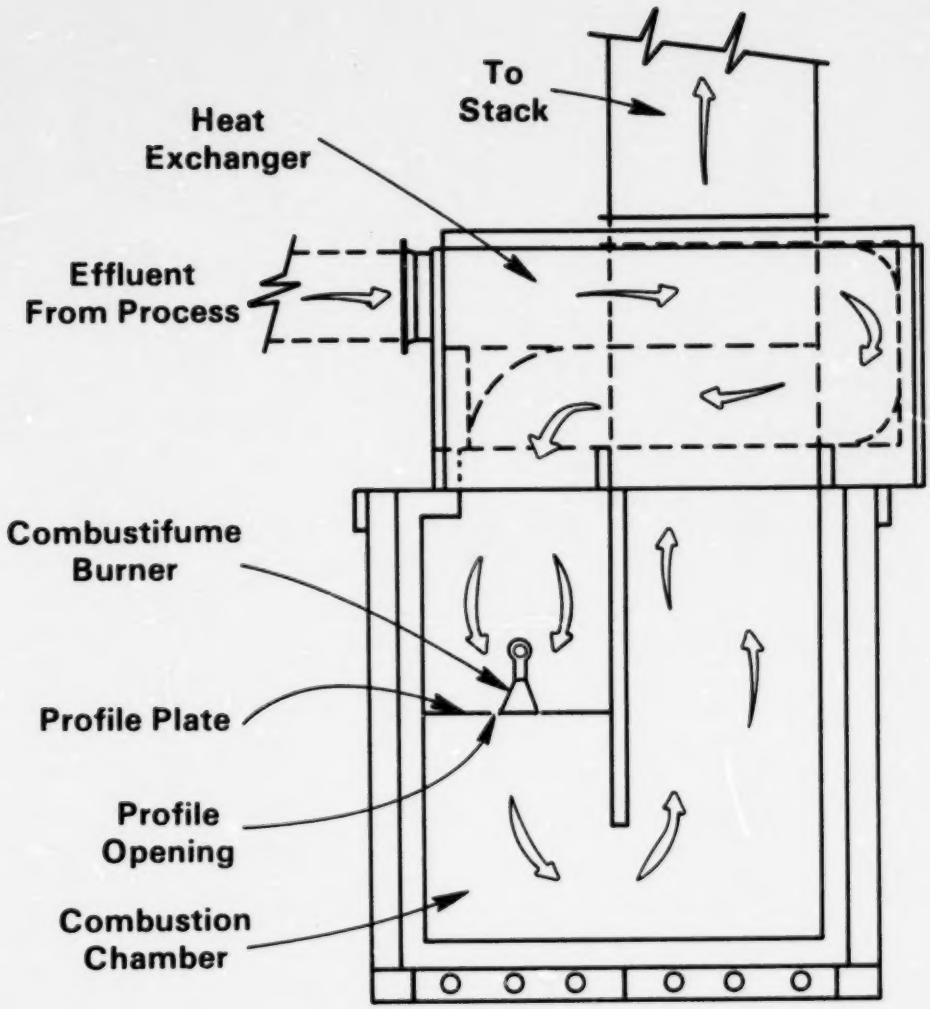

FIGURE 19. COMPACT COMBUSTION CHAMBER

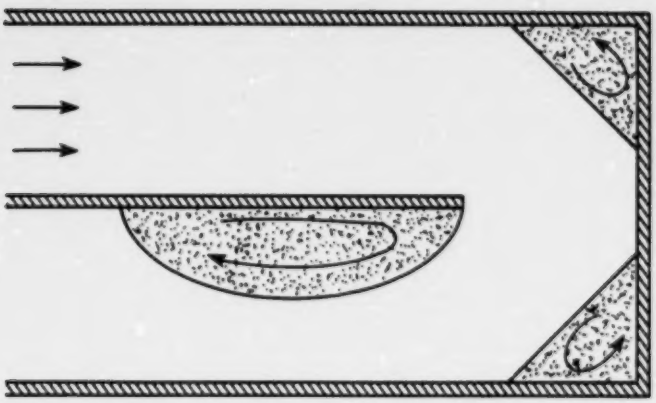

A. U Bend

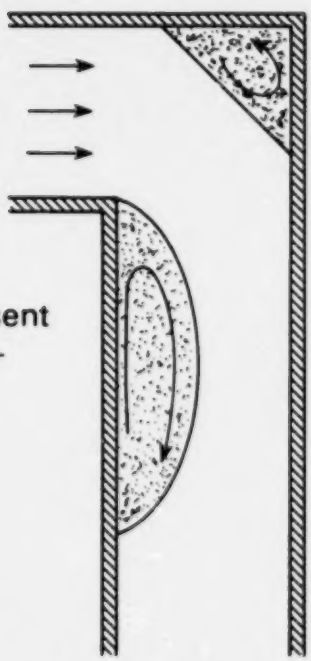

Shaded Areas Represent
Recirculating Flows—
Dead Zones

B. L Bend

FIGURE 20. RECIRCULATION REGIONS WITH 180° AND 90° TURNS

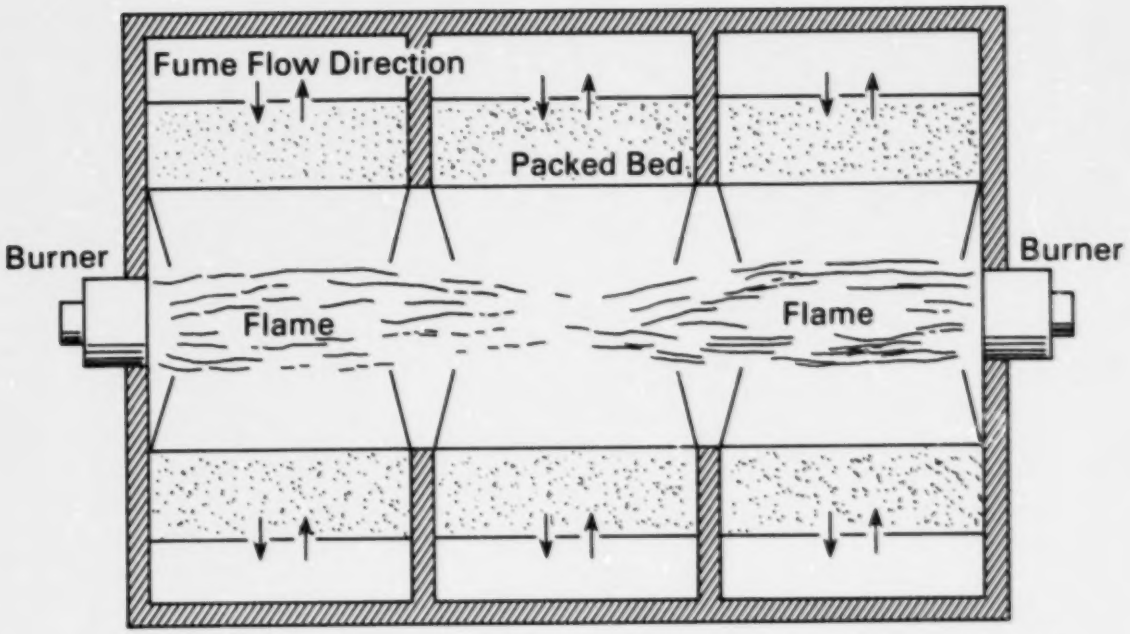

FIGURE 21. PROCTOR-SCHWARTZ SYSTEM WITH REGENERATIVE HEAT RECOVERY

Top View with Ducting Removed

APPROACH SECTION

The purpose of the approach section is merely to carry the fume contaminated air from the recuperator to the burner and combustion chamber. However, the approach section to the burner and to the combustion chamber can have a great effect on the uniformity of flow, and thus the completeness of fume combustion in a given space. Symmetric approaches such as in Figure 4b and 7a result in uniform downstream flows. On the other hand, the turn such as shown in Figure 1 can lead to severe maldistributions, as seen by comparison with Figure 20. Several of the approach sections that might result in problems are discussed below.

Slotted Duct System

Figure 22 shows an afterburner approach section with the fume-air mixture being discharged through slots into the products of combustion of a nozzle-mix burner. The multiplicity of slots with a reasonable pressure drop should remove the effects of the upstream turns, especially if the duct turns are fitted with properly designed turning vanes. However, considering the cross-sectional view, it is seen the passage to supply the fume-air mixture to the bottom three slots might be restrictive. With such a design, the flow through the top slots could be twice that through the bottom slots because of such a restriction. This could lead to a maldistribution in the end of the burner tunnel and in the combustion chamber.

We note that Figure 7a shows a variation on slot principle in which orifices supply the fume-air mixture to the burner, and then the remaining fume-air mixture is supplied to the fume combustion chamber by an annulus. Because of the symmetrical approach section is this case, however, there would be no maldistribution.

Approach With Abrupt Turn

Figures 1, 4c, 6a, 7b, and 13 show approach sections with abrupt turns. This may not be a problem with the distributed sources and high pressure drops of Figure 1, 6a, and 13a. Considering the flow pattern shown in 20b, however, one can see that there could be a severe flow maldistribution in Figures 4c, 7b, and 13b unless proper precautions were taken by inserting vanes, perforated plates, or other corrective devices, or by providing sufficient combustor chamber volume to compensate for the maldistribution.

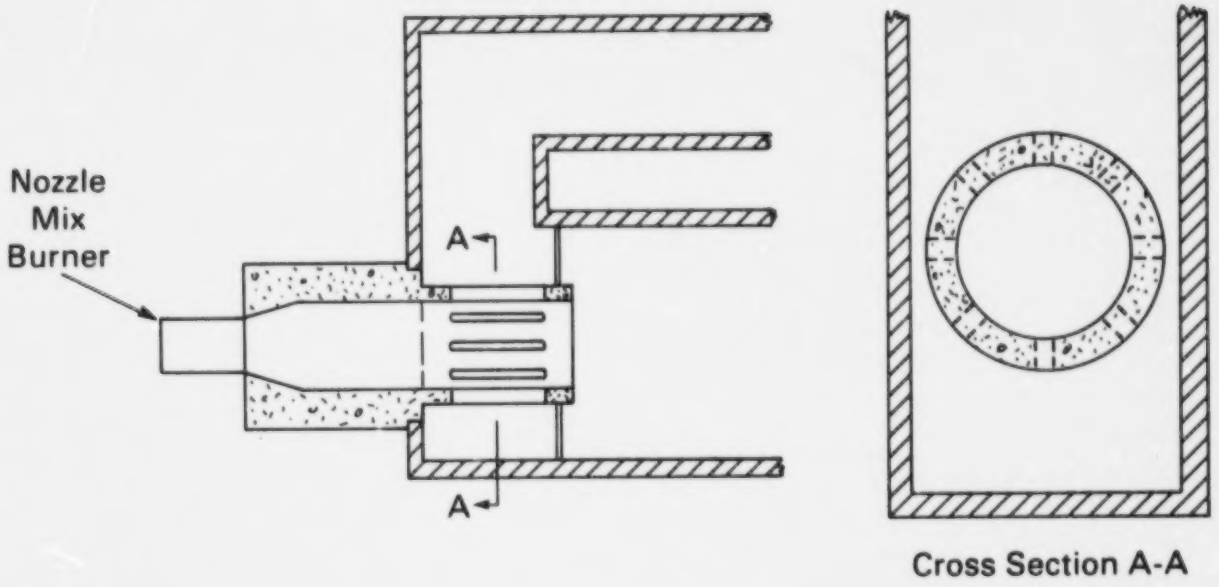

FIGURE 22. AFTERBURNER APPROACH SECTION WITH SLOTTED DUCT

High Velocity Approach Section

Figure 9 shows an extreme case of a high velocity approach section; less extreme cases could also result from too rapid expansion of the supply duct into the burner-combustion chamber system. In the case of Figure 9, a massive recirculation zone would exist around the entrance and extend into the combustion region of the outer burner elements. The ultimate result would be the necessity for a larger combustion chamber section and probably less efficient use of the thermal input.

One should note that in the case of Figure 17d, the high velocity product-jet is desirable since it aspirates in the fumes, which enter along the length of the jet and intimately mix with the product gases as they go through the accelerating section.

SECTION 3

MATHEMATICAL MODELING OF TURBULENT COMBUSTION

At present there are three main types of mathematical models available for predicting the performance of furnaces. These can be classified according to the dimensionality of the model[11]. The simplest model is the zero-dimensional, well-stirred single-zone model. This model has the great advantages of simplicity and computer economy, and is capable of predicting the overall performance of a conventional furnace surprisingly accurately. Thus, despite various shortcomings, the well-stirred model with well-established empirical correction factors is used as the basis for routine design of radiant sections of boilers and fired heaters. Other limitations of the well-stirred model lie in the fact that it does not predict spatial variations in temperature and heat flux along a furnace and it cannot predict the effect of changes in flow pattern and flame length. These limitations are critical to any use in fume reactor design.

The second class of models are one-dimensional, such as the long furnace model in which the gas velocity and temperature transverse to the flow direction are assumed to be uniform and axial radiation is neglected. This model is economical and is capable of predicting axial variations of temperature and heat flux. It can deal with changes in flame length but not recirculation of gases within the furnace. When the recirculation zone is of limited extent a combination of well-stirred and plug flow models can be used successfully. This modeling approach is applicable to certain fume reactor designs.

The third class of models are the multi-dimensional models. Zone and multiflux methods are available for solving that part of the calculation concerned with radiative heat transfer. However, these

must be coupled with some method for calculating the flow and heat release. In principle, this can be done by solving the governing equations for conservation of mass, momentum and energy using (say) a finite-difference solution procedure. However, these methods require considerable expertise and computer time, and often produce unreliable predictions. The unreliable results probably arise from the need for various turbulent mixing coefficients which must be evaluated by trial and error comparison with data on a similar system. For these reasons they are used rarely (if at all) for design of industrial furnaces.

In time (about 1985) these methods are expected to become more reliable and gain wider acceptance in furnace design. Because of some simplifying factors to be mentioned later, practical application of this approach may be even sooner in the fume incinerator field. For this reason, it is felt necessary to present the discussion of multidimensional mathematical modeling covered in this section. However, before proceeding with the discussion, it should be noted that as an alternate method to the above three, the flow and heat releases can be estimated using approximate theories of confined turbulent jets and other components as developed by Thring and Newby[12] and Craya and Curtet[13]. These methods are simple and capable of yielding information which is qualitatively correct. Data for this approach are discussed in the subsequent section.

Considerable progress has been made during the last twenty years in the mathematical modeling of complex turbulent flows, both reacting and non-reacting[14]. The results are generally obtained from the solution of time-averaged conservation equations, in finite difference form. However, in the absence of care, a prediction procedure can rapidly become too expensive for engineering use. Thus, when devising these mathematical models, or choosing a specific model to use, an acceptable balance between economy and accuracy as achieved through physically acceptable simplifications is sought. The scope of this section on mathematical modeling in furnaces is (a) to describe some relevant physical features of turbulence in mixing and reacting flows, (b) to outline the principles involved in the modeling of turbulent combustion, and (c) to suggest a balanced method that could reasonably be employed in afterburner systems studies, stressing

particularly the simplifying assumptions involved and their justification. It is not intended to present any detailed or specific programs; these can be developed from the literature references.

SOME PHYSICAL FEATURES OF TURBULENCE

The physics of turbulence is very complex; therefore the present description is necessarily much simplified (for an exhaustive treatment, see, e.g., Tennekes and Lumley[15] and Hinze[16]. Turbulent fluid motion is a time dependent and inherently three-dimensional condition of flow in which various quantities show a random variation with time and space coordinates. The momentary value of any property $\tilde{\phi}$ is conventionally decomposed into an average value ϕ and a fluctuation ϕ

$$\tilde{\phi} = \phi + \phi \qquad (1)$$

Vortex Stretching

A turbulent flow contains a spectrum of vortex (eddy) sizes; the largest are the order of magnitude of a characteristic flow dimension, the smallest are only two or three orders of magnitude larger than the molecular free path length. The large eddies are the "youngest"; their energy is derived primarily from the mean rate of strain in the flow. The vortices are "stretched" by the viscous interaction between them: the turbulence is three-dimensional and the tendency is for vortices to be stretched along their axes by the relative motion of neighboring vortices whose axes are not parallel to that of the one being stretched (Fig. 23a). The stretching process is repetitive, continually producing new generations of smaller eddies, whose rotational speeds increase because of the conservation of angular momentum (Figure 23b). Finally, vortices become so small in diameter that their identities are destroyed by molecular smearing and their energy is dissipated into internal energy (heat). An eddy "lifetime" can be imagined. This is typical of all turbulence: most of the energy is associated with large-scale motions, most of the vorticity or dissipation (vorticity, which is defined mathematically as the curl of the velocity vector, is a measure of the rate of rotation of a fluid element) is associated

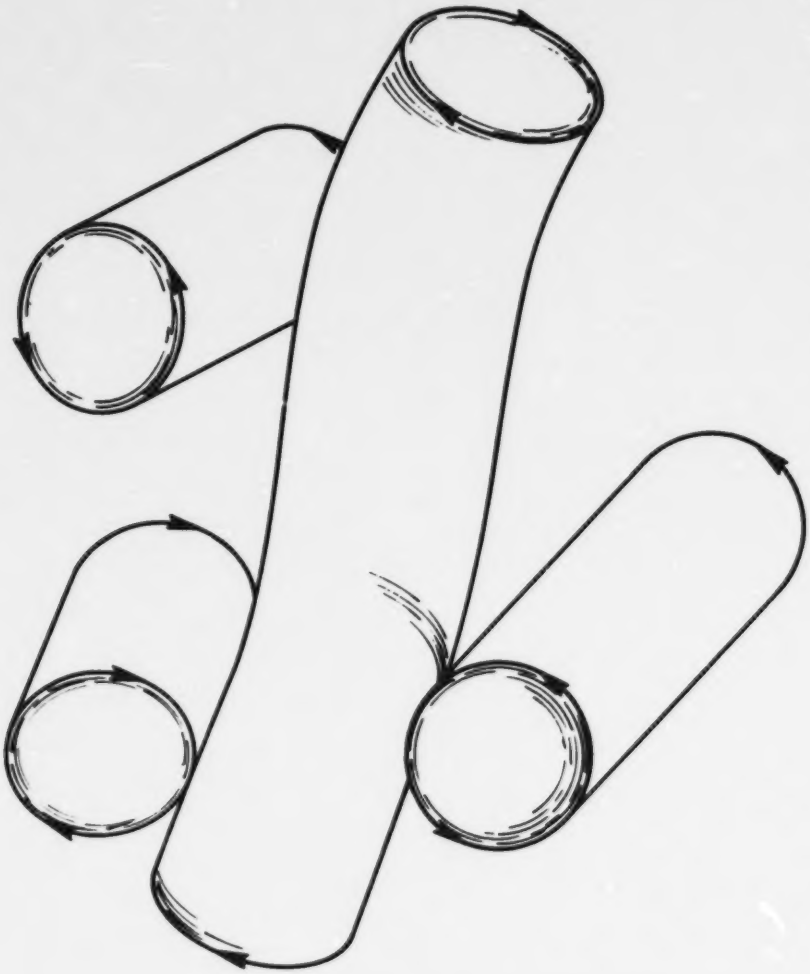

(a) Vortex Stretching Mechanism

(b) Eddy Size Decrease by Stretching

FIGURE 23. VORTEX PHENOMENA

with small-scale motions. The transfer of energy from the larger eddies (smaller velocity gradients) to the smaller ones (larger velocity gradients), brought about by vortex stretching, is called the "energy cascade". At high Reynolds numbers, the fine scale motions responsible for dissipation are isotropic. An illustration of this "local isotropy" is given by Bradshaw[17] (Fig. 24). An initial stretching in the z-direction intensifies the motion in the x and y directions (and reduces the scale). After a few repetitions, small-scale isotropy is approached.

Correlations, Scales, and Spectra

The time average of a fluctuating variable (Eq 1) is defined by

$$\phi = \lim_{t \to \infty} \frac{1}{t} \int_{t_o}^{t_o + t} \tilde{\phi}\, dt \qquad (2)$$

Time averages (mean values) of fluctuations ϕ and of their combinations will be denoted by an overbar; $\overline{\phi}$ is zero by definition.

Consider two fluctuating variables, A + a and B + b. If $\overline{ab} \neq 0$, a and b are said to be correlated; if $\overline{ab} = 0$, the two are uncorrelated. Figure 25 illustrates this concept. a has the same sign as b for most of the time; this makes $\overline{ab} > 0$. The variable c, on the other hand, is uncorrelated with a and b ($\overline{ac} = 0$, $\overline{bc} = 0$) because it has statistically the same chance of having values of the same or the opposite sign as a and b. The correlation coefficient R_{ab}, defined by:

$$R_{ab} \equiv \frac{\overline{ab}}{(\overline{a^2} \cdot \overline{b^2})^{1/2}}, \qquad (3)$$

gives a measure for the degree of correlation between a and b ($\overline{a^2}$ and $\overline{b^2}$ are the variances of a and b, respectively). If $R_{ab} = \pm 1$, the correlation is perfect.

To get an idea of the length scales of the fluctuating motion we consider the correlation between the same fluctuating quantity (e.g.,

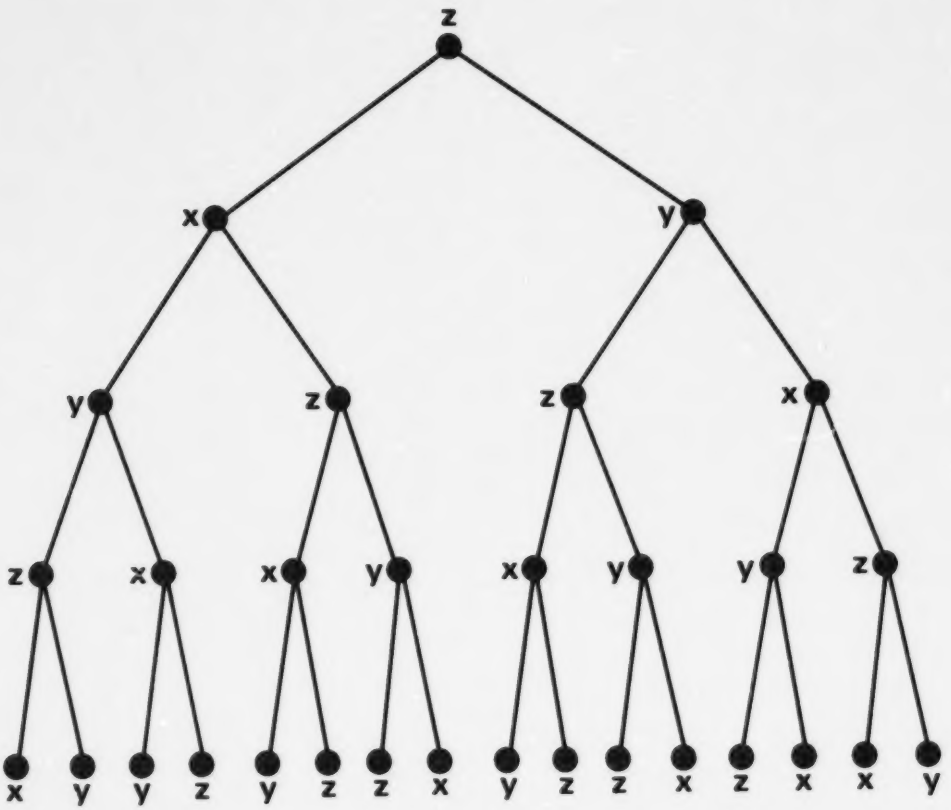

FIGURE 24. PRODUCTION OF SMALL SCALE ISOTROPY BY VORTEX STRETCHING.
The Labels are the Directions of Stretching in each "generation".

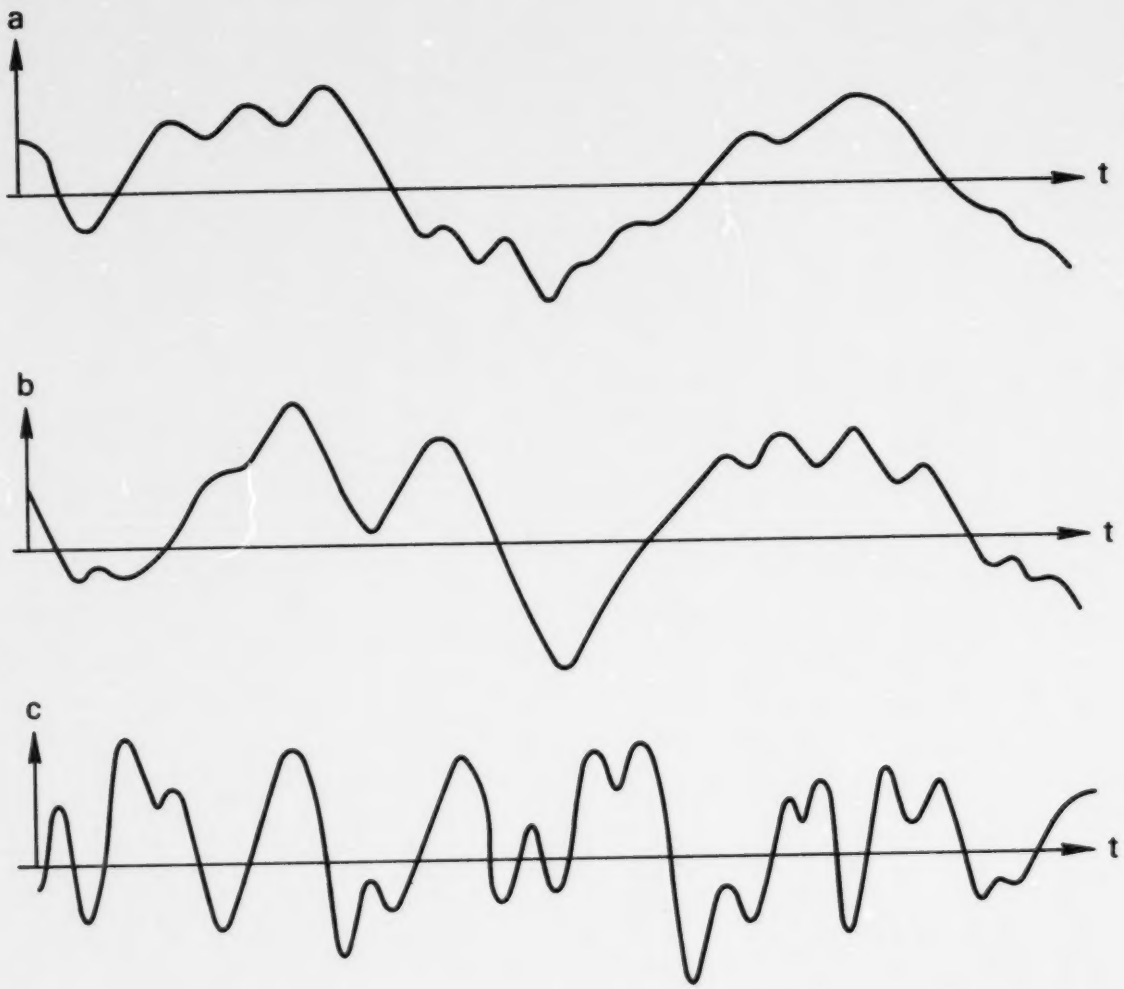

FIGURE 25. CORRELATED AND UNCORRELATED FLUCTUATIONS

the v- component) at two different points in space (e.g. having separation r in the x direction). The correlation (or covariance) of v is therefore $\overline{v(x)\ v(x+r)}$, and the (transverse) correlation coefficient is

$$R_{22}(r,0,0) = \frac{\overline{v(x)\ v(x+r)}}{\left[\overline{v^2(x)}\ \overline{v^2(x+r)}\right]^{1/2}} \tag{4}$$

For convenience, this correlation coefficient is usually approximated by:

$$R_{22}(r,0,0) \simeq \frac{\overline{v(x)\ v(x+r)}}{\overline{v^2(x)}} \tag{4'}$$

Physically, the correlation with separation r is a measure of the strength of eddies whose length in the direction of the vector $\vec{r}$ is greater than the magnitude of r (since eddies smaller than this will not contribute to the correlation). A typical transverse correlation coefficient is sketched in Figure 26.

A length scale of the eddies could be defined as the distance $\bar{r}$ beyond which the correlation is practically zero. However, a more convenient definition is:

$$L \equiv \int_0^\infty R\,dr \tag{5}$$

actually called the "integral scale". When we speak of the length scale of the energy containing eddies we mean a length of order L. This value of L will be comparable to that of $\bar{r}$ if the R curve does not deviate too much from the rectangular. The difference becomes substantial if R obtains a negative value for greater values of $\bar{r}$, which will certainly occur if, e.g., there is a certain constant periodicity in the flow pattern, so that the R curve oscillates about the r-axis at high value of r.

The Fourier transform of the space correlation coefficient is called the wave number spectrum. Much basic theoretical work on turbulence

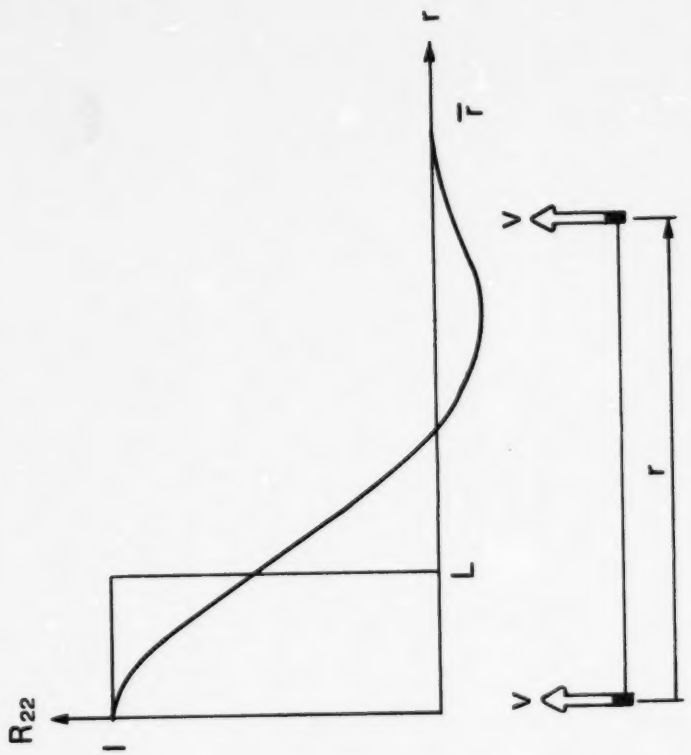

FIGURE 26. TYPICAL TRANSVERSE CORRELATION COEFFICIENT

is concerned with the behavior of one- and three-dimensional wave number spectra, representing the average amount of energy of the turbulent motion between wave numbers k and k + dk. (For periodic functions of space, the wave number $k \equiv \frac{2\pi}{\lambda}$ bears the same relation to the wavelength λ as, for periodic functions of time, the radian frequency $\omega \equiv \frac{2\pi}{T}$ bears to the period T.) A typical isotropic turbulent energy spectrum is plotted in Figure 27. These spectra are useful when dealing mathematically with the transfer of turbulent energy from the low wave numbers (large wavelengths--eddy sizes) to the high wave numbers (small wavelengths--eddy sizes) where it is dissipated.

Turbulence and Combustion

Because they have the greatest specific surface area, and because the stretching process augments the concentration gradients, almost all the molecular mixing occurs across the interface of the smallest vortices[15]. Since the smallest eddies are in equilibrium (i.e., they are eliminated by diffusion as rapidly as they descend from larger ones), the vortex decay time is characterized by the time scale of large vortices. Thus the decay time is of the order L/U, where L and U are a characteristic dimension and velocity of the flow.

For a turbulent diffusion flame, molecular mixing is a prerequisite to combustion. Since fuel and air are initially contained in separate eddies, this can only occur after a period equal to the eddy lifetime. Now the latter are usually long: for a typical engineering flow, L/U might be 0.5 (m)/10 (m/s) = 50 milliseconds. The time scale for overall fuel/oxidant reaction is the order, at most, of a millisecond. Therefore, turbulence, and not chemical kinetics, is rate controlling. Similar arguments apply for premixed combustion, except that in this case the mixing is between separate eddies of burnt and unburnt gas.

Consider mixing of two species a and b, with concentration fluctuations $c_a = c_b = c$ (where $c = \tilde{C}-C$). c decreases by molecular diffusion. To an observer moving with the fluid [18]

$$\frac{dc}{dt} = -\frac{D}{\lambda^2}\, c, \qquad (6)$$

where D is the diffusion coefficient, and λ the eddy diameter ($\frac{\lambda^2}{D}$ is the time scale of molecular diffusion). λ decreases by stretching. Its

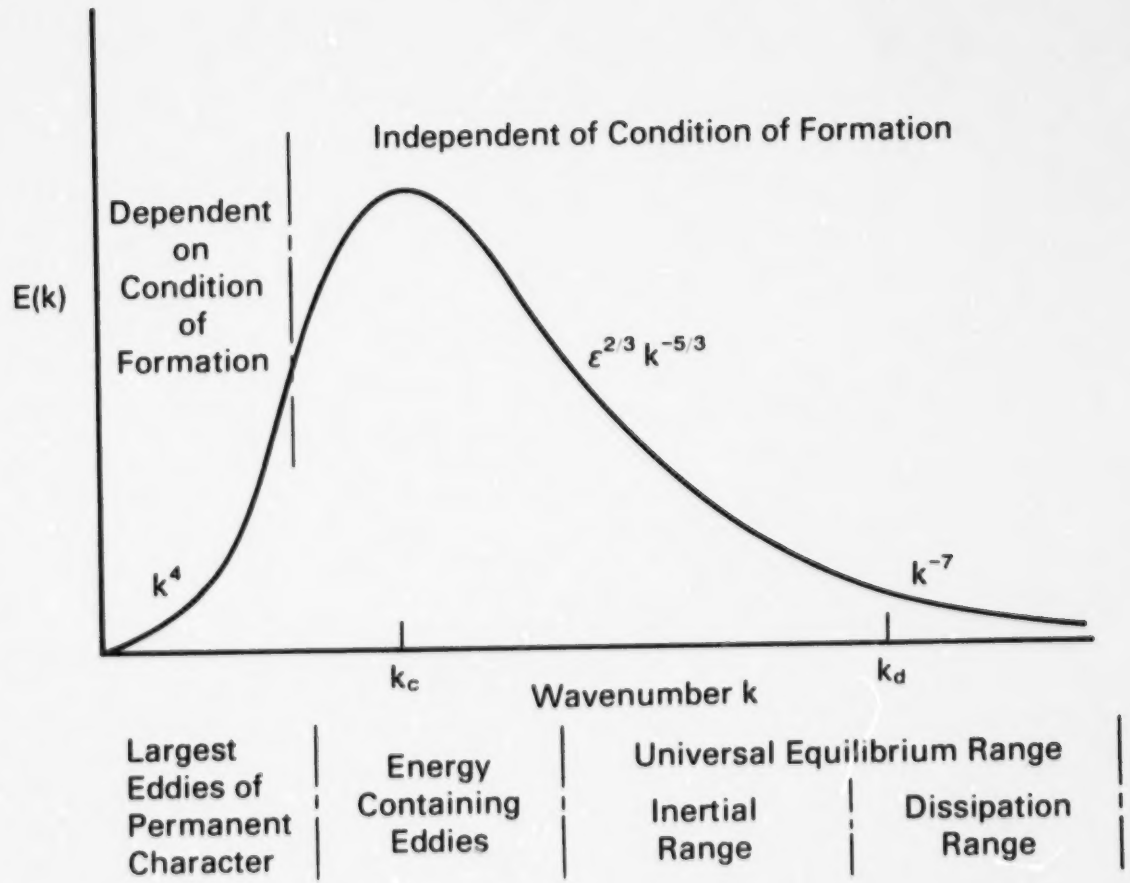

FIGURE 27. TYPICAL ISOTROPIC TURBULENT ENERGY SPECTRUM

decay is assumed proportional to its dimension and inversely proportional to the time scale of the large scale motion[15].

$$\frac{d\lambda}{dt} \sim - \frac{\lambda U}{L} \tag{7}$$

Combining (6) and (7) and integrating, with $\lambda = L$ and $c = c_o$ for $t = 0$ (birth of eddy), gives:

$$t_{mix} \sim \frac{L}{2U} \ln \left(1 + \frac{2LU}{D} \ln \frac{c_o}{c}\right) \tag{8}$$

It can be concluded that the turbulence time scale is of primary importance in the mixing process. The influence of molecular diffusion is secondary, although essential.

FUNDAMENTALS OF TURBULENT COMBUSTION MODELING

The Flow

Conservation Equations--

As already mentioned, turbulent flows are three-dimensional and time-dependent. Calculation over their entire length and time scales is both impossible (with available computers), and unnecessary from a practical viewpoint. As a consequence, mean predictions are sought by solving time averaged equations.

For an isothermal flow with constant density, defining:

$$\tilde{U}_i = U_i + u_i , \quad \tilde{P} = P + p \tag{9}$$

substituting in the continuity and Navier-Stokes equations and averaging, we obtain (cartesian tensor notation, which implies summation over repeated indices, is used):

$$\frac{\partial(\rho U_i)}{\partial x_i} = 0, \tag{10}$$

$$\rho U_j \frac{\partial U_i}{\partial x_j} = - \frac{\partial P}{\partial x_i} + \frac{\partial}{\partial x_j} \left(\mu \frac{\partial U_i}{\partial x_j}\right) - \frac{\partial}{\partial x_j} \left(\rho \overline{u_i u_j}\right) \tag{11}$$

Because convective terms are non-linear, unknown correlations of the form $-\rho\overline{u_i u_j}$ have appeared. They are apparent stresses (for instance, $-\rho\overline{uv}$ represents an extra mean shear stress on the face dxdz of an infinitesimal control volume with sides dx, dy and dz in the coordinate directions). These extra turbulent stresses are called Reynolds stresses; the time-mean Navier-Stokes equations, in which they appear, are called the Reynolds equations. Turbulence models relate these unknown stresses to known or determinable properties. Having more unknowns than equations in the customary description of turbulence is called the "closure" problem.

Turbulence Modeling--

Much of the work on turbulence modeling employs an isotropic turbulent or "eddy" viscosity concept. This assumes that the turbulent stresses act like the viscous stresses, that is, they are proportional to the velocity gradient. In general form:

$$\rho\overline{u_i u_j} = \mu_t\left(\frac{\partial U_i}{\partial x_j} + \frac{\partial U_j}{\partial x_i}\right) - \frac{2}{3}\rho k\,\delta_{ij} \qquad (12)$$

where $k \equiv \Sigma_i \frac{u_i^2}{2}$ is the turbulence kinetic energy, and δ_{ij} is the Kronecker delta ($\delta = 0$ for $i \neq j$, $\delta = 1$ for $i = j$).

The turbulent viscosity μ_t is not a property of the fluid but depends on the dynamic condition of the flow, and its value varies from point to point. If μ_t could be expressed in terms of known or calculable quantities, then Equation (11) could be solved.

Prandtl proposed in 1925 (for a simple shear flow):

$$\mu_t = \rho\ell_m^2\left|\frac{\partial U}{\partial y}\right|, \qquad (13)$$

where ℓ_m is a characteristic length scale of the turbulent motion, called mixing length. ℓ_m must be prescribed algebraically; but in boundary-layer flows, a few simple rules usually serve for its prescription.

Other models require the solution of a differential equation to determine the turbulent viscosity. The local variation of μ_t is assumed to be of the form:

$$\mu_t = C_\mu\rho k^{1/2}\ell \qquad (14)$$

where C_μ is a constant. In this model, the length scale ℓ is still prescribed algebraically (usually a constant fraction of flow width for boundary-free shear flows, but not the same fraction for each flow.) On the other hand, k is determined from the solution of a differential equation expressing the processes by which it is transported. Two-equation models of turbulence require the solution of two transport equations, one for k and another one for a quantity from which ℓ can be derived. These models employ for μ_t the same formula (14) (which is often referred to as the Prandtl-Kolmogorov formula). They do not require ℓ be prescribed algebraically, and this is an advantage in modeling flows with recirculation, in which it is rather difficult to determine the length scale profile by measurement.

More advanced models do not introduce the turbulent viscosity concept, but involve the solution of transport equations for the Reynolds stresses. This is probably the optimum level of closure in terms of physical interpretation, and it has the potential to be generally applicable to a wide range of flows. However, Reynolds stress closures are still in a development stage, and are computationally very expensive.

For an exhaustive discussion of turbulence models, the reader is referred to the works of Launder and Spalding[19], Harlow[20], and Mellor and Herring[21].

Equation (14) contains the constant C_μ, and other constants appear in the transport equations for k and other variables of the turbulence models. These "constants" are semi-empirical quantities, derived by matching experimental and numerical results by computer optimization. They are functions of the specific model employed, and for the same model they depend on the type of flow solved, and sometimes vary with the various investigators. Actually, refinements of these models could involve making these "constants" depend on various non-dimensional arguments. Therefore, when applying one model of turbulence, care should be taken to employ the <u>set</u> of constants which is appropriate to the model and the flow type.

The specification of a length scale ℓ is a dimensional necessity which stems from Equation (11) and the assumption (14). This scale can be visualized as being the size of the largest eddies of the flow, and thus having the order of magnitude of an integral scale L (5). This, of course, does not imply that a single value of ℓ can be assigned at each point for

a specified flow condition. The actual value of ℓ will be a function of the specific turbulence model employed. However, it is plausible that length scales predicted with different models will be locally of the same order of magnitude.

Thermal and Chemical Properties

When dealing with a nonisothermal reacting system, the conservation of energy and a conservation equation for each chemical species have to be considered. If $\tilde{\theta} = \theta + \theta$ is a scalar quantity,

$$\rho U_j \frac{\partial \theta}{\partial x_j} = S_\theta + \frac{\partial}{\partial x_j}\left(\Gamma_\theta \frac{\partial \theta}{\partial x_j}\right) - \frac{\partial}{\partial x_j}\left(\rho \overline{u_j \theta}\right) \tag{15}$$

is the common form of these equations. Again one could put

$$-\rho\overline{u_j\theta} = \Gamma_{\theta,t} \frac{\partial \theta}{\partial x_j} \tag{16}$$

and rewrite Equation (15) as

$$\rho U_j \frac{\partial \theta}{\partial x_j} = S_\theta + \frac{\partial}{\partial x_j}\left(\Gamma_{\theta,\,\mathrm{eff}} \frac{\partial \theta}{\partial x_j}\right), \tag{17}$$

where $\Gamma_{\theta,\mathrm{eff}} \equiv \Gamma_\theta + \Gamma_{\theta,t} \simeq \Gamma_{\theta,t}$ and a turbulence model is required for $\Gamma_{\theta,\,\mathrm{eff}}$ too.

Any detailed chemical model describing the combustion of higher hydrocarbons should take into consideration a large number of species and reaction steps. Each species involved in the modeling of the chemical kinetics necessitates the solution of an additional conservation equation, and hence increases the computer time required. Moreover, uncertainties exist in both the mechanisms and the rates for the high temperature oxidation of hydrocarbons and the resulting intermediates. For these reasons it is common practice (see e.g., Gosman, et al.)[22] to assume a global, one-step reaction between fuel and oxidant. This simple assumption allows the heat release rate to be readily evaluated. However, it cannot be used when trying to predict pollutant formation

and emissions. Some slight improvement is possible by supposing a two-step reaction in which the hydrocarbon reacts to form CO and H_2O followed by the oxidation of CO to CO_2 [23]. A three-step mechanism was used by Arbib, et al., [24], for hydrocarbon attack (to CO and H_2), CO oxidation and water formation. All of the above-mentioned investigations employed global reaction rate expressions. Altenkirch and Mellor [25] used a kinetic scheme based on the quasi-global concept, which combined a global expression for irreversible partial oxidation of the fuel (developed by Edelman and Fortune [26], and subsequently corrected by Edelman and Harsha [27]), with a set of 15 elementary reactions for CO and H_2 oxidation. But the results obtained by this and by even more detailed models so far are not such as to justify the enormous amount of computer time that they require.

Instantaneous global reaction rates are usually expressed as

$$\tilde{R}_j = \tilde{K}\, \tilde{C}_{fu}\, \tilde{C}_{ox}\,, \tag{18}$$

where $\tilde{K}$ is the rate constant, usually written the Arrhenius form:

$$\tilde{K} = A \exp\left(-\frac{E}{R\tilde{T}}\right)\,. \tag{19}$$

The time-averaging of $\tilde{R}_j$ represents one of the central difficulties of combustion modeling. Calculations have often been performed by the simple expedient of expressing the time-averaged reaction rate as

$$R_j = K\, C_{fu}\, C_{ox}, \tag{20}$$

but, since the concentration and temperature fluctuations can be large, this practice is not, in general, justifiable. In addition to the highly non-linear dependence of reaction rate on temperature, a situation can occur in which the instantaneous values of fuel or oxidizer concentrations vanish for finite periods of time, leading to a time-average rate of reaction which is less than the one computed using time-averaged values of the concentration (the "unmixedness" problem).

A number of approaches exist to circumvent this difficulty, and they are reviewed by Gosman, et al. [28].

The Computation

Once the differential equations have been set up, they have to be solved numerically. To this end, adequate algorithms exist today. They usually involve writing the conservation equations in a common form, and solving them by the finite difference procedure. The basic differential equation solved by most hydrodynamic codes is:

$$\rho \frac{D\Phi}{Dt} = \nabla \cdot (\Gamma_\Phi \nabla_\Phi) + S_\Phi \qquad (21)$$

where Φ is any dependent variable and $\Gamma_{\Phi,eff}$ and S_Φ are functions of Φ.

Computational codes to solve particular cases of Equation (21) are described by Gosman[22] and Gosman and Pun[29], for two-dimensional recirculating flows; by Patankar and Spalding[30], for boundary-layer type flows; and in the TEACH-3E program developed at the Imperial College (and so far unpublished) for three-dimensional recirculating flows. A considerable degree of sophistication is being achieved by using these techniques to predict combustor performance, with a fair amount of success (see e.g., Ref. 31).

The presence of chemical source terms generally leads to a numerical difficulty known as "stiffness" of the equations. This is a property that, in the current context, stems from the range of disparate time scales that are related to reactive collision times. In multicomponent, multireaction systems, the smallest characteristic time dictates the maximum permissible time step (or mesh size for steady reacting flows) for numerical integration. The latter may be prohibitively small, so that the computation of species concentrations becomes an unviable proposition. Stiffness exhibits itself in the form of excessively high temperatures, and mass fractions that are greater than one or negative. Greenberg and Presser[32] have recently reviewed the various techniques employed to handle "stiffness", and have suggested a new method to deal effectively with the problem for elliptic internal reacting flows.

Some Remarks About Radiation Transfer

Usually radiation heat transfer is neglected in most computations of turbulent reacting flows. This assumption is good for small combustors. The fraction of the total heat transfer due to thermal radiation grows with the combustor size, attaining prominence (for gaseous firing) for characteristic combustion lengths in excess of about 1 m. The accounting for radiation requires the solution of a complex integro-differential equation which is time consuming to solve. However, techniques capable to handle reacting flows with radiation exist [31], and they could be employed whenever the latter is expected to play a dominant role.

RECOMMENDATIONS FOR MODELING TURBULENT COMBUSTION IN INDUSTRIAL AFTERBURNERS

Because of the great variety of afterburner systems and the wide range of fuel and waste gas combinations employed, it is difficult to choose a specific model suitable for all or most fuel-gas combinations. However, a number of recommendations can be made in the light of previous experience.

Flow Geometry

Most industrial afterburners have a complicated geometrical form, and the flow in them presents zones of recirculation. Therefore, in principle, the full three-dimensional conservation equations would need to be solved. Although, as already mentioned, there are nowadays methods for doing that, they would be probably uneconomical for applications of this kind. Moreover, in many combustion chambers the burners generate in their immediate vicinity very nearly axisymmetric flames, which are often relatively insensitive to the details of the flow elsewhere. This would suggest that a two-dimensional procedure for axisymmetric flows with recirculation would suit most afterburner systems. This would lead to elliptic conservation equations in cylindrical-polar coordinates.

Turbulence Model

The most established turbulence model to date is the two-equation model in which equations are solved for the turbulence kinetic energy, k, and its dissipation rate, ε. The turbulent viscosity may then be related to k and ε by dimensional arguments as

$$\mu_t = C_\mu \rho \frac{k^2}{\varepsilon} \qquad (22)$$

where C_μ is a constant of the model. The effective exchange coefficient $\Gamma_{\Phi,eff}$ for a variable Φ may be expressed as

$$\Gamma_{\Phi,\,eff} = \frac{\mu_{eff}}{\sigma_{\Phi,\,eff.}} \,, \qquad (23)$$

where $\sigma_{\Phi,\,eff}$ is a turbulent Prandtl or Schmidt number, and $\mu_{eff} = \mu_t + \mu \tilde{-} \mu_t$.

Most two-equation models of turbulence provide predictions of roughly the same level of accuracy. The reason why the k-ε model has been favored by more workers than any other lies partly in the relative ease with which the exact equation for ε can be derived, and partly in the mainly esthetic fact that ε appears directly as an unknown in the equation for k. In addition, the equation for ε has the advantage to contain fewer terms. The k-ε model also appears to give better results for flows near walls (Launder and Spalding [33]).

A usual approximation is to assume $\sigma_{\Phi,\,eff.} = 1$ in Equation (23) for any variable Φ. This makes the effective diffusive transport coefficients, $\Gamma_{\Phi,\,eff}$ all equal ($= \mu_{eff}$) at every location for all variables. This approximation is usually quite acceptable since the σ_Φ's are all of order unity.

Kinetic Model

The chemical aspects of afterburner systems have been reviewed by Barnes, et al., [8]. All that needs to be told here is that for some applications, in particular those in which the waste gas contains mostly inerts and only the temperature distribution in the combustor is important, a global one-step reaction between the fuel and the oxidant would probably be sufficient. The effect of free radicals and atoms is small. CO and H_2 have a significant role in highly loaded combustors, but it is good enough to ignore them when one seeks only heat release. The overall reaction does not depend on trace species (e.g., NO_x) chemistry. When this approach is not possible, it is of course necessary to keep the number of chemical species involved to a minimum, since every one requires the solution of an additional differential equation.

The time averaged reaction rate could be acceptably approximated by Equation (20), in applications of this kind. This is because, due to the minute fuel concentrations, the chemical kinetics is relatively slow and the fluctuations in concentration are smoothed out by mixing (Lockwood [34]). Moreover, use of Equation (20) would plausibly be justified whenever global reaction-rate expressions are employed, if these were determined experimentally through average concentration and temperature measurements inside a combustor having a configuration similar to the one being modeled.

SECTION 4

JETLIKE COMPONENTS OF AFTERBURNERS

Examination of afterburner components reveals that many of them can be classified as resulting in jetlike action in the flow field. Looking at the components as regions in the flow field, one could consider the regions as jet flow regions. For instance, the discrete source burners of Figures 7a and 7b can be treated as hot gas jets interacting with the surrounding fume laden air. While the simple jet in an infinite environment of identical properties to the jet has been discussed in many reports, some consideration of the jetlike flames in an afterburner shows that there are many variations in the jet and environmental flow patterns that can lead to significant differences in results. On the other hand, the smaller variations in temperature and reaction rate in the combustion chamber section of an afterburner as contrasted to normally expected combustor rates in the combustion region of a furnace permit the use of the simpler nonreacting jet results in analysis. In this section, such a viewpoint is taken; emphasis is placed on "cold jet" results that are applicable to afterburner design.

For initial orientation, Table 1 lists several sets of type variations that one might encounter in a combustion system. For a given jet, a type must be specified from each set; it is seen that this leads to a large number of variations in jets even without consideration of details. For the present study, several examples in the literature that are pertiennt to afterburners will be cited.

Table 1. JET-TYPE VARIATIONS CLASSIFIED IN SETS

a. Geometry of jet exit

1. Axially symmetric
2. Two-dimensional
3. Rectangular
4. Wall
5. Radial
6. Annular
7. Other

b. Environmental velocity

1. Zero
2. Coaxial positive
3. Coaxial negative
4. 90° cross flow
5. Non 90° cross flow

c. Environmental properties

1. Temperature and composition same as in jet
2. Temperature different
3. Composition different
4. Temperature and composition different

d. Number of jets

1. Single jet
2. Multiple parallel jets in line
3. Multiple parallel jets in pattern
4. Multiple nonparallel jets

e. Relation of jet to wall

1. Nonimpinging jet
2. Jet impinging at 90°
3. Jet impinging at other than 90°

f. Environmental geometry

1. Jet in open
2. Jet in enclosure without recirculation
3. Jet in enclosure with recirculation

g. Swirl condition

1. Zero swirl
2. Low swirl
3. High swirl

h. Buoyancy

1. No buoyancy effect
2. Positive buoyancy parallel to jet direction
3. Negative buoyancy parallel to jet direction
4. Nonparallel buoyancy effects

CIRCULAR TURBULENT FREE JETS

The circular turbulent free jet has been studied in great detail, and the essential properties are quite well known[35,36,37]. While no jet in the combustion chamber portion of a fume afterburner is free, some may be essentially so for large distances, sufficient to analyze the mixing adequately. Two possible examples are Figures 11c and 17d.

Figure 28, with $U_s = 0$, shows the usual interpretation of this type of jet, in which a potential core region is followed by transition region and finally a region of fully established flow. The fluid energy from the nozzle interacts with the surrounding media and is gradually eroded away with the potential core disappearing in about 5 diameters. By about 10 diameters, a stable flow pattern with similarity properties is established. On the axis, the velocity is then given by

$$U_m/U_o = A/\left[(x/d) + B\right]$$

where U_m is the velocity on the axis, U_o is the core velocity, x is the distance from the nozzle end, d is the nozzle diameter, Bd is the experimentally determined location of the virtual source upstream of the nozzle, and A is an experimentally determined multiplying coefficient. Figure 29 shows a set of data plotted in this form, assuming B = 0. Depending on the details of the turbulence in the jet, and the details of the original velocity profile, A and B both vary somewhat, and B can even be negative. Considering all factors, Rajaratnam[36] recommends A = 6.3 and B = 0. To compute the estimated volume rate of flow, he recommends $Q_{(x)}/Q_o = 0.32\ (x/d)$, and to compute the kinetic energy of flow, $E_{(x)}/E_o = 4.1\ (d/x)$. These values are shown in Table 2. Field, et al., (37), add the concentration equation, for concentration on the axis, $C_m/C_o = 5.0\ (d/x)$.

TABLE 2. COEFFICIENTS FOR INCOMPRESSIBLE TURBULENT JETS

	Axially Symmetric, $A/[(x/d)+B]$								Plane, $A/[(x/w)+B]^{1/2}$							
	U_m/U_o		C_m/C_o		$E_{(x)}/E_o$		$Q_o/Q_{(x)}$		U_m/U_o		C_m/C_o		$E_{(x)}/E_o$		$Q_o/Q_{(x)}$	
	A	B	A	B	A	B	A	B	A	B	A	B	A	B	A	B
Rajaratnam	6.3	0	--	--	4.1	0	3.13	0	2.47	0	--	--	1.87	0	1.61	0
Field, et al.	6.3	0	5.0	0	--	--	3.13	0	2.48	.6	2.00	.6	--	--	1.97	0
Sforza, et al.	6.25	0	4.65	0	--	--	3.57	0	--	--	--	--	--	--	--	--
Becker, et al.	--	--	5.4	-2.4	--	--	--	--	--	--	--	--	--	--	--	--

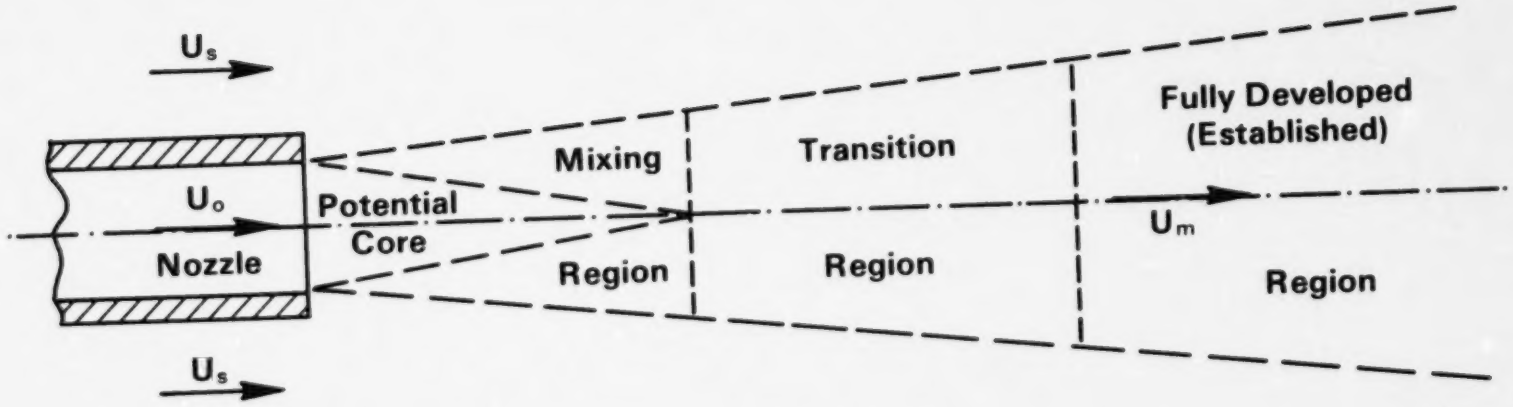

FIGURE 28. REGIONS OF JET

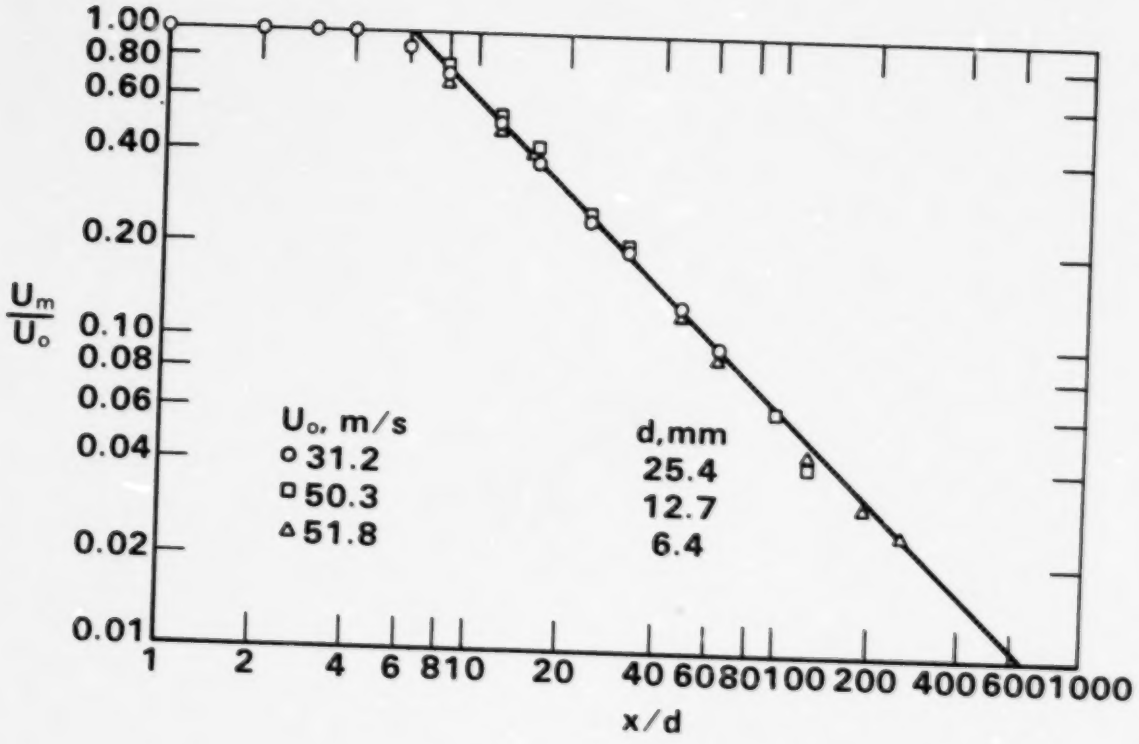

FIGURE 29. DISTRIBUTION OF CENTERLINE VELOCITY FOR FLOW FROM ORIFICE ACCORDING TO ALBERTSON, ET AL.

The velocity profile at any distance, x, can be normalized to the half-velocity radius, b. Rajaratnam suggests using for the half-velocity radius, b = .10 x in the fully developed flow region, while Field, et al., use b = .085 x. The corresponding value of b for concentration, as given by Field, et al., is .109. This is close to the value of .107 average for both concentration and temperature for the data reviewed by Becker, et al.[38].

In a recent review of the fluctuating temperature measurements in a free jet, Lockwood and Moneib[39] suggest a value of b/x = .124 for the half-temperatures increment radius. (These authors also note the slow approach to a constant value of the temperature fluctuates on the axis ($\theta'/\bar{\theta} \approx .20$ at x/d >35) and suggest this confirms the fact that turbulence has a rather long memory). If this value is ratioed to Rajaratnam's half-velocity b/x value, the ratio is close to Field's concentration to velocity ratio b/x values. Considering the observations on plane turbulent jets discussed later, it would appear a consistent set of value of b/x would have the same value for concentration and temperature.

As seen in Figure 30, the variation of U/U_m with r/b in the fully developed flow region is Gaussian in general shapes but not in detail. Several semi-empirical relations have been suggested in the literature for correlating these velocity distribution data; for instance, Schlichting[40] suggests

$$U/U_m = \left(1 + (\sqrt{2}-1)(r/b)^2 \right)^{-2} , \qquad (25)$$

which fits data out to r/b = 1.5, beyond which it is a little high. The 3/2 power curve and error curve show a similar characteristic, while the cosine curve

$$U/U_m = \left(1 + \cos (\pi r/2b)\right)/2 \qquad (26)$$

fits quite well[41]. We note that since the half width b expands faster for concentration than for velocity, the mass diffusion is faster than the momentum diffusion.

Golubev and Klimkin[42], using helium, air, and freon jets in air, obtained the profiles shown in Figure 31, normalized to $r/b^* = 1$ at the 50 percent momentum rather than 50 percent velocity point. One notes that $b/b^* = 1.35$ and $b_c/b^* = 1.69$. Thus the turbulent Prandtl number (ratio of diffusivity of momentum to thermal diffusivity) becomes 1.35/1.64 = 0.82, which is same as Steward and Guruz[43] suggest from studies of the spread ratio in confined jets.

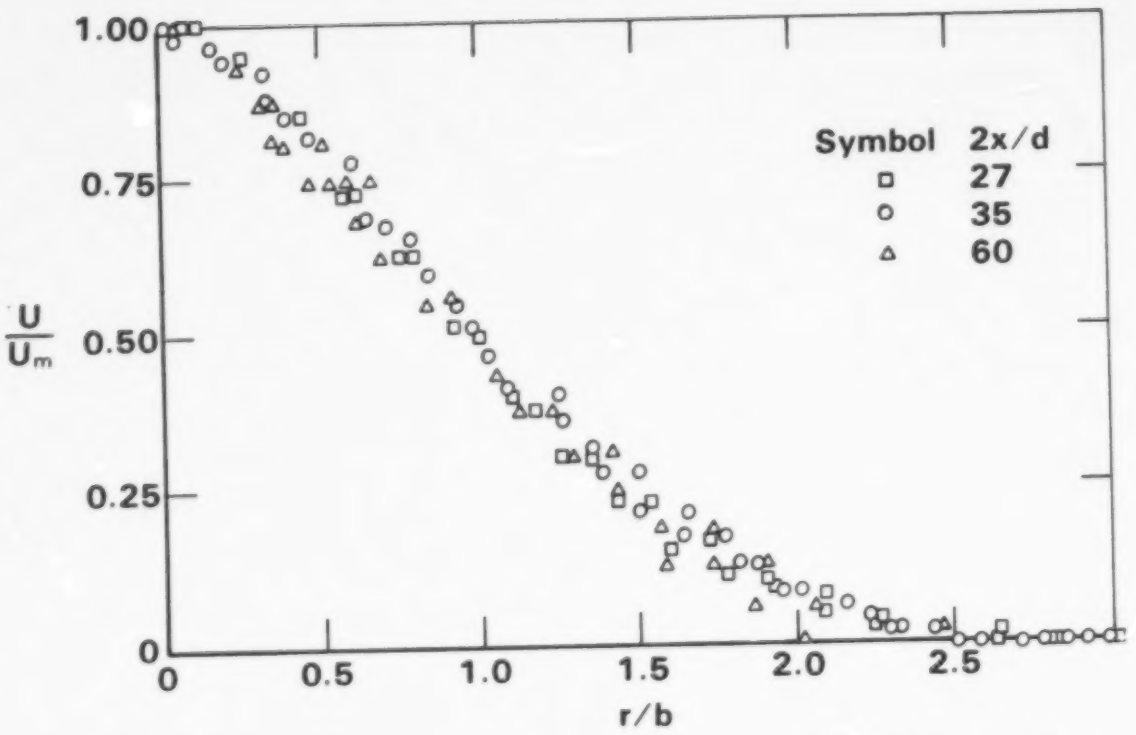

FIGURE 30. REICHARD'S VELOCITY PROFILE IN THE DOWNSTREAM PART OF A CIRCULAR JET

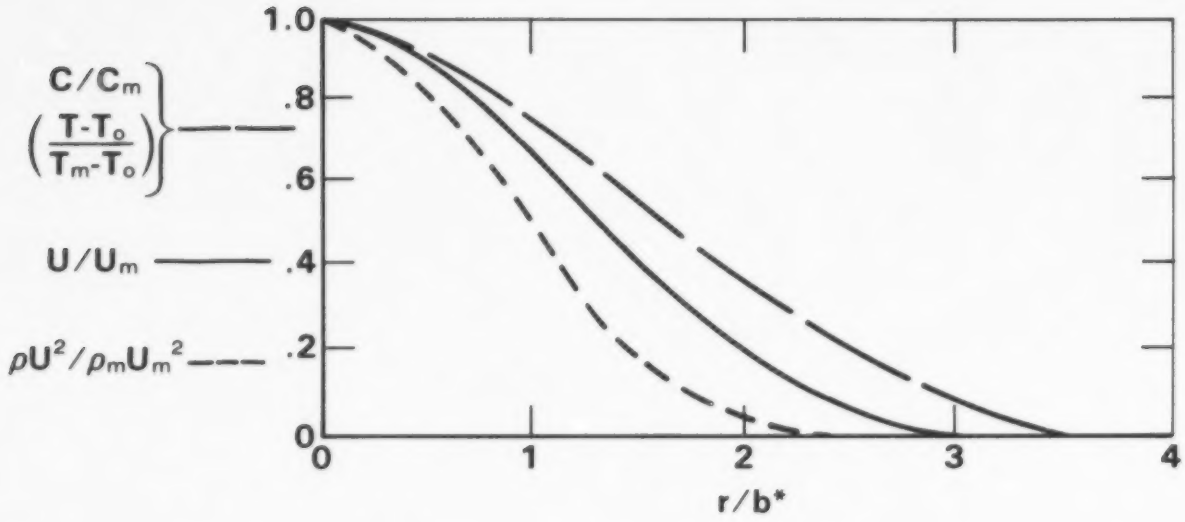

FIGURE 31. GOLUBEV-KLIMKIN PROFILES OF DOWNSTREAM PART OF CIRCULAR JET

PLANE TURBULENT FREE JETS

The plane turbulent free jet, like the circular jet, has been the subject of much study[35,36,37]. The flow region downstream of systems such as shown in Figure 2 can be averaged on the basis of the plane turbulent jet. The character of the jet is similar to that outlined for the circular jet. However, the velocity on the axis does not fall off as rapidly with distance. For a slot width, w, an equation of the form

$$U_m/U_o = A/(\frac{x}{w} + B)^{1/2} \qquad (27)$$

is commonly used to determine the velocity. As shown in Table 2, Rajaratnam suggests A = 2.47 and B = 0, and Field, et al., suggest A = 2.48 and B = .6. For the kinetic energy ratio, Rajaratnam recommends A = 1.87 and B = 0, while Field, et al., suggest A = 2.00 and B = .6. In the case of the total flow, $Q_o/Q_{(x)}$ (note ratio inversion) Rajaratnam suggests 1.61 for A. For C_m/C_o, Field, et al., suggest 2.00 for A and .6 for B.

Again the velocity profile at any distance, x, can be normalized relative to the half-velocity, half-width of the jet, b. Rajaratnam suggests the same b = .10x, as for the circular jet, while Field, et al., suggest the coefficient of .096 for the velocity and .14 for the concentration. As for the circular jet, a variety of equations have been suggested for the velocity profile, in many cases of the same form as for the circular jet. It should be noted, however, that some investigations have been able to correlate the velocity profile data back into the core region by using the core edge as the zero point for the measurements in the transverse plane.

For both the circular jet and the plane jet, Field, et al., suggest that when density differences are present, $(U_m/U_o)(\rho_s/\rho_o)^{1/2}$ be substituted for (U_m/U_o), $(C_m/C_o)(\rho_s/\rho)^{1/2}$ for (C_m/C_o), and $(Q_{(x)}/(Q_o)\ (\rho_s/\rho_o)^{1/2}$ for $(Q_{(x)}/Q_o)$. With these substitutions, Field, et al., also suggest that $(T_m-T_s)/(T_o-T_s)$ can be substituted for C_m/C_o when temperature differences are present. Recent studies by Sforza and Mons[44] and by Golubev and Klimkin[42] confirm these suggestions.

It may be noted that these relations are consistent with Thring's[45] early suggestion for modeling in a uniform temperature system of cold jets discharging into a hot furnace system. In this approach, before

size scaling is considered, a charge is made in jet size so that the same temperature fluid is used in the jet and the surroundings; as a result, $d_{model} = d_o(\rho_o/\rho_b)^{1/2}$, where ρ_o is the prototype nozzle fluid density and ρ_b is the furnace gas density used with the adjusted jet diameter, d_{model}. Similarly, the relation corresponds to the Ricou-Spalding[46] assumption for aspiration of the surrounding media by a jet.

FREE COMPOUND JETS

In the compound jets considered herein, (Fig. 28), the simple circular jet is surrounded by a flow of uniform positive velocity, U_s, rather than a medium at zero velocity. A similarity is noted to the combustion chamber burner systems of Figures 6a, 13b, and 15b. Using the relation $(U-U_s)/(U_m-U_s)$ in place of U/U_m, the velocity profile for both the plane jet and circular jet are found to be independent of U_s. Thus, general curves such as Figure 30 can be used. However, this is not the case when the expansion of the jet with distance is considered. As shown in Figures 32 and 33, the width of the jet does not increase linearly as with a zero ambient velocity, but shows a curving inward toward the plane of symmetry. One should note these curves are for the jet boundary; assuming a cosine velocity distribution, the corresponding value of b/d and b/w would be half as large. This can be seen by a comparison of Figure 4.7 of Rajaratnam[37] for b/b_o and Figure 33[35] for y_{edge}/b_o. Madni and Pletcher[47] reported data from the literature in a logarithmic form and obtained straight lines, as in Figure 34. These data agree with those of Rajaratnam and of Abramovich, but the different coordinates aid in extrapolation. However, the Madni and Pletcher's plot of Figure 35 indicates a somewhat higher intercepts for $U_s/U_o = .2$ and .5.

The relation between the velocity on the axis and the distance along the jet is not as clear in the literature. For a plane jet, Rajarantnam suggests using

$$\frac{U_m - U_s}{U_o - U_s} = 2.41 \left(\frac{U_o}{U_o - U_s}\right) \Big/ (x/w)^{1/2}. \qquad (28)$$

We note that the coefficient here is a little less than the same authors suggested for the free jet. This general form of equation fits the curve suggested by Abramovich for $U_s/U_o < .6$ but requires a slightly higher

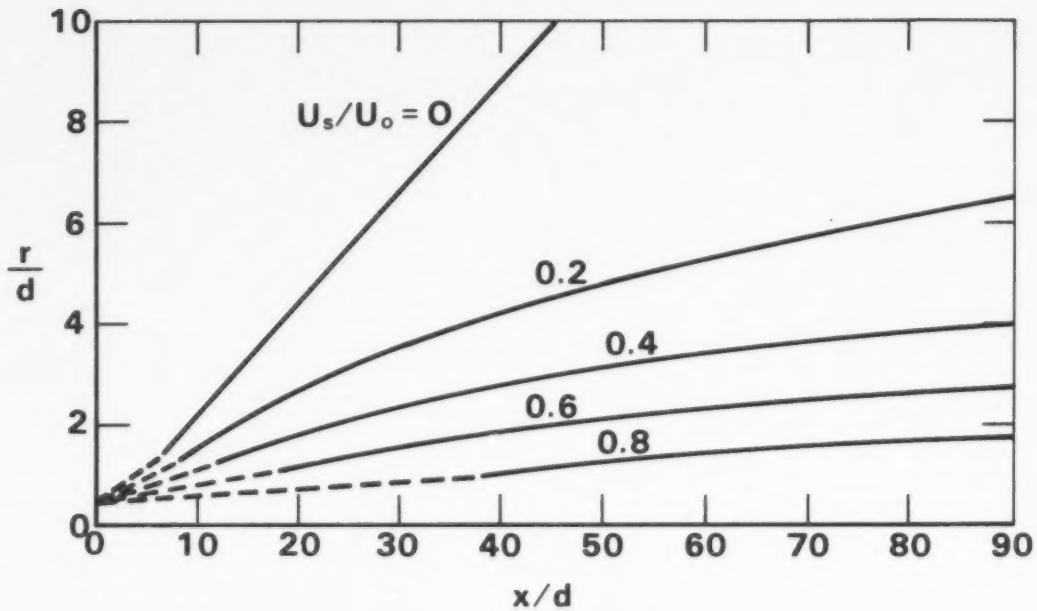

FIGURE 32. BOUNDARY OF AN AXIALLY SYMMETRIC JET

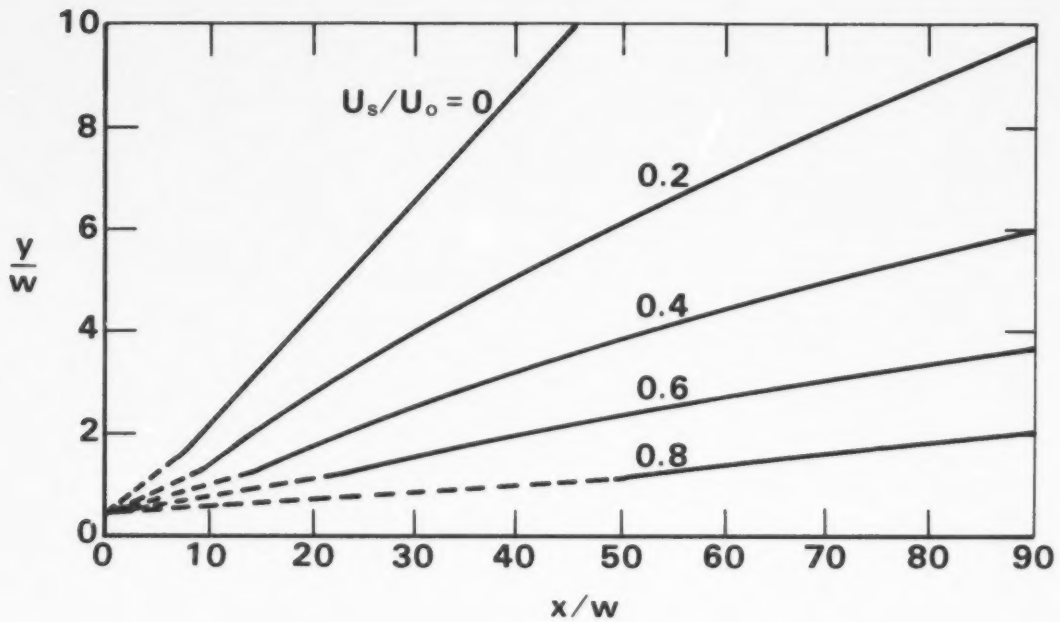

FIGURE 33. BOUNDARY OF A PLANE JET.

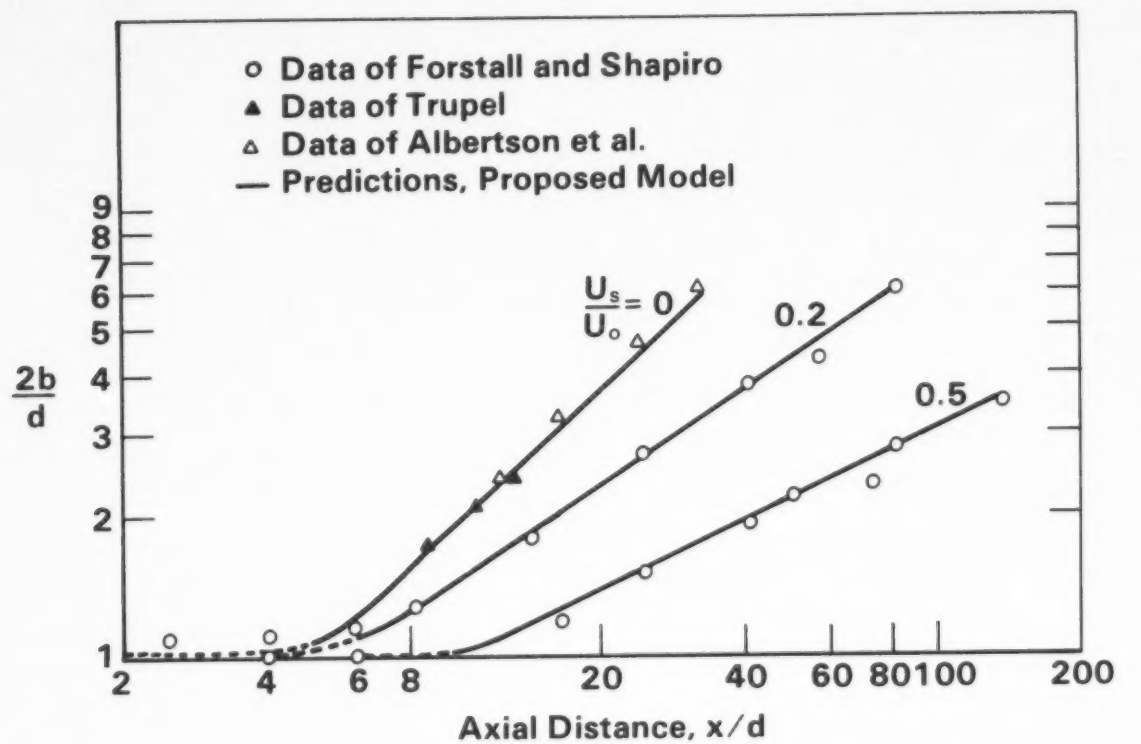

FIGURE 34. PREDICTED AND EXPERIMENTAL HALF-RADIUS FOR DIFFERENT VELOCITY RATIOS

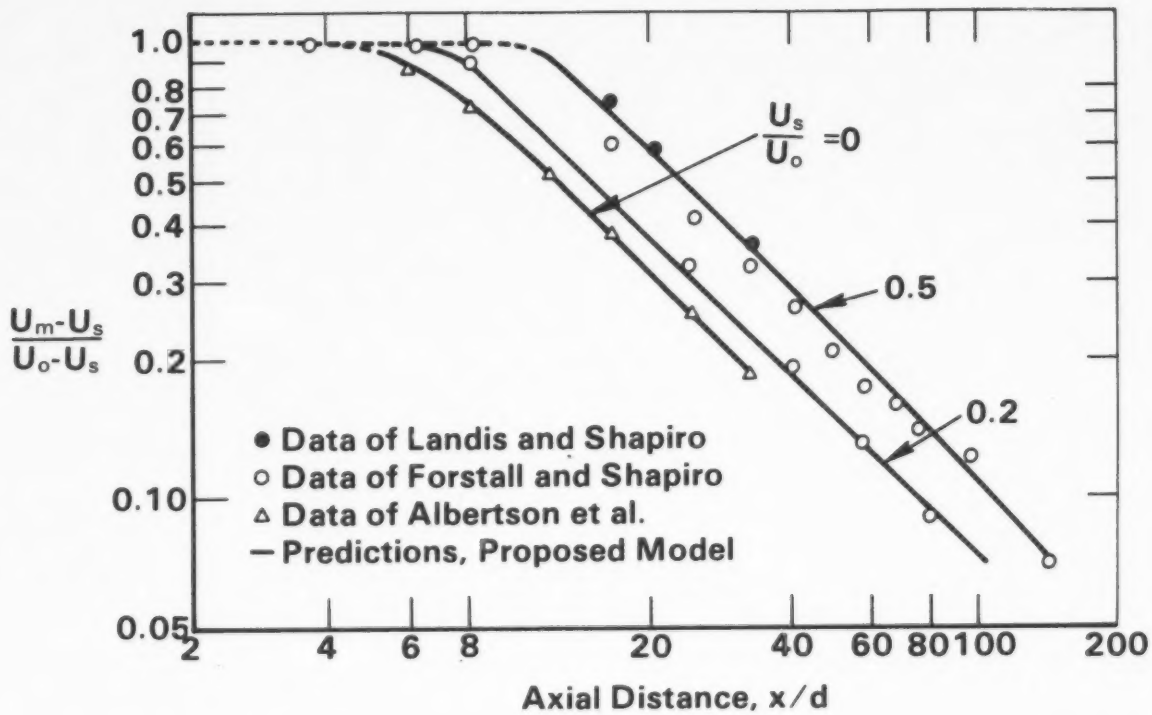

FIGURE 35. PREDICTED AND EXPERIMENTAL CENTER LINE VELOCITY FOR DIFFERENT VELOCITY RATIOS

coefficient. For a circular jet, Rajaratnam (following Bradbury[47]) suggests

$$\frac{U_m - U_s}{U_o - U_s} = 6.3 \left(\frac{U_o}{U_o - U_s}\right)^{1/2} / (x/d)$$

As U_s/U_o increasesover 1, simple equations for correlation are not available. One might use, however, data such as that of Abramovich, et al.[49], which cover ratios of U_s/U_o from 0 to 3 and ratios of external density to jet density from .27 to 8.2.

ENCLOSED COMPOUND JETS

When a compound or coaxial jet is confined, the expansion of the central jet causes an adverse pressure gradient until it reaches the wall, where further entrainment is prevented. Figure 13b, and single burner elements of 13a, together with their corresponding downstream region, can be considered as examples of this type of flow. If the annular flow is insufficient, compared to the jet flow, an annular recirculator region will occur, as shown in Figure 36[50]. Increasing the jet diameter compared to the enclosure diameter decrease the tendency for the recirculation to occur. A criterion dimensionless group, the Craya-Curtet parameter, C_T, characterizes the flow. This parameter is given by

$$1/C_T^2 = C = -3(q/Q)^2/2 + (q/Q) + (q/A)^2/A \qquad (30)$$

where Q is the total volume flow rate in the duct, q is the excess flow rate of the jet (deducting a flow through the nozzles area corresponding to the velocity external to the nozzle, and A is the ratio of the jet orifice area to the duct cross sectional area. This parameter can be considered a measure of the excess momentum available for mixing of the two streams. A slightly different Thring-Newby parameter is also used for the characterization. It has essentially the same value as the Craya-Curtet parameter over a wide range of variables[51]. Figure 37 shows how this parameter defines the size of the recirculation zone. The downstream end is very close to the impact region assuming an unconfined jet. The upstream boundary of the recirculation region moves toward the nozzle entrance as the value of C_T decreases. The maximum recirculation occurs at about the halfway point.

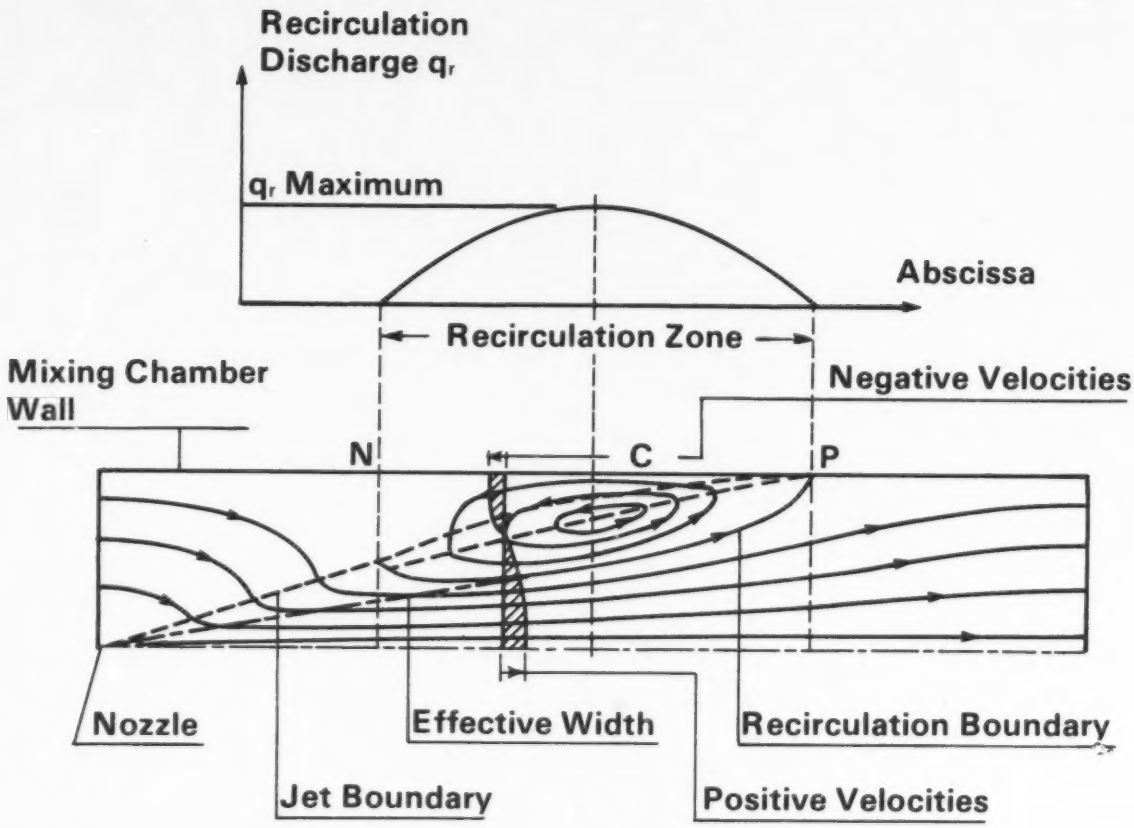

FIGURE 36. MAP OF THE RECIRCULATION FOR A DUCTED AXISYMMETRIC JET

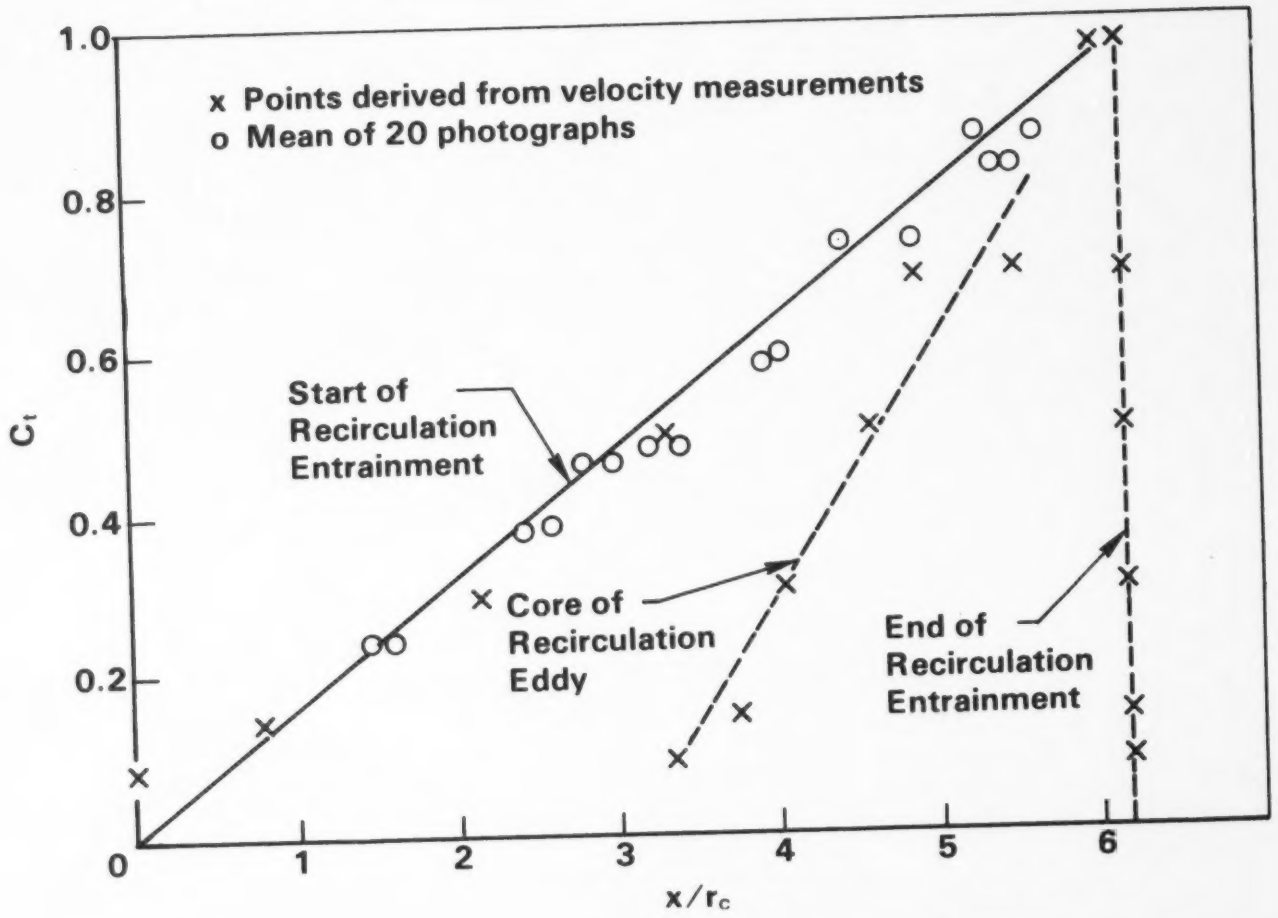

FIGURE 37. POSITION OF RECIRCULATION EDDY IN CONFINED JET

Figure 38[49] shows the variation of the maximum amount of recirculation, $(q_r)_{max}$, with the inverse of the simulation parameter, $1/C_T$.

The parameter C_T also affects the decay rate of the velocity on the axis and the spread rate of the jet. Figure 39 shows this influence on the velocity on the axis, U_m, (u_f is average velocity outside jet region). Figure 40 presents the rate of growth of the jet as a function of distance, for various values of C_T. Becker, et al.[52], put the relation of C_T in the form

$$1/C_T = (u_d^2 - u_k^2/2)^{1/2}/u_k \tag{31}$$

where

$$u_k = Q/\pi r_2^2 \tag{32}$$

and

$$u_d^2 = (u_1^2 - u_2^2)(r_1/r_2)^2 + u_2^2/2, \tag{33}$$

where u_1 is the jet velocity and u_2 is the outer annular velocity in the plane of the nozzle, and r_1 and r_2 are the nozzle and duct radii. Steward and Guroz[53] show that when there was a difference in density between the jet and annular flow, Becker's formulation of C_T could be modified simply by including density terms, thus

$$u_k' = (r_1^2 u_1 \rho_1 + (r_2^2 - r_1^2) u_2 \rho_2)/(r_2^2 \rho_e), \tag{34}$$

$$(u'_d)^2 = (u_1^2 \rho_1 - u_2^2 \rho_2)(r_1/r_2)^2/\rho_e + (u_2^2 \rho_2/2\rho_e) \tag{35}$$

where ρ_e is the mean density of the exit fluid defined on a mass basis.

Steward and Guroz find the velocity and temperature profiles are related in a similar manner to those for free jets, that is, the effective Prandtl number is the same as for the simple free jet.

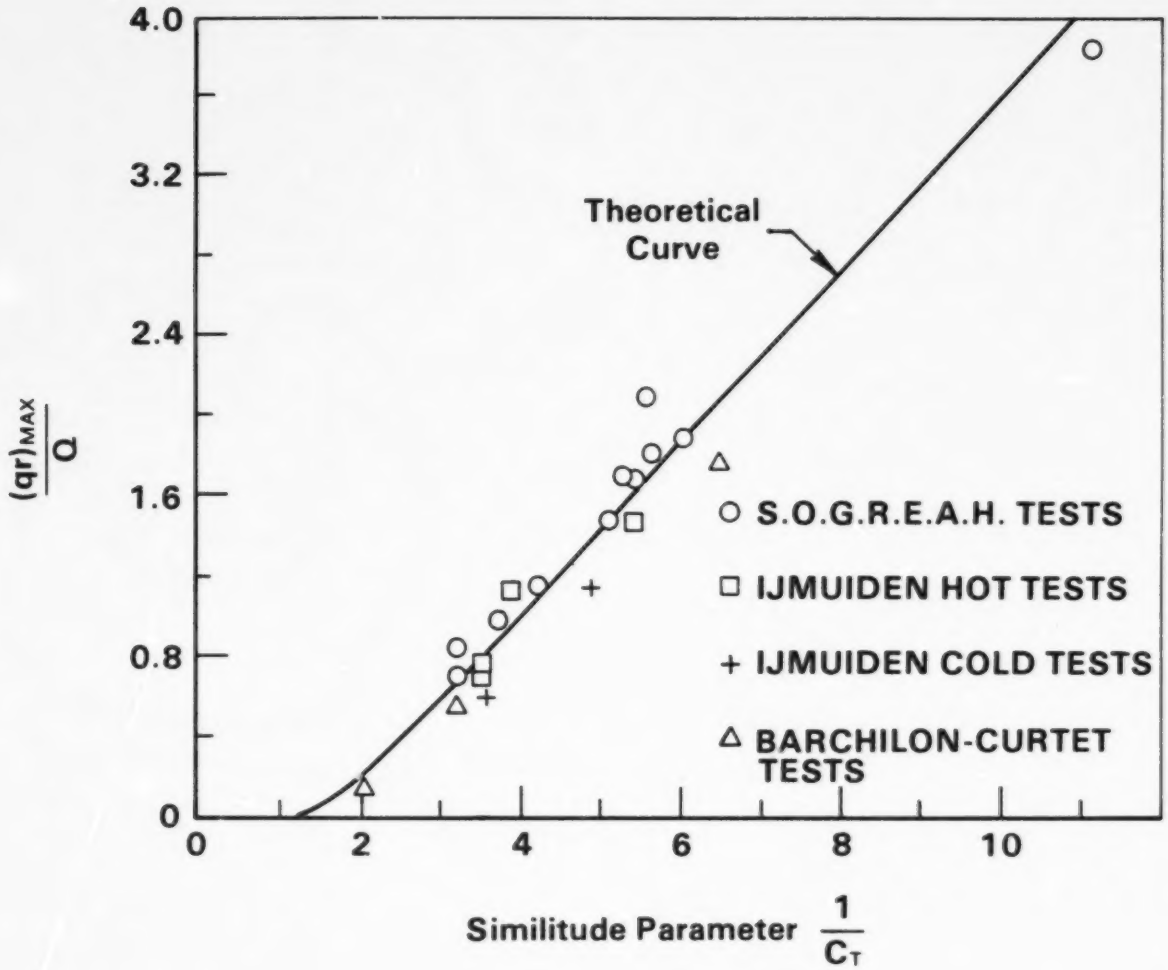

FIGURE 38. MAXIMUM RECIRCULATION FLOW RATE VERSUS $m^{1/2}$

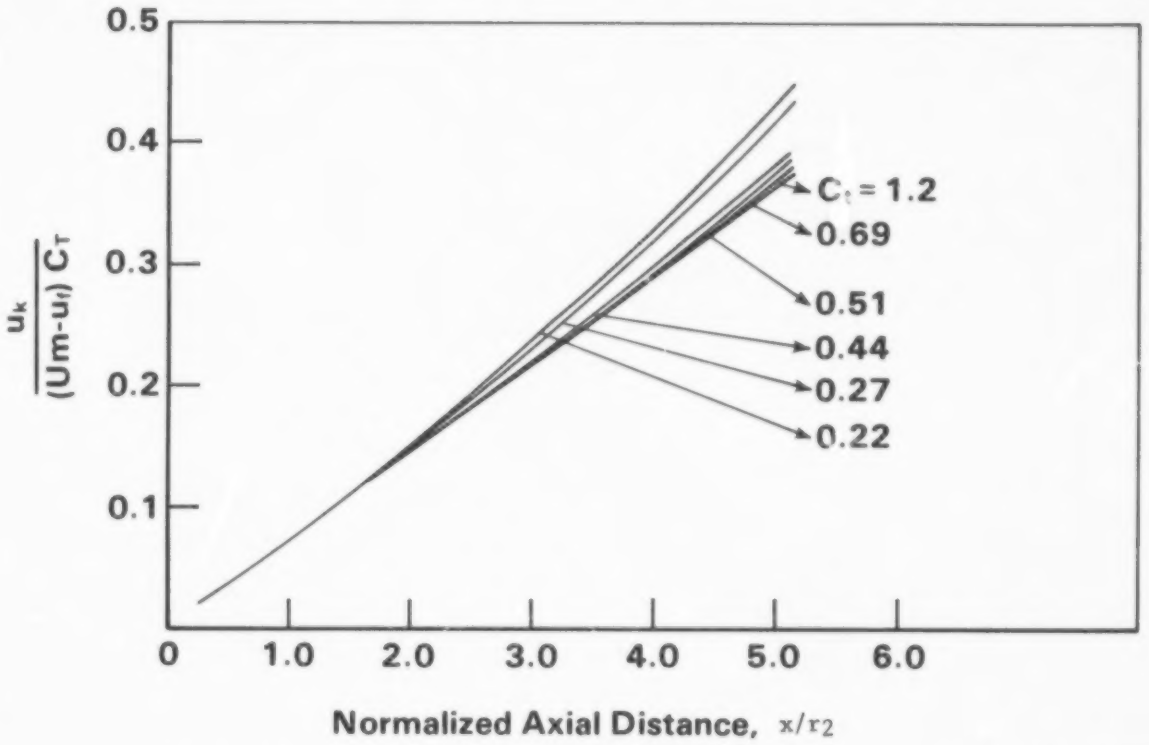

FIGURE 39. INVERSE MAXIMUM MEAN EXCESS VELOCITY (NORMALIZED) AS A FUNCTION OF AXIAL DISTANCE DIVIDED BY DUCT RADIUS FOR VARIOUS NON-ISOTHERMAL CRAYA-CURTET NUMBERS

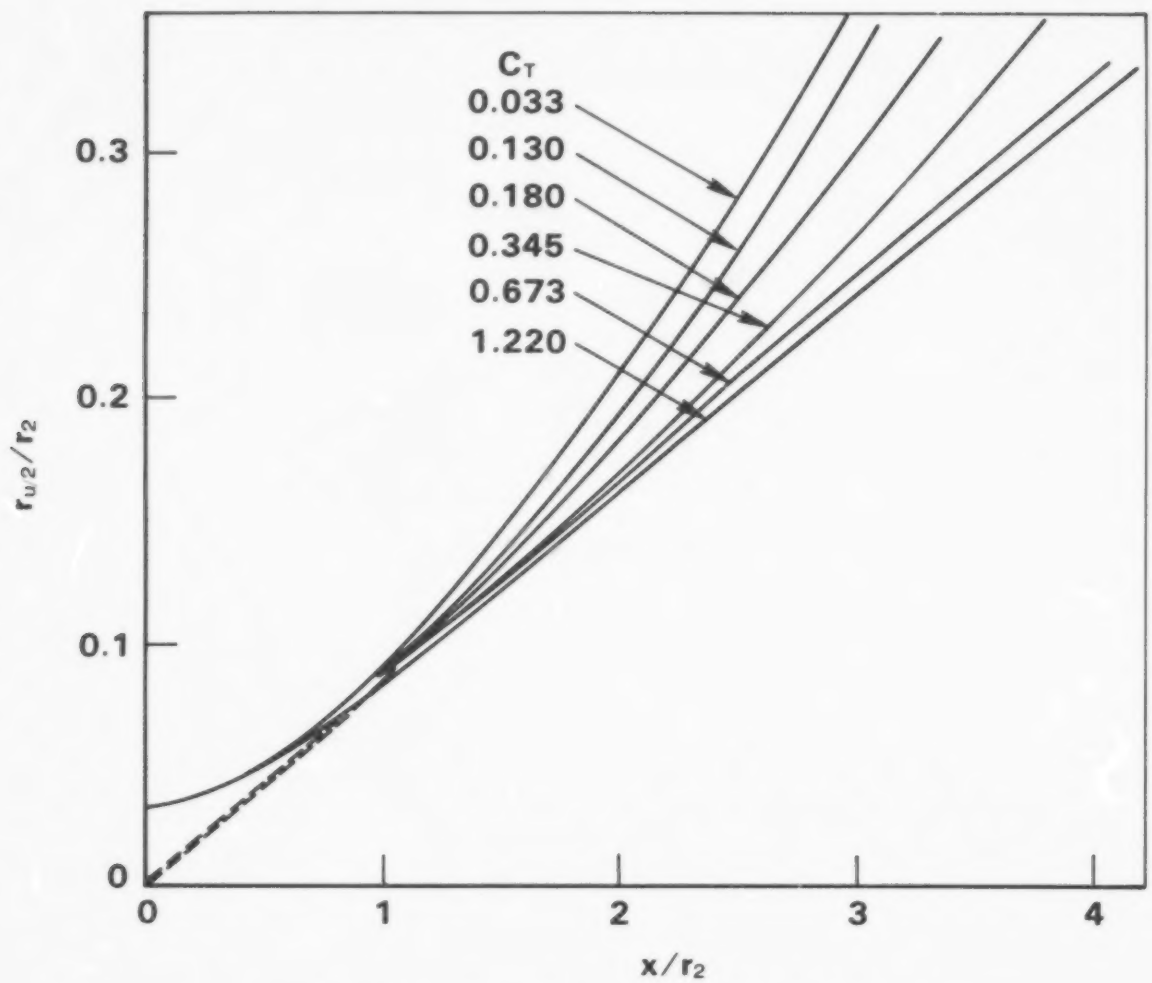

FIGURE 40. THE AXIAL GROWTH OF THE VELOCITY HALF-RADIUS

CIRCULAR JET WITH SWIRL

If an axially symmetric jet is given a certain amount of swirl before it exits from a nozzle, the jet spreads more rapidly and the velocity field decays more rapidly. Figure 16 b shows one use of such a jet. If the swirl is relatively strong, reverse flow can be produced on the axis in the region of the exit. Many nozzle mix burners have various degrees of swirl imparted to the fuel and/or air, with a resultant swirl flow of the exit gases from the burner. This flow can be treated as a swirling jet flow in the present study. Swirl combustors with a well-stirred region external to the burner are not used in incinerator afterburners and are not treated here. However, extensive reviews of this type of combustor are available in the literature[54,55,56].

The criterion term in predicting the performance of a swirl jet is the swirl number, S, where

$$S = G_\phi / G_z r_o. \tag{36}$$

In this formulation, G_z is the axial flux of axial momentum, comprised of momentum and pressure terms. The constant axial flux of angular momentum is designated as G_ϕ, and the orifice radius is specified by r_o (some investigators have used $2r_o$).

Chigier and Chervinski[57] studied the jet flow patterns resulting from various degrees of swirl at the exit of a duct. They distinguish three regions on the basis of their tests, a weak swirl region, a moderate swirl region, and a strong swirl region. As shown in Figure 41, the radial distribution of axial velocity spreads slowly outward, and then seems to halt. However at the same time, when the strong swirl region is reached ($S \tilde{=} .5$) a dip occurs in the velocity profile near the nozzle (see Curve f) and the dip becomes increasingly strong as the swirl increases. In the very strong swirl region, reverse flow on the axis occurs. From Figure 42, it is seen that weak swirl is characterized by a narrow high velocity swirl region. For moderate swirl, the region widens and also moves outward. In the strong swirl region, the wide swirl region moves back toward the axis.

The half velocity jet is defined in terms of the angle α (where $b/x = \tan \alpha$) as $\alpha = 4.8 + 14\ S$. The axial velocity relation is defined as

$$(u_m/u_{mo})[(x+a)/d] = 1/(.147 + S^2) \tag{37}$$

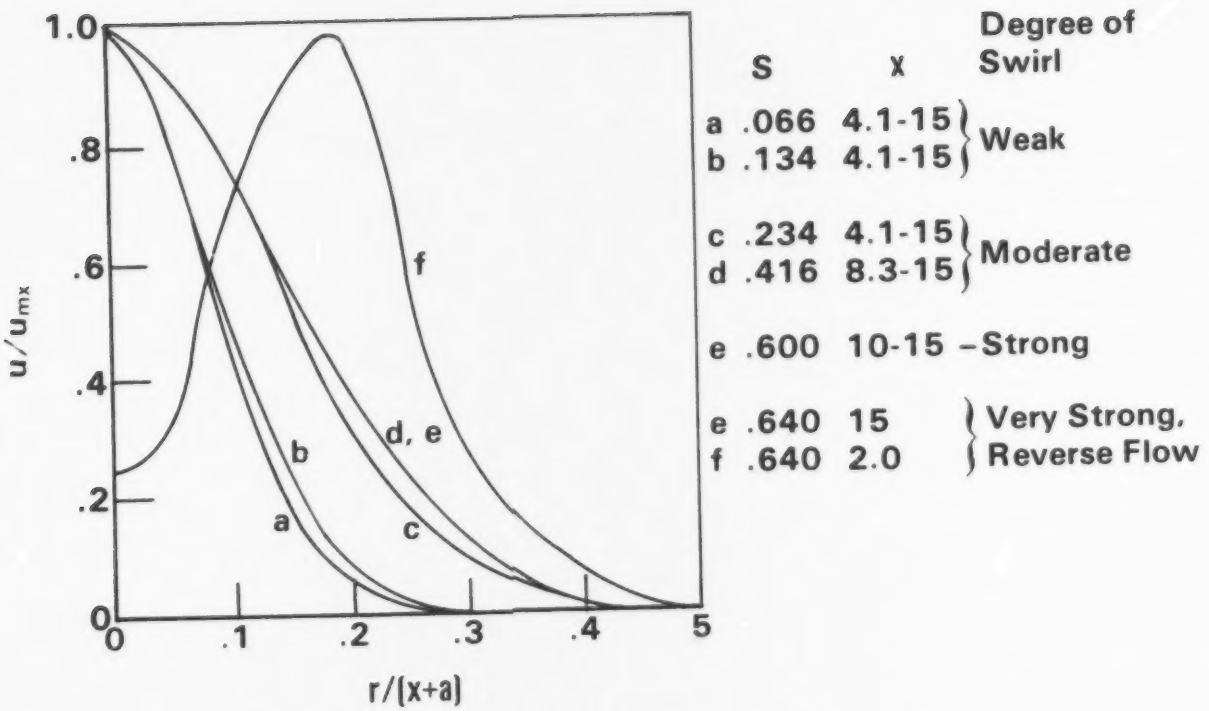

FIGURE 41. RADIAL DISTRIBUTION OF AXIAL VELOCITY

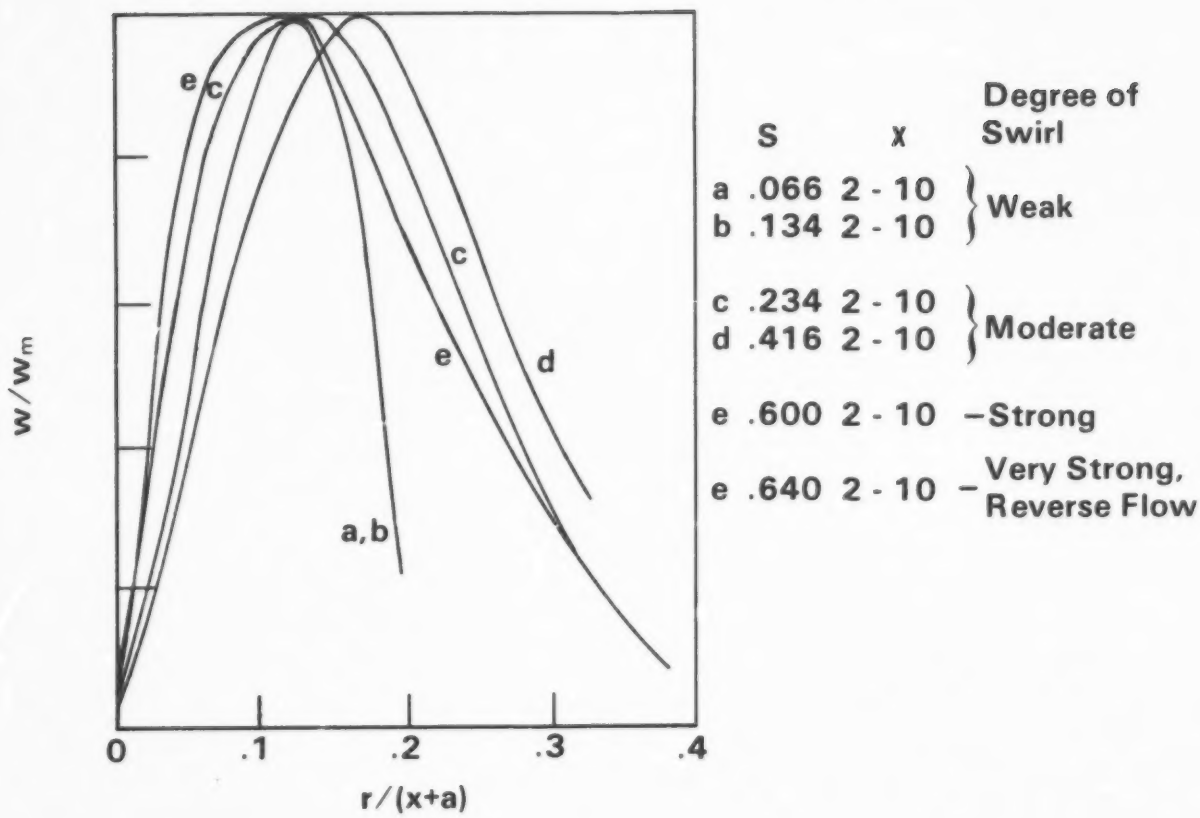

FIGURE 42. RADIAL DISTRIBUTION OF SWIRL VELOCITY

and the mass flow rate is defined by[36]

$$(Q/Q_o)(d/x) = (.32 + .8S). \qquad (38)$$

The intercept value "a" is equal to 2.3d.

It is clear that for mild swirl with no depressed central velocity, the swirl essentially increases the mixing rate.

JETS IN CROSS FLOW

The jet combinations that have been discussed thus far have involved a jet flow parallel to the general flow axis of the system. Many afterburners involve single or multiple jets at other angles to the general flow axis. Examples are shown in Figures 4c, 6b, and 22. For jets in cross flow, the angle is usually 90°, corresponding to the area of major research effort and information, but may be at other values. To a first approximation, the flow can be considered on the basis of a distortion of a normal jet. In fact, one of the significant coordinates of the jet is the distance along the jet axis. (At least four different definitions of the jet axis are considered in the literature, although not always specifically defined. The first is defined by the maxima of the velocity. The second is defined by the maxima of the total prssure. The third is defined by a maximum of composition. The fourth, termed the centerline of the jet by Rajaratnam[36], is photographically defined. All are quite close together.) As the jet emerges, the shear forces of the cross-flow act on the jet. They gradually force the jet over and, at the same time, force the jet from a circular shape into a kidney shape formed by the two counter-rotating vortices that are generated. The length of the potential core is also reduced, roughly by a fractional reduction equal to $3.2\ U_{\text{cross wind}}/U_{\text{jet}}$ for small relation values of cross-wind velocity.

In terms of the x coordinate along the direction of crosswind flow and the y coordinate at right angles, in the original jet direction, the outer profile, centerline profile, and inner profile fit rather closely to straight lines on log-log plots. Pratte and Baines[58] give the relation

$$(y/d)(U_{CW}/U_o) = K\ [(x/d)(U_{CW}/U_o)]^{0.28} \qquad (39)$$

for a large variation of the velocity ratio, where K is 2.63 for the outer profile, 2.05 for the centerline profile, and 1.35 for the inner profile.

A closer examination of the data, however, does show a break in the data. Using the distance along the jet centerline, however, does show a break in the data. Using the distance along the jet centerline, s, rather than x as a coordinate, the data are found to fit very closely the relation y = s up to 2.08, where the relation

$$(y/d)(U_{CW}/U_o) = 1.63\ [(s/d)(U_{CW}/U_o)]^{1/3} \qquad (40)$$

becomes valid.

In cases where the injection angle is other than 90 , Platten and Keffer[36,59] gave values of axial position from 45° (downstream) to 135° (upstream), for ratios of U_o/U_{CW} of 4.05 to 8.32. Margason[36,60] gives values from 30° to 150°, at ratios of U_o/U_{CW} from 2 to 10. Bergeles, et al.[61] noted two contrasts between the discharge from a jet pointed downstream, at 30° from the overall flow direction, and a jet directed normal to the flow (90°). In the angled jet, the disturbance in the flow field are mainly downstream of the orifice; these included large variations in streamwise recirculation. For jet velocities about .3 the free stream velocity (uniform density) the jet remains essentially attached to the surface; for values above .5, the jet lifts completely from the surface and penetrates the main flow.

The exact shape of the kidney-shaped jet and the rate of growth is now considered. Rajaratnam suggests that b_{CW}, the half velocity radius, be given for the jet in cross wind by $b_{CW} = .215\ s$; this corresponds to the radial distance in the plane of the original jet flow and wind direction, and normal to the jet axis. Comparing this with the unblown jet coefficient of 0.1, and noting that the distance to the half velocity from the axis is larger in other directions in the plane normal to the axis, it is seen that the cross wind causes a large increase in the rate of mixing. This is important in afterburner design.

The velocity profile is of the same character as found with unblown jet flow, and also does not vary in character with direction from the axis[36]. Rajaratnam has also collected in Figure 43 several results on the variation of the shape in the plane normal to the jet axis, which are plotted against the dimensionless distance along the jet (note the square term on the velocity ratio); these results cover the ratio of the jet perimenter, p, to the square root of the cross sectioned area, the jet width to total depth, and the width to the depth, on the centerline. From this information, profiles for computing the mixing may be derived.

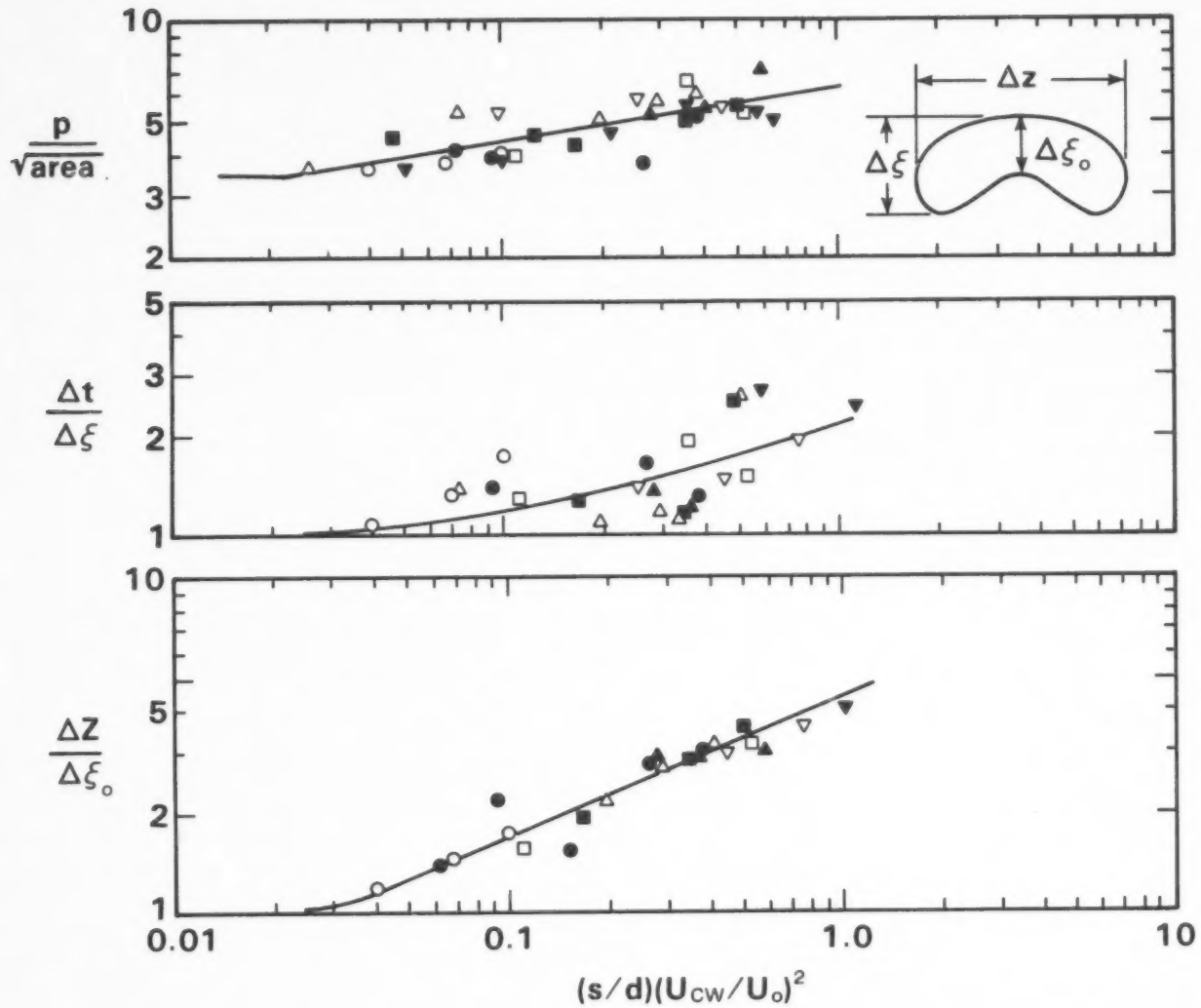

FIGURE 43. GEOMETRY OF THE KIDNEY SHAPE OF THE CIRCULAR JET IN CROSS-FLOW

In an extensive series of tests on cross flow of jets of four different fuel gases over a range of jet temperatures, Hoehne and Luce[62] found the data could be correlated by using the same square root of density modification to the velocity ratio terms as outlined previously. That is, the momentum term ρU^2 was considered to be the significant term. While a small but consistent additional effect of temperature was also found, for present purposes this may be disregarded.

One of the authors has found that satisfactory predictions of combustion performance can be made in the case of multiple jets in a crosswind by the simple addition of the concentrations of the individual jets.

JET IMPINGEMENT

Impingement of a gas jet upon a surface can occur in an afterburner, either accidentally or in the process of inducing cross-channel mixing[9] (i.e., Figures 8b and 17b). This section outlines the main features of the impinging flow and the relevant variables involved.

Flow Field

The flow field produced by the impingement of a turbulent subsonic jet against a surface (whose diameter is large compared to that of the jet) can be subdivided into three characteristic regions (Figure 44): (1) the free jet, upstream of any strong local interaction effects due to impingement; (2) the stagnation flow, where the strong (essentially inviscid) interaction of the jet with the surface produces a change in flow direction; (3) the wall jet, consisting essentially of flow along the surface beyond the point at which the strong interactions of impingement cause any local effects[63,64,65]. The following discussions will be limited to axially symmetric geometry; qualitatively the results will be valid for plane geometry too, but the quantitative expressions will, in general, be different.

The jet broadens linearly in the flow direction z' by momentum exchange with the surrounding gas up to a distance z_g from the solid surface, which marks the boundary of the stagnation region. Immediately downstream from the nozzle exit (where the velocity profile is nearly uniform) there is a "potential core" in which the velocity on the axis

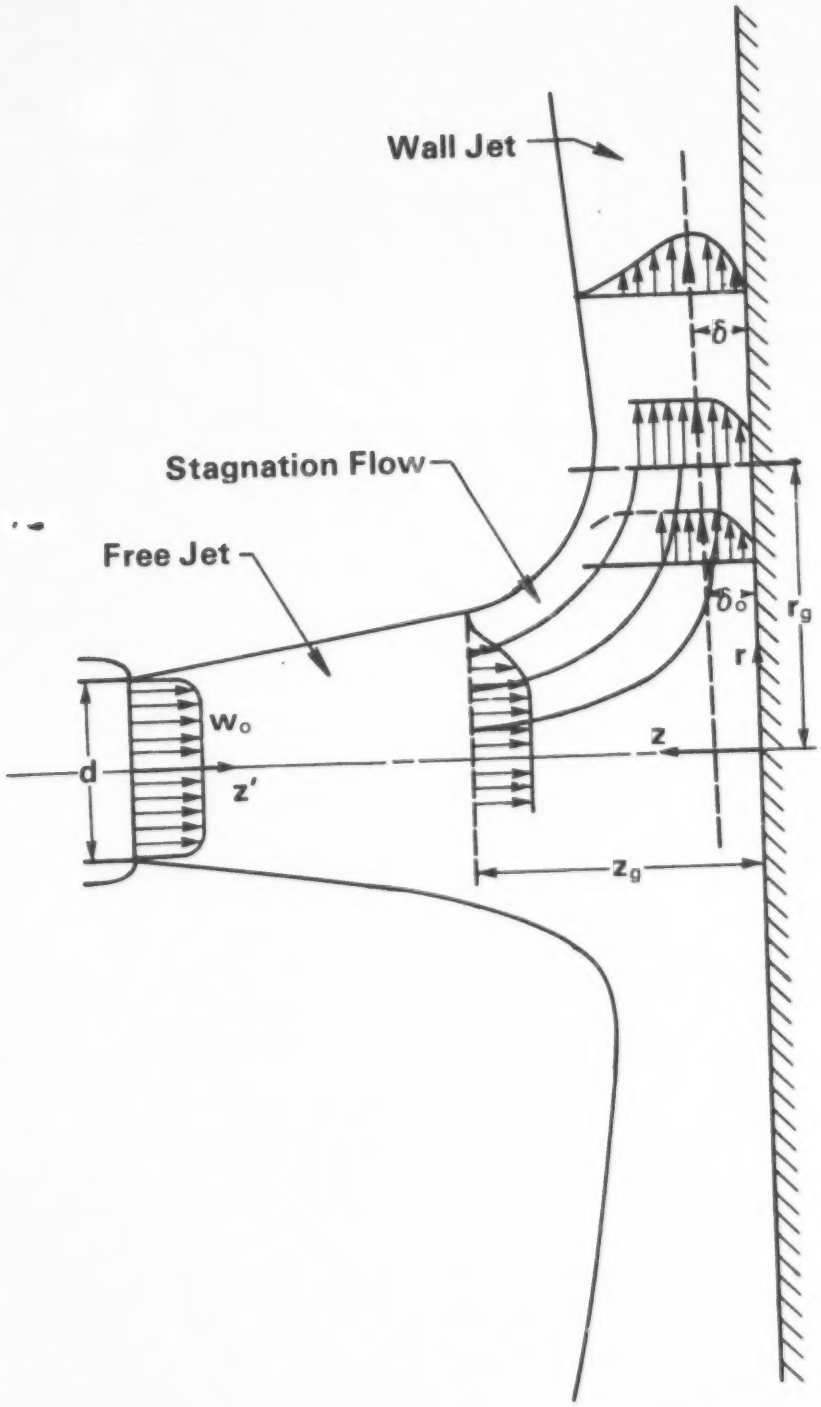

FIGURE 44. FLOW FIELD OF NORMALLY IMPINGING JET

is nearly constant. The core length z'_k is normally about five to seven nozzle diameters. For a sufficient length of the free jet, the velocity profile approaches a Gaussian distribution:

$$\frac{w(r, z')}{w(0,z')} = \exp\left[-\left(\frac{r}{Cz'}\right)\right] \tag{41}$$

where $C \simeq 0.1$. Equation 41 is valid between z'_k and z_g. The velocity on the axis in the whole free jet region can be calculated by[66]

$$\frac{w(0,z')}{w_d} = \left\{1-\exp\left[-\left(\frac{d/z'}{\sqrt{2}\ C}\right)\right]^2\right\}^{1/2} \tag{42}$$

With increasing jet length ($z' \gg z'_k$) Equation 42 asymptotically approaches the well-known hyperbolic law for the dependence between axial velocity and distance from the exit:

$$\frac{w(0,z')}{w_d} \rightarrow \frac{1}{\sqrt{2}\ C}\frac{d}{z'} \tag{43}$$

Stagnation flow begins relatively close to the surface ($z_g \simeq 0.14$ H, according to Beltaos and Rajaratnam[67]. Here the axial velocity component is decelerated and transformed to an accelerated radial one. The velocity components outside the boundary layer are given by:

$$w_z = -2a_R z, \qquad w_r = a_R r \tag{44}$$

where, for real stagnation flows due to impinging jets of finite diameter[68]

$$a_R = \left(\frac{w_d}{D}\right)\left(1.04 - 0.034\ \frac{H}{D}\right), \quad (1 \leq H/D \leq 10) \tag{45}$$

The boundary layer thickness (defined as the distance from the surface where w_r reaches 99 percent of the value in Equation 44) is

$$\delta_o = 1.95 \left(\frac{\upsilon}{a_R} \right)^{1/2} = \frac{1.95}{\sqrt{Re}} \left(1.04 - 0.034 \frac{H}{D}\right)^{-1/2} \qquad (46)$$

and is therefore inversely proportional to the exit Reynolds number.

The wall parallel velocity component w_r initially increasing linearly from zero must reach a maximum value at a certain distance r_g from the stagnation point and finally decrease to zero in the fully developed wall jet. The end of the stagnation flow region is at about[67] $r_g = 0.22H$. Whereas the stabilizing effect of acceleration keeps the boundary layer laminar in the stagnation zone, transition to turbulence generally will occur immediately after r_g in the decelerating flow region. Wall boundary layer and free jet boundary grow together, forming the typical wall jet profile where the boundary layer δ is defined as the locus of the maxima of the velocity $[z(w_{r_{max}})]$. This maximum velocity is expressed as

$$w_{r_{max}} \propto 1/r^n \qquad (47)$$

where values of n ranging from 1.1 to 1.143 have been reported.

Entrainment of surrounding air by the jet is larger than that of a free jet[69].

Angle of Impact. For impact angles smaller than 90°, the initially axisymmetric flow field spreads out after impingement across the surface, and tends toward a two-dimensional flow[70]. The radical changes occurring in the structure of the jet cause a change in the velocity decay function so that for

$$\begin{aligned} x < 0 \quad & w_{x_{max}} \sim 1/x \\ x > 0 \quad & w_{x_{max}} \sim 1/x^{1/2} \end{aligned} \qquad (48)$$

where x is the axial distance along the impact plate from the point of impingement. The flow distribution after impingement can be derived approximately from the inviscid solution for the two-dimensional case[71]. From this, if Q is the jet flow rate, and ϕ the impact angle (Figure 45), the flow rate in the direction making an acute angle with the jet axis is

$$Q' = \frac{1-\cos\phi}{2} Q \qquad (49)$$

while that in the opposite direction is

$$Q'' = \frac{1+\cos\phi}{2} Q \quad . \qquad (50)$$

Arrays of Nozzles. The impinging flow from arrays of nozzles generally shows the same three flow regions--free jet, stagnation zone, wall jet--but in addition there are secondary stagnation zones where the wall jets of adjacent nozzles impinge upon each other. These secondary stagnation zones are characterized by boundary layer separation and eddying of the flow. This can lead to a considerable influence on the other flow regions, especially for smaller spacings among the nozzles of an array.

Heat Transfer

External variables influencing heat and mass transfer in impinging flows are on one hand mass flow rate, kind and state of the gas, and on the other hand shape, size, and position of the nozzles relative to each other and to the solid surface. An exhaustive review of impinging jet flow heat and mass transfer has been given by Martin[72].

The local heat-transfer coefficient at the stagnation point on the impingement plate reaches a maximum value at the apex of the potential core. Since the centerline velocity is constant in the potential core, the observed increase in heat transfer coefficient must be due to the effects of turbulence. The centerline jet velocity decreases beyond the apex of this core; therefore, maximum heat transfer will be obtained if the impingement plate is separated from the nozzle exit by the length of the potential core.

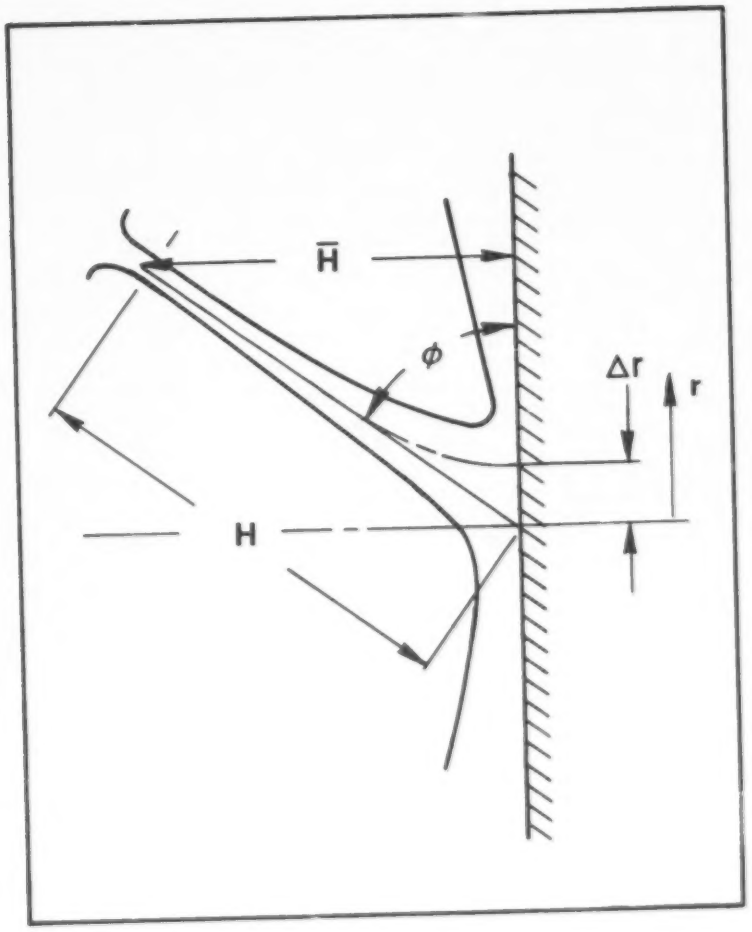

FIGURE 45. INCLINED IMPINGING JET

In the radial direction, the local heat transfer coefficient decreases monotonically with r for large H/D, but has a more or less distinct hump or second maximum for small H/D. This increase of the transfer coefficient begins immediately after the end of the accelerated flow region, where the disappearance of the stabilizing streamwise pressure gradient leads to a sudden step in turbulence level. Arrays of nozzles show qualitatively similar results. In addition, there may occur further peaks in the lateral variation of the transfer coefficients where the wall jets of adjacent nozzles impinge upon other forming secondary stagnation zones.

For a single round nozzle, the integral mean values of the heat transfer coefficient over a radius r can be correlated by the following empirical equation[72]

$$\frac{\overline{Nu}}{Pr^{0.42}} = \frac{D}{r} \frac{1 - 1.1\ D/r}{1+0.1\left[(H/D)-6\right]D/r} F(Re) \qquad (51)$$

where

$$F(Re) = 2Re^{1/2}\left(1 + \frac{Re\ 0.55}{200}\right)^{0.5}, \qquad (52)$$

[72]

Range of validity:

$2000 \leq Re \leq 400{,}000$

$2.5 \leq r/D \leq 7.5$

$2 \leq H/D \leq 12$

Equation 34 may approximately be used for impact angles smaller than 90°. Only the nozzle to plate distance must not be used normal to the plate, but normal to the nozzle exit cross section (Fig. 45):

$$H = \bar{H}/\sin \phi \qquad (53)$$

The stagnation point (or the point of maximum heat transfer) shifts by a length Δr toward the part of the jet being deflected in the acute angle. This length may be approximated by:

$$\Delta r = A \cot \phi \qquad (54)$$

where

$$A = 1.4\ (D + 0.11\ H) \qquad (55)$$

NOMENCLATURE FOR SECTION 4 ONLY

A	Multiplying coefficient, (Eq. 24)
a_r	Stagnation coefficient (Eq. 45)
B	Additive coefficient (Eq. 24)
b	half velocity radius
b^*	half momentum radius
b_c	half concentration radius
b_{cw}	half velocity radius of jet in cross wind
C	$1/C_T^2$
C_T	Craya-Curtet parameter (Eq 30)
C_m	concentration on jet axis
C_o	concentration in nozzle
d	nozzle diameter
d_o	prototype nozzle diameter
d_{model}	diameter of nozzle as adjusted for density ratio
D	nozzle diameter
$E_{(x)}$	kinetic energy of jet
E_o	kinetic energy of nozzle
G_ϕ	axial flux of angular momentum
G_z	axial flux of axial momentum
H	nozzle to wall distance
Q	total flow rate
Q_o	volume flow rate from nozzle
$Q_{(x)}$	volume flow rate of jet
q	excess flow rate of jet
q_r	recirculation flow
r	radial dimension
r_c	chamber radius
r_o	orifice radius for swirl flow
r_g	distance from wall of maximum velocity parallel to surface in impinging flow

r_1	nozzle radius
r_2	duct radius
S	swirl number (Eq 36)
s	distance along centerline of jet in cross wind
T	temperature
T_o	nozzle temperature
T_m	temperature on axis
T_s	ambient temperature
U	velocity
U_{CW}	cross-wind velocity
U_m	velocity on axis
U_o	core velocity
U_s	ambient velocity
u_d	see Eq 33
u_d'	see Eq 35
u_f	average velocity outside jet region
u_k	$Q/\pi r_2^2$
u_k'	value of u_k corrected for density differences (Eq 34)
u_m	axial velocity
u_{mo}	axial velocity at throat
u_1	jet velocity
u_2	outer annulus velocity
w	swirl velocity (tangential velocity)
w	velocity of impinging jet
w	slot width
w_m	maximum swirl velocity
w_d	nozzle velocity for impinging jet

x	axial distance
y	distance normal to x-axis to plane jet
z'	flow direction of impinging jet
z_g	stagnation region thickness
z_K	core length of impinging jet
α	half angle of jet spread
δ_o	boundary layer thickness (Eq 46)
θ'	temperature fluctuation
$\bar{\theta}$	average temperature
υ	kinematic viscosity
ρ_b	furnace gas density
ρ_e	mean density of exit fluid from duct
ρ_o	nozzle density
ρ_s	ambient density
ϕ	impact angle

SECTION 5

SUMMARY AND CONCLUSIONS

This report on afterburner mixing phenomena is a companion to an earlier report, Reference 8, which discussed chemical aspects of afterburner systems. The report on chemical kinetics brought together information for estimating time-temperature-composition relations necessary to carry out the oxidation of various organic fumes. In the present report, sufficient information is given to permit the estimation of comparative values for various fluid dynamic systems that can be used as afterburners. These values can then be compared to the requirements based on Reference 8 to determine if a design is acceptable. The report is divided into three phases, namely, a review of direct flame afterburner systems, a consideration of the possibilities of using mathematical modeling in designing such systems, and a review of the empirical relations that can be used in the description of the mixing associated with various jet-like components of an afterburner.

Direct flame afterburner systems may be considered as composed of a fume polluted air source, a recuperator section (usually), an approach section to the burner section, a burner section, a combustion chamber section, possibly a catalytic section, the other side of the recuperator section (usually), and an exhaust. In this study, the sections involved in the mixing process related to the incineration of the fumes, namely, the approach section, the burner section, and the combustion chamber section, are considered. A large variety of designs in these three sections is found, with no clear-cut preference for any particular combination. This is because of conflicting requirements relative to capital cost, maintenance cost, size, complexity, fuel consumption, needed flexibility, and pollutant type, as well as variations in code restrictions and contract specifications. However, well-documented field studies of actual performance would undoubtedly eliminate many of the available fume afterburner systems as viable products[74].

Mathematical modeling of combustion systems is receiving great attention in the current literature. Therefore, the pertinence of these studies to the design of practical fume afterburners is considered in

some detail. It is pointed out that mathematical modeling is only one of many possible design approaches. In the proper formulation of the pertinent equations, the character of the turbulence must be understood before suitable approximation can be made in mathematically specifying the turbulence at any point in a combustion system. Even then, the mathematical models contain arbitrary coefficients based on the fit of analytical results to experimental results for a particular experimental flow system. For best results, then, the particular system on which the coefficients are based should resemble the afterburner design of interest. Comparing the complexity of the typical afterburner with the simplicity of most experimental systems used in connection with specifying the parameters of a mathematical model, some pitfalls of this design approach become apparent. On the other hand, because the flow and reaction region of interest in the primary fume incineration process does not involve the high fuel concentration, high reaction rate and high temperatures of the more usual types of combustion systems, there are simplifications possible in the application of mathematical modeling to fume incinerator design. It is concluded that the practical use of mathematical modeling for fume afterburner designs is at least 5 years away.

For the same reason that there appears to be a possible simplification in the use of mathematical modeling, there also appears to be a possible simplification in using literature on various forms of jets to estimate the time-temperature-composition profiles as the hot combustion gases are mixed into the fume-laden secondary air flow. From such information, one can check whether the time-temperature-composition requirements predicted for a specific fume are met. Because of the low reaction rate, "cold jet" data may be used rather than having to invoke the complications of intense combustion process taking place in the jet flow. This opens up a wide range of applicable data in the literature, with rather simple relationships available for predicting the mixing features of a jet and its surroundings. Specifically, in this study, the following types of turbulent jets are reviewed--circular free jet, plane free jet, free compound jet, enclosed

compound jet, circular jet with swirl, jets in cross flow, and impinging jets. The information in this literature is believed to be sufficient to permit the calculation of adequate time-temperature-composition curves for most reasonable fume afterburner designs.

REFERENCES

1. Hawthorne, W. R., D. S. Weddell, and H. C. Hottel. Mixing and Combustion in Turbulent Gas Jets. Third Symposium on Combustion, The Combustion Institute. 1949. 266-288.

2. Brown, G, and A. Roshko. The Effect of Density Difference on the Turbulent Mixing Layer. Turbulent Shear Flows, AGARD-CP-93. 23.1-23.12. 1971.

3. Yule, A. J. Observations of Late Transitional and Turbulent Flow in Round Jets. Symposium on Turbulent Shear Flow, Penn State University. 11.13-11.21. April, 1977.

4. Roshko, A. Open Forum. Free Turbulent Shear Flow, Vol. 1, NASA SP-321, 629-635. 1973.

5. Jimenez, J. On the Visual Growth of a Turbulent Mixing Layer. J. Fluid Mech., 96:447-460, 1980.

6. Pauletta, C. Fume Incineration. Pollution Engineering, 2:21-23, Mar-Apr, 1970.

7. Gruzdev, V. W., M. D. Targer, and A. V. Talantov. Self-Ignition of Kerosene in a Flux of Non-Equilibrium Combustion Products. Combustion, Explosions, and Shock Waves, 490-492. Jan, 1980.

8. Barnes, R. H., M. J. Saxton, R. E. Barrett, and A. Levy. Chemical Aspects of Afterburner Systems, EPA-600/7-79-096. 1979.

9. Rolke, R. W., R. D. Hawthorne, C. R. Garbett, E. R. Slater, and T. T. Phillips. Afterburner Systems Study. EPA-R2-72-062, PB 212,560. Aug, 1972.

10. Reed, R. J. North American Combustion Handbook, 2nd Edition, North American Manufacturing Co., Cleveland, OH. 1978.

11. Michelfelder, S. Survey on Prediction Methods for Calculation of Furnace Performance. Fourth Members' Conference, International Flame Research Foundation. 1976.

12. Thring, M. W. and M. P. Newby. Combustion Length of Enclosed Turbulent Jet Flames. Fourth Symposium on Combustion. 789-796. 1953.

13. Curtet, R. Confined Jets and Recirculation Phenomena with Cold Air. Combustion and Flame, 2:383-411. 1958.

14. McDonald, H. Combustion Modeling in Two and Three Dimensions--Some Numerical Considerations. Prog. Energy Combust. Sci. 5:97-122. 1979.

15. Tennekes, H. and J. L. Lumley. A First Course in Turbulence. The MIT Press. 1972.

16. Hinze, J. O. Turbulence. Second Ed., McGraw-Hill. 1975.

17. Bradshaw, P. An Introduction to Turbulence and Its Measurement. Pergamon Press. 1971.

18. Spalding, D. B. Mathematical Models of Turbulent Flames; A Review. Combus. Sci. Technol., 13:3-25. 1976.

19. Launder, B. E. and D. B. Spalding. Mathematical Models of Turbulence. Academic Press. 1972.

20. Harlow, F. H. Turbulence Transport Modeling. AIAA Selected Reprint Series, V. XIV, AIAA, New York. 1973.

21. Mellor, G. and H. Herring. A Survey of the Mean Turbulent Field Closure Models. AIAA J. 11:590. 1973

22. Gosman, A. D., et al. Heat and Mass Transfer in Recirculating Flows. Academic Press. 1969.

23. Schefer, R. W. and R. F. Sawyer. Pollutant Formation in Fuel Lean Recirculating Flows. NASA CR-2785. 1976.

24. Arbib, H. A., Y. Goldman, J. B. Greenberg, and Y. M. Timmat. A Numerical Model of High Intensity Confined Hydrocarbon Combustion. Combustion and Flame. 38:259-270. 1980.

25. Altenkirch, R. A. and A. M. Mellor. Continuous Flow Predictions of Measured Species Concentrations with a Prevaporizing Combustor. Report No. PURDU-CL-75-01, Purdue University, West Lafayette, IN. 1975.

26. Edelman, R. B. and O. F. Fortune. A Quasi-Global Chemical Kinetic Model for the Finite-Rate Combustion of Hydrocarbon Fuels. AIAA Paper No. 69-86. 1969.

27. Edelman, R. B. and P. T. Harsha. Laminar and Turbulent Gas Dynamics in Combustors-Current Status. Progress Energy Comb. Sci., 4:1-62, 1978.

28. Gosman, A. D., F. C. Lockwood, and A. P. Salooja. The Prediction of Cylindrical Furnaces Gaseous Fueled with Premixed and Diffusion Burners. 17th Symp. (Int'l) on Combustion. 1979. pp 747-760.

29. Gosman, A. D. and W. M. Pun. Calculation of Recirculating Flow. Heat Transfer Report No. HTS/74/2, Imperial College, London. 1973.

30. Patankar, S. V. and D. B. Spalding. Heat and Mass Transfer in Boundary Layers, 2nd ed. Intertext, London. 1970.

31. Abou Ellail, M.M.M., A. D. Gosman, F. C. Lockwood, and I.E.A. Megahed, Description and Validation of a Three-Dimensional Procedure for Combustion Chamber Flows. Progress in Astronautics and Aeronautics. 58:163-190. 1978.

32. Greenberg, J. B. and C. Presser. A Fully Automatic Method for Predicting Internal Reacting Flows. TAE No. 389, Dept of Aeronautical Engineering, Technion, Haifa, Israel. 1979. To appear in J. Comp. Phys.

33. Launder, B. E. and D. B. Spalding. The Numerical Computation of Turbulent Flows. Computer Methods in Applied Mechanics and Engineering, 3:269-289. 1974

34. Lockwood, F. C. The Modeling of Turbulent Premixed and Diffusion Combustion in the Computation of Engineering Flows. Combustion and Flame, 29:111-122. 1977.

35. Abramovich, G. The Theory of Turbulent Jets. M.I.T. Press. 1963.

36. Rajaratnam, N. Turbulent Jets. Elsevier. 1976.

37. Field, M. A., et al. Combustion of Pulverized Fuel. Part 2. Flow Patterns and Mixing. British Coal Utilization Research Association Bulletin. 30:455-522. 1966.

38. Becker, H. A., H. C. Hottel, and G. C. Williams. The Nozzle-Fluid Concentration Field of the Round, Turbulent, Free Jet. J. Fluid Mechanics, 30:285-303. 1967.

39. Lockwood, F. C. and H. A. Moneib. Fluctuating Temperature Measurements in a Heated Round Free Jet. Combustion Science and Technology, 22:63-81. 1980.

40. Schlichting, H. Bounday Layer Theory. McGraw-Hill. 1968.

41. Forstall, W., Jr. and A. H. Shapiro. Momentum and Mass Transfer in Coaxial Gas Jets. ASME J. Applied Mechanics, 399-408. 1950.

42. Golubev, V. A. and V. F. Klimkin. Investigation of Submerged Turbulent Gas Jets with Different Densities. J. Eng. Phys., 333-338. 1978.

43. Steward, F. R. and A. G. Guroz. Aerodynamics of a Confined Jet with Variable Density. Combustion Science and Technology, 16:29-45. 1977.

44. Sforza, P. M. and R. F. Mons. Mass, Momentum, and Energy Transport in Turbulent Free Jets. Int. J. Heat Mass Transfer. 21:371-384. 1978.

45. Thring, M. W. Some Recent Developments in the Physics of Fuel Combustion. British J. Applied Physics, 8:89-97. 1957.

46. Ricau, F.P.E. and D. B. Spalding. Measurements of Entrainment by Asymmetrical Turbulent Jets. J. Fluid Mechanics, 11:21-32. 1961.

47. Madni, I. K. and R. H. Pletcher. Prediction of Turbulent Jets in Coflowing and Quiescent Ambients. J. Fluid Engineering, Trans. ASME, 97:558-567. 1975.

48. Bradbury. L.J.S. Simple Expressions for the Spread of Turbulent Jets. Aeronautical Q., 18:133-142. 1967.

49. Abramovich, G. N., et al. An Investigation of the Turbulent Jets of Different Gases in a General Stream. Astronautica Acta, 14:229-240. 1969.

50. Barchilon, M. and R. Curtet. Some Details of the Structure of an Axisymmetric Confined Jet with Backflow. J. Basic Engineering. D, Trans ASME, 86:777-787. 1964.

51. Beér, J. M. and N. A. Chigier. Combustion Aerodynamics, Wiley, 1972.

52. Becker, H. A., H. C. Hottel, G. C. Williams. 9th Symposium (Int'l) on Combustion, The Combustion Institute, 7-20. 1963.

53. Steward, F. R., and A. G. Guroz, Aerodynamics of a Confined Jet with Variable Density. Combustion Science and Technology, 16:29-45. 1977.

54. Lilley, D. G. Swirl Flows in Combustion: A Review. AIAA Journal, 15:1063-1078. 1977.

55. Syred, N. and J. M. Beér. Combustion in Swirling Flows: A Review, Combustion and Flame, 23:143-201. 1974.

56. Beér, J. M. and N. A. Chigier. Combustion Aerodynamics, Wiley, 1972.

57. Chigier, N. A. and A. Chervinsky. Experimental Investigation of Swirling Vortex Motion in Jets. J. Appl. Mech., Trans ASME, E, 443-451. 1967.

58. Pratte, B. D. and W. D. Baines. Profiles of the Round Turbulent Jets in a Crossflow. Proc. ASCE, J Hydraulics Div, 93:53-64. Nov, 1967.

59. Platten, J. L. and J. P. Keffer. Deflected Turbulent Jet Flows. Trans ASME, J. Appl. Mechanics, 756-758. 1968.

60. Margason, R. J. The Path of a Jet Directed at Large Angles to a Subsonic Stream. NASA TN.D-4919. 1968.

61. Bergeles, G., A. D. Gosman, and B. E. Launder. Near-Field Character of a Jet Discharged through a Wall at 30° to a Mainstream. AIAA J., 15:499-504. 1977 1977.

62. Hoehne, V. O. and R. G. Luce. The Effect of Velocity, Temperature, and Molecular Weight on Flammability Limits in Wind-Blown Jets of Hydrocarbon Gases. American Petroleum Inst, Div of Refining Proceedings. 50:1057-1081. 1970.

63. Donaldson, C. duP and R. S. Snedeker. A Study of Free Jet Impingement, Part 1. Mean Properties of Free and Impinging Jets. J. Fluid Mech. Part 2, 45:281-319. 1971.

64. Donaldson, C. duP, R. S. Snedeker, and D. P. Margolis. A Study of Free Jet Impingement, Part 2. Free Jet Turbulent Structure and Heat Transfer. J. Fluid Mech. Part 3, 45:477-512. 1971.

65. Gauntner, J. W., J.N.B. Livingood, and P. Hrycak. Survey of Literature on Flow Characteristics of a Single Turbulent Jet Impinging on a Flat Plate. NASA TN D-5652. 1970.

66. Schlünder, E. U. Über die Ausbreitung Turbulenter Freistrahlen Z.Flugwiss. 19:108-113. 1971.

67. Beltaos, S and N. Rajaratnam. Impinging Circular Turbulent Jets. Proc. ASChE, J. Hydraul Div. 100:1313-1328. 1974.

68. Dosdogru, G. A. Chem.-Ing. Tech. 44:1340. 1972.

69. Era, Y., and A. Saima. An Investigation of Impinging Jet. Bulletin of the JSME, 19:133, p 800. 1976.

70. Beér, J. M. and N. A. Chigier. Impinging Jet Flames. Combustion and Flame, 12:575-586. 1968.

71. Milne-Thomson, L. N. Theoretical Hydrodynamics. 3rd Ed. MacMillan. 1955.

72. Martin. H. Heat and Mass Transfer Between Impinging Gas Jets and Solid Surfaces. Advances in Heat Transfer, 13:1-60. 1977.

73. Schlünder, E. U. and V. Gnielinski. Chem.-Ing. Tech. 39:578. 1967.

74. Barrett, R. E. and R. H. Barnes. Some Aspects of Afterburner Performance for Control of Organic Emissions. EPA-600/7-79-050c. US EPA, Research Triangle Park, NC. Feb, 1979.